Technische Universität München
TUM School of Medicine and Health

Dietary Influence, Novel Targeted Therapies, and Richter Transformation in Chronic Lymphocytic Leukemia: Insights and Potential Strategies

Lisa Veronika Kracher

Vollständiger Abdruck der von der TUM School of Medicine and Health der Technischen Universität München zur Erlangung einer

Doktorin der Naturwissenschaften (Dr. rer. nat.)

genehmigten Dissertation.

Vorsitz:	Prof. Dr. Marc Schmidt-Supprian
Prüfende der Dissertation:	1. Priv.-Doz. Dr. Maike Buchner-Mayr
	2. Prof. Dr. Matthias Feige

Die Dissertation wurde am 23.11.2023 bei der Technischen Universität München eingereicht und durch die TUM School of Medicine and Health am 05.06.2024 angenommen.

Zusammenfassung

Chronische lymphatische Leukämie (CLL) gehört zu den häufigsten bösartigen B-Zell-Erkrankungen in der westlichen Welt, doch trotz verfügbarer gezielter Behandlungen stellen arzneimittelresistente Verläufe eine klinische Herausforderung dar. Im Rahmen dieser Doktorarbeit wurden verschieden Aspekte der CLL behandelt. Der erste Teil beschäftigt sich mit dem Einfluss der Ernährung von Patienten, die die Entstehung einer CLL begünstigen und den Fortschritt der Krankheit verstärken kann. Dabei lag der Schwerpunkt der Forschung auf Lipiden, wie z.B. Cholesterin, die in der Blutbahn von Patienten transportiert werden und sich dort in direkter Umgebung zu CLL Zellen befinden. Bei einer Umstellung der Ernährung auf eine fettreiche Westliche Diät konnten schon nach kurzer Zeit Anstiege der Lipidwerte im Blut von Mäusen, aber auch humanen Probanden, nachgewiesen werden. CLL belastete Mäuse auf Westlicher Diät starben deutlich früher als Kontrolltiere auf einer rein pflanzlichen und fettarmen Diät und zeigten zudem quantitativ Veränderungen der Zellpopulationen in der Milz. Humane CLL Zellen, die *in vitro* in unterschiedlichen Diät-Seren inkubiert wurden, zeigten verbesserte Viabilität und Aktivierung von Signalwegen und Metabolismus mit höherem Fettgehalt im eingesetzten Medium.

Der zweite Teil dieser Arbeit befasst sich mich einem möglichen neuen Behandlungsansatz für CLL. Dabei handelt es sich um die Hemmung negativer Regulatoren, die essentiell für den Erhalt eines Signalgleichgewichts innerhalb der Zelle sind. Speziell wurden der MAPK-Signalweg und seine beteiligten Phosphatasen DUSP1 und DUSP6 untersucht. Der MAPK-Signalweg ist wesentlich beteiligt in der Entstehung einer CLL, da er u.a. Zellproliferation und -differenzierung steuert. Durch die Hemmung von DUSP1/6 mittels des Inhibitors BCI war es möglich eine verstärkte Signalweitergabe ohne negative Rückkopplung zu induzieren, die eine intensive Ansammlung von reaktiven Sauerstoffspezies (ROS) in den Mitochondrien zur Folge hatte. Diese führte zu unwiderruflichen DNA-Schäden, die in Zelltod der CLL Zellen endeten.

Der dritte und letzte Teil dieser Dissertation behandelt das Krankheitsbild der Richter Transformation (RT), seine Charakteristika und mögliche Ursachen für seine Entstehung. Die Richter Transformation beschreibt den Übergang einer chronischen lymphatischen Leukämie zu einem aggressiven Lymphom Typ, der dem diffus großzelligen B-Zell-Lymphom ähnelt (DLBCL). Im Rahmen dieser Forschung wurden verschiedene CLL Mausmodelle getestet, die mit Tamoxifen (TAM)-induzierbaren Mutationen versehen sind, die eine RT nacharmen könnten. Eine Induktion der konstitutiv aktiven Proteine $CARD11^{L225LI}$ und AKT^{E17K} resultierten nicht in einem Krankheitsbild, das einer RT ähnelte. Die genetische Aktivierung des TAM-induzierbaren Transkriptionsfaktors MYC hingegen führte zu einem Phänotyp, der in vielen Aspekten einer Richter Transformation entspricht. Zusammen mit einem MYC Expressionsmodell nach retroviraler Transduktion, wurden Krankheitsverlauf nach Transplantation, sowie intrazelluläre Signalwege, metabolische Vorgänge und Veränderungen des Proteoms in den transformierten Zellen untersucht. Interessanterweise schien eine Zellveränderung in Richtung RT verzögert zu sein, was auf eine zelluläre Anpassung an die übermäßige MYC-induzierte

Signalweitergabe hindeutet. In transformierten Zellen wurden die Stoffwechselwege Glykolyse und Glutaminolyse hochreguliert, möglicherweise gesteuert durch mTOR- und HIF-1α-Signalwege, was zu einer gesteigerten Energieproduktion und veränderten Stoffwechselprozessen beitrug. Die schützende Mikroumgebungen der Lymphknoten und der Bauchhöhle schienen zusammen mit antioxidativen Systemen und DNA-Reparaturmechanismen MYC überexprimierende Zellen zu begünstigen. Diese Studie legt nahe, dass das Zusammenspiel von intrazellulären MYC-induzierten Signalwegen, Stoffwechselanpassungen und Bestandteile des Immunsystems zu einem Übergang zu einem RT Phänotyp beitragen und damit neue therapeutische Möglichkeiten für die Behandlung einer RT mit aktiver MYC-induzierter Signalübertragung bieten.

Zusammenfassend befasst sich diese Studie mit möglichen Ursachen der CLL Entwicklung, neuen Therapiemöglichkeiten einer akuten CLL und mit dem Verhindern des Übergangs einer CLL zur aggressiven Richter Transformation. Dabei stellte sich heraus, dass das Überleben und die Steuerung von CLL Zellen stark von einem intrazellulären Signalgleichgewicht beeinflusst werden, aber auch intra- und extrazelluläre Metaboliten und Stoffwechselwege das Schicksal von CLL Zellen steuern können.

Abstract

Chronic lymphocytic leukemia (CLL) is one of the most common B-cell malignancies in the Western world, but despite the availability of targeted treatment therapies, drug-resistant progression remains a clinical challenge. Various aspects of CLL were addressed in this thesis. The first part deals with the influence of the patient's diet, which can promote the development of CLL and accelerate the progression of the disease. The focus of the research was on lipids, such as cholesterol, which are transported in patients' bloodstream and located in the immediate vicinity of CLL cells. When the diet was changed to a high fat Western diet, increases in lipid levels in the blood of mice and human test subjects could be detected after a short time. CLL-burdened mice on a Western diet died significantly earlier than control animals on a purely plant-based low fat diet. Also, they showed quantitative changes in the cell populations in the spleen. Human CLL cells incubated *in vitro* in medium conditions with different diet sera showed improved viability, activation of signaling pathways, and metabolic alterations with higher fat content in the used medium.

The second part of this thesis deals with a possible new treatment approach for CLL. This involves the inhibition of negative regulators that are essential for maintaining a signal balance within the cell. Specifically, the MAPK signaling pathway and its involved phosphatases DUSP1 and DUSP6 were examined. The MAPK signaling pathway plays a key role in the development of CLL, as it controls cell proliferation and differentiation, among other things. By inhibiting DUSP1/6 with the inhibitor BCI, it was possible to induce increased signaling without negative feedback, resulting in an intensive accumulation of reactive oxygen species (ROS) in the mitochondria. This led to irreversible DNA damage, which resulted in cell death of the CLL cells.

The third and last part of this thesis deals with the clinical picture of the Richter transformation (RT), its characteristics, and possible causes for its development. The Richter transformation describes the transition from CLL to an aggressive type of lymphoma resembling diffuse large B-cell lymphoma (DLBCL). The performed research tested various CLL mouse models carrying tamoxifen (TAM)-inducible mutations that could mimic RT. Induction of the constitutively active proteins CARD11^{L225LI} and AKT^{E17K} did not result in a clinical picture resembling RT. In contrast, genetic activation of the TAM-inducible transcription factor MYC resulted in a phenotype that corresponds in many aspects to a Richter transformation. Together with a MYC expression model after retroviral transduction, the course of the disease after transplantation, as well as intracellular signaling pathways, metabolic processes, and changes in the proteome in the transformed cells were investigated. Interestingly, the shift towards RT appeared delayed, suggesting cellular adaptation to excessive MYC signaling. Glycolysis and glutaminolysis were upregulated, potentially regulated by mTOR and HIF-1α pathways, contributing to enhanced energy production and altered metabolic processes. The protective microenvironment of lymph nodes and peritoneal cavity, along with antioxidant systems and DNA repair mechanisms, seemed to favor MYC-overexpressing lymphoma cells.

This comprehensive study suggests that the interplay of MYC signaling, metabolic adaptations, and immune responses contribute to the transition towards a Richter transformation phenotype, offering new therapeutic avenues for managing RT with activated MYC signaling.

In summary, this study investigates possible causes of CLL development, new treatment options for acute CLL, and preventing the transition of CLL to aggressive Richter transformation. It turned out that the survival and control of CLL cells are strongly influenced by an intracellular signal balance, but that intra- and extracellular metabolites and metabolic pathways can also control the fate of CLL cells.

List of publications

First author (shared):
Negative feedback regulation of MAPK signaling is an important driver of chronic lymphocytic leukemia progression
DOI: 10.1016/j.celrep.2023.113017

Co-authorship:
Targeted PI3K/AKT-hyperactivation induces cell death in chronic lymphocytic leukemia
DOI: 10.1038/s41467-021-23752-2

Analysis of immune responses in patients with CLL after heterologous COVID-19 vaccination
DOI: 10.1182/bloodadvances.2022008445

Abbreviations

4-OHT	4-hydroxytamoxifen
ACC	acetyl-CoA carboxylase
ACLY	ATP citrate synthase
ALL	acute lymphoblastic leukemia
ASCT2	neutral amino acid transporter 2
ATP	adenosine triphosphate
ATP5A	ATP synthase F1 subunit alpha
BCI	(E)-2-benzylidene-3-(cyclohexylamino)-2,3-dihydro-1H-inden-1-one
BCI-HCl	BCI hydrochloride
BCL10	B-cell lymphoma/leukemia 10
BCR	B-cell receptor
CARD11	Caspase recruitment domain-containing protein 11
CD	cluster of differentiation
CLL	chronic lymphocytic leukemia
CPT1A	carnitine palmitoyltransferase 1A
Cre	cyclization recombinase
CXCL12/13	C-X-C motif chemokine 12/13
CXCR4/5	C-X-C chemokine receptor type 4/5
CYANUS	CYtometry Analysis Using Shiny
CyTOF	Cytometry by Time-Of-Flight
DC	dendritic cell
DUSP1/6	dual-specificity phosphatase 1/6
Eco	expressing ecotropic receptor
ERK	extracellular-signal regulated kinase
ERT2	estrogen receptor
FACS	fluorescence-activated cell sorter
FAO	fatty acid oxidation
FDG	2-[^{18}F]fluoro-2-deoxy-D-glucose
FSC	forwards-scatter
G6PDH	glucose-6-phosphat-dehydrogenase
GAPDH	glyceraldehyde 3-phosphate dehydrogenase
GFP	green fluorescent protein
GLS	glutaminase
GLUT1	glucose transporter 1
GM-CSF	granulocyte-macrophage colony-stimulating factor
GOT	glutamic oxaloacetic transaminase
GPT	glutamic pyruvic transaminase
HDL	High-density lipoprotein
HIF-1α	hypoxia-inducible factor alpha
HIPK2	homeodomain-interacting protein kinase 2
HK	hexokinase
Hsp70	heat shock protein 70
i.p.	intraperitoneal
i.v.	intravenous
IDH1/2	isocitrate dehydrogenase 1/2
IFN-β/γ	interferon-β/γ
IL	interleukin
JNK	c-Jun N-terminal kinase
LDHA	lactate dehydrogenase A
LDL	low-density lipoprotein
LN	lymph node
loxP	locus of x-over, P1

M-CSF	macrophage colony-stimulating factor
MALT1	Mucosa-associated lymphoid tissue lymphoma translocation protein 1
MAP3K	MAP kinase kinase kinase
MAPK	mitogen-activated protein kinase
MCP-1	monocyte chemoattractant protein-1
MFI	mean fluorescent intensity
MHC	major histocompatibility complex
MRI	magnetic resonance imaging
n.s.	not significant
NF-κB	nuclear factor kappa-light-chain-enhancer of activated B cells
NK	natural killer
OS	overall survival
PB	peripheral blood
PB	plant-based
PBMC	peripheral blood mononuclear cell
PBS	phosphate-buffered saline
PC	peritoneal cavity
PDL1	programmed death-ligand 1
PET	positron emission tomography
PFK	phosphofructokinase
PLC	phospholipase C
pMIG	plasmid MSCV IRES GFP
R2b	B6(Cg)-Rag2tm1.1Cgn/J
RAG1/2	recombinase activating genes 1 and 2
ROS	reactive oxygen species
rRNA	ribosomal ribonucleic acid
RT	Richter transformation
rtTA	reverse tet-controlled transcriptional activator
SSC	sidewards-scatter
TAM	tamoxifen
TAM	tumor-associated macrophage
TCA	tricarboxylic acid cycle
TCR	T-cell receptor
Tet	tetracyline
tetO	tet operon
TetR	tet respressor
TG	triglyceride
TME	tumor microenvironment
TNF-α/β	tumor necrosis factor-α/β
TUM	Technical University of Munich
WFPB	whole food plant-based
wt	wild type
ZPF	Zentrum für Präklinische Forschung

List of contents

List of tables

List of figures

1. Introduction

The immune system is a complex network of cells, tissues, and molecules that work together to defend the body against harmful pathogens, such as bacteria, viruses, and fungi. It consists of two main components: the innate immune system and the adaptive immune system. These systems collaborate to provide a multi-layered defense mechanism against a wide range of threats. The innate immune system is the body's first line of defense and is present from birth. It provides rapid and non-specific responses to a broad range of pathogens. Key features of the innate immune system include physical barriers (skin and mucous membranes), phagocytes (neutrophils and macrophages), natural killer (NK) cells, and the complement system (proteins that can opsonize pathogens and trigger inflammation). The adaptive immune system is a more specific and tailored defense mediated by B and T lymphocytes. B cells mainly produce antibodies that can bind to specific antigens on pathogens. This can neutralize the pathogen or mark it for destruction by other immune cells. T cells have various roles, including helper T cells that coordinate immune responses, cytotoxic T cells that directly kill infected cells, and regulatory T cells that control the immune response.[1,2] B and T lymphocytes carry unique antigen recognition receptors, which are generated during a process called V(D)J recombination. V(D)J recombination involves the rearrangement of gene segments coding for the variable (V), diversity (D), and joining (J) regions of the B-cell receptor (BCR) and T-cell receptor (TCR) genes. RAG1 and RAG2 (Recombination Activating Gene 1/2) form a complex known as the RAG complex. This complex is responsible for recognizing specific DNA sequences known as recombination signal sequences (RSSs) located at the boundaries of V, D, and J gene segments.[3] Therefore, RAG2 is an essential component of the V(D)J recombination machinery and a RAG2 knockout in mice leads to a loss of the adaptive immune system.[4]

Before B and T lymphocytes are released into the periphery, their receptor affinities are tested in processes called positive and negative selection. During positive selection, it is ensured that developing lymphocytes express functional antigen receptors that are capable of recognizing antigens presented by major histocompatibility complex (MHC) molecules. Positive selection ensures that lymphocytes with receptors that are too weak or too strong are eliminated. Negative selection is a process that eliminates developing lymphocytes that strongly recognize self-antigens. This helps prevent the development of autoimmunity, where the immune system attacks the body's tissues.[5]

Since every cell in the human body can undergo a malignant transformation towards cancer, so can cells of the immune system. Cancer is a complex and multifaceted disease characterized by uncontrolled cell growth, invasion of surrounding tissues, and the potential for metastasis to distant sites. Over the years, researchers have identified a set of interconnected biological capabilities that collectively drive the development and progression of cancer. These fundamental characteristics, known as the "hallmarks of cancer," provide insights into the underlying mechanisms that allow cancer cells to thrive and evade the body's normal regulatory mechanisms.[6]

The hallmarks of cancer encompass several key traits, such as sustaining proliferative signaling, evading growth suppressors, resisting cell death, enabling replicative immortality, inducing angiogenesis, activating invasion and metastasis, avoiding immune destruction, deregulating cellular energetics, tumor-promoting inflammation, and genome instability and mutations. The concept of the hallmarks of cancer has provided a framework for understanding the underlying principles that govern the behavior of cancer cells. These interconnected traits reflect the adaptability and resilience of cancer cells, allowing them to overcome barriers that typically constrain normal cellular behavior. Targeting these hallmarks holds promise for the development of novel therapeutic strategies aimed at disrupting the fundamental processes driving cancer progression.[6,7]

Chronic lymphocytic leukemia (CLL) is the most common adult leukemia in Western countries, with an age-adjusted incidence of 4.1 per 100,000 inhabitants in the United States.[8] It is characterized by the accumulation of mature CD5-positive B cells in peripheral blood (PB), bone marrow (BM), lymph nodes (LN), and spleen (SP). CLL's leukemogenic event may involve mutations as early as the hematopoietic stem cell stage, and its genomic landscape is increasingly understood. Key chromosomal aberrations include del(13q), del(11q), trisomy 12, and del(17p), each associated with distinct clinical outcomes.[9] Whole exome sequencing revealed recurrent mutations in genes like *NOTCH1*, *MYD88*, *TP53*, and *ATM*, indicating several pathways involved in CLL pathogenesis. These abnormalities can lead to the dysregulation of critical genes involved in cell cycle control and apoptosis. These include the over expression of anti-apoptotic proteins, such as Bcl-2, that allow CLL cells to evade programmed cell death. In addition to genetic modification, dysregulation of intracellular signaling pathways contributes to the survival, proliferation, and resistance of CLL cells.[9,10] Atypically for B-cell malignancies, BCR signaling in CLL is induced antigen-independently and cell-autonomously, but is dependent on the heavy-chain complementarity-determining region (HCDR3) and an internal epitope of the BCR.[11] Downstream of the BCR, the protein tyrosine kinases LYN, SYK, PI3K, and BTK are involved in some of the most critical signaling pathways in CLL.[12] Beside other signaling pathways, SYK kinase activation functions as an origin for the activation of the mitogen-activated protein kinases (MAPK) cascades, which result in the activation of ERK1/2, p38, and JNK (Figure 1).[13]

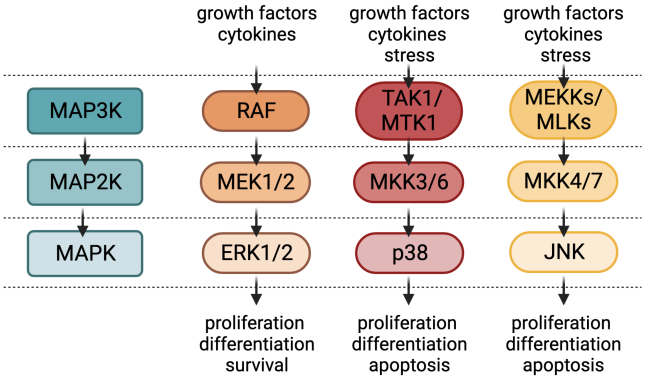

Figure 1: Signaling kinase cascades within the MAPK pathway family. Adapted from Johnson et al. and Turner et al. [14,15]

Further, the microenvironment plays a role in CLL cell survival, influencing treatment response, as CLL cells interact with stromal cells and immune cells of lymph nodes, bone marrow, and spleen. Signals from the microenvironment activate the BCR and MAPK signaling pathway and thereby provide survival and growth advantages to CLL cells, enabling them to evade cell death.[16] One of the central focuses of this thesis revolves around elucidating the critical significance of signal downregulation of the MAPK signaling pathway, resulting in phosphorylation events of ERK1/2, through the negative regulators DUSP1 and DUSP6. Clinical management of CLL has strongly improved over the last three decades, with chemo-immunotherapies and targeted small molecules, such as ibrutinib (BTK inhibitor) and venetoclax (Bcl-2 inhibitor).[17,18] While advances have transformed CLL therapy, ongoing research continues to enhance our understanding and management of this complex disease. With the existing treatment methods, two major difficulties remain in the care of CLL patients. One is a relapsed or refractory disease course. Patients who relapse or become refractory to initial treatments with the mentioned small molecules face limited options. Developing effective alternative salvage therapies for these cases is challenging, but irrevocably necessary. Another drastic course of a CLL disease is the development of a Richter transformation (RT), also known as Richter syndrome.

RT is a serious complication that can convert CLL, a slow-growing indolent lymphoma, into a more aggressive disease mostly resembling diffuse large B-cell lymphoma (DLBCL). It is often accompanied by rapidly enlarging lymph nodes, fever, night sweats, weight loss, and worsening clinical status. Richter transformation takes place in up to 10% of all CLL cases and is found in treatment-naive patients, although it is more common following therapy.[19] The treatment of RT typically involves chemotherapy regimens used for aggressive lymphomas, such as DLBCL. However, the response rates are often lower compared to de novo DLBCL cases. Stem cell transplantation may be considered for eligible patients, as even with novel treatment approaches, the median overall survival of patients with RT is predicated to only estimate 8-16 months. Interestingly, patients who received no prior treatment for CLL had significantly better OS.[20-22]

RT often arises due to genetic changes and clonal evolution within the CLL cells. Genetic abnormalities in DLBCL-type RT frequently target genes like *MYC*, *TP53*, *NOTCH1*, and *CDKN2A/B*. These genes play a crucial role in controlling cell proliferation and apoptosis. The disruption of these mechanisms likely contributes to the aggressive clinical presentation of RT, leading to both resistance to chemotherapy and rapid disease progression.[23]

Notably, approximately 70% of all DLBCL-type RT cases show deregulation in the network of the transcription factor MYC, caused by various genetic alterations.[24] The MYC signaling network is a complex regulatory system involving the MYC family of proto-oncogenes, which includes c-MYC, N-MYC, and L-MYC.[25] Any mention of MYC in this thesis describes c-MYC. Thereby, MYC is a transcription factor that is described to be a universal amplifier of gene expression increasing output at all active promoters.[26] In RT, amplifications and translations of MYC and loss-of-function mutations of the MYC suppressor MGA (Max-gene-associated) occur most frequently.[22,27] In B-cell lymphoid malignancies, MYC signaling is closely associated with BCR, PI3K, Toll-like receptors (TLR), and CD19 signal transduction, providing growth and survival signals.[28] In contrast to that, MYC expression can trigger apoptosis through the induction of BIM (member of the Bcl-2 family) and consequently inhibit B Bcl-2. A disruption of apoptotic processes through enforced expression of Bcl-2, or loss of either BIM or p53 function, can therefore enable lymphomagenesis.[29] Further, MYC activity-increasing mutations often co-occur with mutations causing loss of p53, CDKN2A/B, or gain of Bcl-2/Bcl-6 activity, contributing to the progression of an increasingly malignant phenotype in human lymphomas.[21,30]

Interestingly, the majority of lymphomas with MYC alterations descend from cells lacking MYC expression, highlighting the necessity of additional oncogenic events to overcome MYC suppression.[28] Additionally, the MYC family transcription factors play critical roles in controlling cell metabolism. In detail, MYC stimulates glycolysis, glutaminolysis, and other metabolic pathways to generate the necessary building blocks for cell growth.[31,32] Importantly, the MYC network is tightly regulated through feedback loops involving various proteins and microRNAs. Thus, the MYC proteins can regulate the expression of their own regulators, creating a complex regulatory circuit.[33]

Additionally, in high-risk CLL patients with p53 and NOTCH1 mutations and in RT patients, elevated AKT signaling levels were detected. In murine CLL, AKT activation was identified as an initiator of transformation towards an aggressive lymphoma by inducing NOTCH1 signaling between CLL cells and microenvironmental T cells.[34] AKT is a downstream target of growth factor receptors and the BCR that signal through the PI3 kinase. In patient CLL and RT, enhanced AKT signaling is reached through increased upstream signaling. In solid tumors and T cell lymphomas, mutations in AKT have been identified to elevate AKT signaling.[35,36] The substitution of glutamic acid (E) for lysine (K) mutation in the lipid binding domain of $AKT1^{E17K}$ increases binding to the phosphatidylinositol-3,4,5-trisphosphate (PIP3) ligand, forming new hydrogen bonds that accelerate the transfer of AKT from the cytoplasm to the cell membrane.[36]

This mutation induces constitutive AKT signaling through its localization to the plasma membrane, resulting in permanent AKT phosphorylation and enzymatic activity. The expression of $AKT1^{E17K}$ or myrAKT (AKT equipped with myristylation signal) in stem cells from the Eμ-MYC transgenic mice was described to lead to a disease resembling B-cell leukemia.[36]

Further, although CARD11 (Caspase Recruitment Domain-Containing Protein 11) mutations are found with lower frequencies in RT, they are of great interest.[22] CARD11–BCL10–MALT1 (CBM) signalosomes are multiprotein signaling platforms, which play a significant role in downstream signaling of the BCR and TCR. MALT1 (Mucosa-associated lymphoid tissue lymphoma translocation protein 1) holds scaffold and protease functions while it is found pre-assembled with the adapter protein BCL10 (B-cell lymphoma/leukemia 10). BCR/TCR-initiated phosphorylation of CARD11 linker regions ends autoinhibition and leads to CARD11 oligomerization that nucleates BCL10-MALT1 heterodimers, resulting in the assembly of functional CARD11–BCL10–MALT1 complexes in lymphocytes.[37] The point mutation L225LI in the coiled-coil domain of CARD11, with leucine being substituted for isoleucine at position 225, was recurrently found in DLBCL.[38] Described coiled-coil mutations in CARD11 result in spontaneous CBM signalosome formation and constitutive NF-κB and JNK activation.[39,40] This constitutive activation of signaling pathways downstream of the BCR, leads to cell survival, proliferation, and expansion of malignant B cells and contributes to the development of B-cell lymphomas.

It's important to note that Richter transformation is a complex and heterogeneous phenomenon, and the genetic landscape can vary among individual cases. The presence of mutations and genetic alterations may influence the behavior of transformed cells, their response to treatment, and patient outcomes. Genetic profiling and understanding these mutations are crucial for improving our ability to diagnose and treat Richter transformation effectively. However, the ultimate reasons for the occurrence of RT are unknown, and various factors can play a role in the malignant transformation. Recent studies showed that RT cells with outright altered genomic and transcriptomic characteristics were found to emerge already at the time of CLL diagnosis up to 19 years before the clonal expansion associated with the clinical diagnosis.[41] Further, the downregulation of BCR signaling was described in RT cells, which could be compensated by elevated activation of MYC and MAPK signaling pathways.[41-43]

Moreover, the tumor microenvironment (TME) and immune dysfunction in CLL patients may contribute to the development of Richter transformation. RT is described to induce an adaptive immune resistance environment with tumor-infiltrating lymphocytes (TIL) and PD-L1 expression, while CLL, on the other hand, seems to be characterized by an immunologically ignorant microenvironment. Thus, the TME in RT can be targeted with checkpoint inhibitors.[44,45]

Additionally, metabolic reprogramming, which plays a fundamental role in the development of cancer,[6] is being recognized as a process in the shift from CLL towards RT.[41] In general, non-malignant, as well as cancerous cells, saturate their energy demand utilizing the metabolic pathways of aerobic glycolysis. It occurs in the cytoplasm of cells and involves a series of enzymatic reactions that break down glucose into pyruvate, generating a small amount of adenosine triphosphate (ATP) and nicotinamide adenine dinucleotide (NADH) in the process. The pyruvate produced then feeds the tricarboxylic acid (TCA) cycle for energy production under normoxic conditions (Figure 2).[46]

The Warburg effect describes the utilization of pyruvate predominantly to generate lactic acid by fermentation (anaerobic glycolysis), even in the presence of oxygen. Thus, the amount of pyruvate entering the TCA cycle is decreased, resulting in low ATP yields, but in the supply of essential metabolites for quick proliferation. Therefore, this phenomenon is primarily described in fast-multiplying cancer cells.[47] However, slow proliferating CLL cells are not predominantly dependent on glycolysis to produce energy, but mitochondrial oxidative phosphorylation (OXPHOS).[48] Moreover, RT cells have been described to have differential chromatin configurations and altered transcriptional programs, further implementing OXPHOS reactions.[41]

The process of OXPHOS involves a series of electron transport chain (ETC) reactions that occur across protein complexes (I to IV), enabling proton transportation into the mitochondrial intermembrane space (Figure 2). In detail, NADH donates electrons to complex I (NADH dehydrogenase), while $FADH_2$ transfers electrons to complex II (succinate dehydrogenase) of the ETC. The electrons are then further passed to ubiquinone (coenzyme Q), complex III (cytochrome c reductase), cytochrome c, and complex IV (cytochrome c oxidase), pumping protons through the inner mitochondrial membrane. This creates a proton gradient, fueling the associated transmembrane ATP synthase (complex V) to generate ATP.[49,50] With 32 molecules of ATP per glucose molecule, OXPHOS is highly efficient in generating ATP, but primarily requires oxygen as the terminal electron acceptor and is therefore classified as an aerobic process.[51] Thus, byproducts of mitochondrial respiration are reactive oxygen species (ROS), which have a variety of intracellular effects, including harmful DNA damage.[52,53]

One source of NADH and $FADH_2$ utilized in OXPHOS reactions is the TCA cycle, also known as the citric acid cycle or Krebs cycle. TCA cycle reactions take place in the mitochondrial matrix and are a central hub of cellular metabolism, as they serve as a source of energy and as a supplier of precursors for various biosynthetic pathways (Figure 2). The TCA cycle is fueled by the entry of acetyl-CoA, derived from the breakdown of glucose, fatty acids, or amino acids. During each cycle, acetyl-CoA combines with oxaloacetate to form citrate. Through a series of enzymatic reactions, citrate is gradually metabolized, releasing carbon dioxide and generating NADH and $FADH_2$, which then feed into the ETC of OXPHOS.[54]

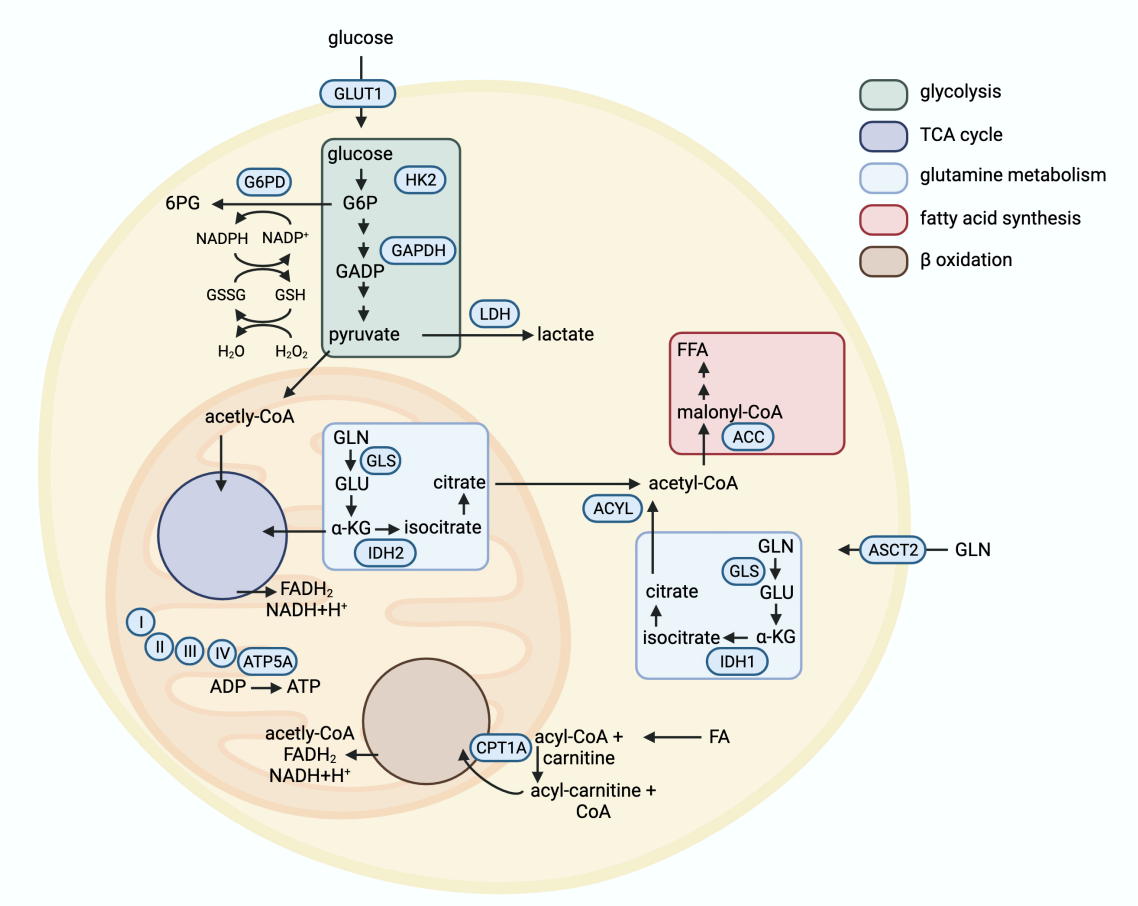

Figure 2: Metabolic pathway overview. Green: In the process of glycolysis one molecule of glucose is converted into two molecules of pyruvate generating two molecules of ATP. It serves as a key step in both aerobic and anaerobic respiration. Blue: The TCA cycle is a central metabolic pathway that completes the oxidation of glucose-derived pyruvate. It generates NADH and $FADH_2$ while releasing carbon dioxide in the mitochondria. These electron carriers play a crucial role in oxidative phosphorylation, the final stage of cellular respiration in the mitochondria. Electrons from NADH and $FADH_2$ are used to generate a majority of the cell's ATP by coupling electron transport with proton pumping across the inner mitochondrial membrane, driving ATP synthesis through ATP synthases. Grey: During glutaminolysis, glutamine is converted into glutamate and further intermediates to fuel the TCA or other metabolic processes. Red: During the process of fatty acid synthesis long-chain fatty acids are built from acetyl-CoA. It's essential for storing energy in the form of fat and producing lipids for cell membranes and other functions. Brown: β-oxidation is crucial for utilizing fats as an energy source, as it breaks down fatty acids into acetyl-CoA generating NADH and $FADH_2$ for oxidative phosphorylation. Abbreviations: GLUT1: glucose transporter 1, G6PD: glucose-6-phosphate-dehydrogenase, HK2: hexokinase 2, GAPDH; glyceraldehyde 3-phosphate dehydrogenase, LDH: lactate dehydrogenase, GLS: glutaminase, IDH: isocitrate dehydrogenase, ATP5A: ATP synthase F1 subunit alpha, CPT1A: carnitine palmitoyltransferase 1A, ACYL: ATP citrate synthase, ACC: acetyl-CoA carboxylase, ASCT2: neutral amino acid transporter 2, TCA: tricarboxylic acid

Glutaminolysis is a metabolic pathway that is based on the enzymatic conversion of glutamine to glutamate in the first step (Figure 2). Glutamate can be further metabolized to α-ketoglutarate, a key intermediate in the TCA cycle. This step is catalyzed by glutamate dehydrogenase and links the metabolism of amino acids to energy production through the TCA cycle.[55] This process is particularly important in cancer cells, where nutrient demands increase to sustain rapid cell growth and survival. Further, α-ketoglutarate can be converted to acetyl-CoA, which also can be inserted into the TCA cycle, or used in the process of fatty acid synthesis.[56] Importantly, glutamine consumption was shown to be increased in CLL cells[57] and was observed to be an adaption strategy to hypoxic conditions.[58]

Naturally, fatty acids are metabolized as a source of energy. The process of fatty acid catabolism is called β-oxidation and consists of a series of enzymatic reactions that sequentially remove two-carbon units from the fatty acid chain (Figure 2). These units are transformed into acetyl-CoA, which enters the TCA cycle to further generate energy in the form of ATP. During this process NADH and $FADH_2$ are generated additionally, fueling the ETC.[59] CLL cells can utilize more free fatty acids to produce energy compared to normal B cells and have aberrant phospholipid levels.[48] In line with that, CLL cells express increased lipoprotein lipase (LPL) levels, which contributes to free fatty acids metabolism.[60]

Also, the involved mitochondrial fatty acid transporter CPT1 and CPT2 were found to be upregulated in CLL cells.[61] The intracellular anabolism of fatty acids utilizes acetyl-CoA to feed fatty acid biosynthesis, in parallel in the mevalonate pathway, acetyl-CoA is used to generate cholesterol, steroid hormones, and isoprenoids. Statins inhibit the mevalonate pathway and are therefore classified as cholesterol-lowering drugs. The inhibited intracellular cholesterol synthesis leads to compensatory up-regulation of low-density lipoprotein-cholesterol import and consequently to lower plasma cholesterol levels.[62,63] As the mevalonate pathway also influences processes of cancer progression, including cell replication of CLL cells, it was shown that statin intake is linked to reduced CLL risk in a dose-dependent manner.[64,65]

Cholesterol is a type of lipid essential for cell membrane structure, hormone synthesis, and bile acid production. However, excess cholesterol in the bloodstream can lead to atherosclerosis, a major risk factor for cardiovascular diseases, and plays an important role in cancer development.[62,66] As cholesterol and triglycerides are insoluble in water, their transport is a complex process involving proteins. Lipoproteins are particles built from cholesterol esters and triglycerides surrounded by phospholipids and apolipoproteins, facilitating lipoprotein formation and function. Plasma lipoproteins can be distinguished based on size, lipid composition, and apolipoproteins. Inside intestinal tissue, the exogenous lipoprotein pathway starts with the absorption of triglycerides (TG) derived from dietary lipids into chylomicrons which circulate through the bloodstream after absorption.[67] In muscle and adipose tissue, TG are subsequently metabolized and chylomicron remnants are formed, which are then taken up by the liver, where very-low-density lipoprotein (VLDL) particles are produced. Further metabolization in various tissues forms intermediate-density lipoproteins (IDL) and low-density lipoproteins (LDL).[67]

LDL, often referred to as "bad cholesterol," are lipoproteins that transport cholesterol from the liver to peripheral tissues. LDL particles contain a high proportion of cholesterol and are more likely to contribute to the formation of arterial plaques, leading to atherosclerosis.[68] Reverse cholesterol transport is mediated by high-density lipoprotein (HDL) particles and are therefore often referred to as "good cholesterol". HDL lipoproteins contain a higher proportion of proteins, transports excess cholesterol from peripheral tissues back to the liver for excretion, and hence help prevent the buildup of excess cholesterol in arteries.[67]

Additionally, HDL particles show antioxidant, anti-inflammatory, and antithrombotic properties and promote endothelial repair.[69] These lipoproteins play crucial roles in maintaining lipid homeostasis and imbalances can contribute to a variety of diseases including atherosclerosis, heart disease, and cancer.[70] Therefore, managing these lipid levels through a healthy diet, exercise, and, if necessary, medication is important for a healthy lifestyle.

The differential activation of metabolic pathways depends on various factors. On the one hand, intracellular conditions, such as oxygen or nutrient availability, influence the various metabolic processes. On the other hand, genetic mutations or transcriptional alterations can change the metabolic profile of cells considerably. Together with aberrant intracellular singling and immune dysfunction, these factors can promote the transformation of non-malignant cells towards cancer, and also the transformation of CLL to RT. Especially the deregulation of the MYC signaling network plays a crucial role in this transformation.

Understanding these factors is essential for improved diagnosis and treatment strategies for RT, but targeting the tumor microenvironment, immune checkpoints, and metabolic pathways holds the potential for more effective therapies. Further research is needed to fully comprehend the intricate molecular mechanisms underlying Richter transformation and to develop innovative treatments for this complex condition.

2. Material

2.1. Antibodies

Table 1: Flow cytometry antibodies

Human	
Target	**Company**
CD2	BioLegend
CD5	BioLegend
CD19	BioLegend
Murine	
Target	**Company**
CD3	BioLegend
CD4	BioLegend
CD5	BioLegend
CD8	BioLegend
CD19	BioLegend
CD44	BioLegend
CD62L	BioLegend
c-MYC	BioLegend
DUSP6	BioLegend
Ki-67	BioLegend
p4E-BP1	BioLegend
pAKT	BioLegend
pERK	BioLegend
pH2AX	CellSignaling
pmTOR	BioLegend

Table 2: Western blot antibodies

Target	**Company**
AKT	CellSignaling
pAKT	CellSignaling
Aldolase	CellSignaling
CARD11	CellSignaling
DUSP6	CellSignaling
ERK	CellSignaling
pERK	CellSignaling
GAPDH	Merck
GLUT1	CellSignaling
Hexokinase 2	CellSignaling
Hsp70	CellSignaling
IKKα/β	Santa Cruz
pIKKα/β	CellSignaling
p65	CellSignaling
pp65	CellSignaling
PFK-1	RnD
PLCγ	CellSignaling
pPLCγ	CellSignaling
pSTAT3	NEB
RAS^{G12D}	CellSignaling

Table 3: CyTOF antibodies and their coupled metals

Target	Clone	Metal
ACC	C83B10	155Gd
ACLY	4D11	142Nd
ASCT2 (SLC1A5)	V501	175Lu
ATP5A	7H10BD4F9	159Tb
B220	53-7.3	176Yb
CD3e	145-2C11	152Sm
CD4	RA3-6B2	172Yb
CD5	4D11	146Nd
CD8a	53-6.7	168Er
CD11c	N418	142Nd
CD11b [MAC1]	M1/70	148Nd
CD19	6D5	149Sm
CD25	3C7	151Eu
CD44	IM7	171Yb
CD45	30-F11	147Sm
CD62L	MEL-14	160Gd
CD69	H1.2F3	145Nd
Cisplatin	-	195Pt
CPT1A	8F6AE9	164Dy
G6PDH	EPR20668	169Tm
GAPDH	6C5	144Nd
GFP	APC003	163Dy
GLS	PA5-35365	156Gd
GLUT1	EPR3915	153Eu
HIF-1α	16H4L13	173Yb
HK	EPR10134(B)	166Er
IDH2	EPR7577	147Sm
Ki-67	B56	168Er
LDHA	EP1566Y	171Yb
Ly6G/C [Gr1]	RB6-8C5	141Pr
NK1.1	PK136	170Er
PDL1	10F.9G2	153Eu
TCRβ	H57-597	169Tm
TER-119	TER119	154Sm

2.2. Inhibitors

Table 4: In vitro inhibitors and stimulants

Name	Target	Company
Antimycin A	mETC complex III	Sigma-Aldrich
BCI HCL	DUSP1/6	MedchemExpress
CTPI-2	mitochondrial citrate carrier SLC25A1	Selleckchem
PD0325901	MEK1/2	Biozol
SB 202190	p38	MedchemExpress
SP600125	JNK	Selleckchem
Oligomycin	ATP synthase	Thermo Fisher
PD98059	MEK1/2	Hölzel Biotech
Rapamycin	mTOR	Tocris Bioscience
Rotenone	mETC complex I	Biomol
Trametinib	MEK1/2	Selleckchem
Telaglenastat	GLS1	MedchemExpress
Etomoxir	CPT1A	MedchemExpress

2.3. Other chemicals, kits, and dyes

Table 5: Chemicals, kits, and dyes

Product	**Company**
2-deoxy-D-glucose	Sigma-Aldrich
AmershamTM ECLTM Western Blotting Detection Reagents	GE Healthcare
BSA	Roth
Carbonyl cyanide 4-(trifluoromethoxy)phenylhydrazone (FCCP)	Sigma-Aldrich
CD2 MicroBeads, human	Miltenyi Biotec
CD19 MicroBeads, mouse	Miltenyi Biotec
CellROX™ Deep Red Flow Cytometry Assay Kit	Thermo Fisher
Cell-Tak	Corning™
CellTrace™ CFSE Cell Proliferation Kit	Thermo Fisher
Cholesterol	Sigma-Aldrich
cOmpleteTM EDTA-free protease inhibitor cocktail	Roche
D-Glucose	Sigma-Aldrich
eBioscience™ Cell Proliferation Dye eFluor™ 670	Thermo Fisher
FBS	Thermo Fisher
Ficoll® Paque Plus	Sigma-Aldrich
JetFlex™ Genomic DNA Purification Kit	Thermo Fisher
L-Glutamine	Thermo Fisher
LEGENDplex™ Mouse Inflammation Panel (13-plex)	BioLegend
Lipofectamine 2000	Thermo Fisher
MitoSOX™ Red Mitochondrial Superoxide Indicator	Thermo Fisher
MitoSpy™ Red CMXRos	BioLegend
MitoTracker™ Red CMXRos	Thermo Fisher
Penicillin-streptomycin	Thermo Fisher
Phosphatase inhibitor cocktail	Roche
Pierce® BCA Protein Assay Kit	Thermo Fisher
RetroNektin	Takara Bio
RNeasy Micro Kit	Qiagen
Sodium butyrate	Sigma-Aldrich
Sodium pyruvate	Thermo Fisher
Tamoxifen	Sigma-Aldrich
ThiolTracker™ Violet	Thermo Fisher
(Z)-4-Hydroxytamoxifen	Sigma-Aldrich
Zombie Aqua Fixable Viability Kit	BioLegend

2.4. Buffers

Table 6: Buffers and their recipes

RIPA Buffer, pH 8.0	
150 mM	NaCl
1%	IGEPAL® CA-630
0.5%	Deoxycholic acid
0.5%	20% SDS
50 mM	50 mM Trizma® base
Running Buffer (10X) – 1 l	
30.2 g	Trizma® base
144 g	Glycine
50 ml	20% SDS
Transfer Buffer (10X) – 1 l	
58.2g	Tris
29.4 g	Glycine
1.6 ml	20% SDS
Transfer Buffer (1X) – 1 l	
100 ml	Transfer Buffer (10X)
200 ml	Methanol
700 ml	dH_2O
Separating Gel (10%) – 10 ml	
4.150 ml	dH_2O
2.5 ml	1.5 M Tris/HCL pH 8.8
3.3 ml	30% acrylamide
50 µl	20% SDS
50 µl	10% APS
5 µl	TEMED
Stacking Gel (4%) – 10 ml	
6.13 ml	dH_2O
2.5 ml	0.5 M Tris/HCL, pH 6.8
1.32 ml	30% acrylamide
50 µl	20% SDS
50 µl	10% APS
5 µl	TEMED
6X Leammli Loading Buffer, pH 6.8 – 90 ml	
2 g	SDS
60 mg	Bromphenolblue
47 ml	Glycerol
12 ml	0.5 M Tris
TBST (10X), pH 7.4	
20 mM	Tris
137 mM	NaCl
0.1%	Tween® 20

2.5. Mouse lines

All animal work was conducted in accordance with the German Animal Welfare Act and approved by the federal government of Upper Bavaria and the veterinarians of the "Zentrum für Präklinische Forschung" (ZPF), the institutional animal care of the TUM.

Table 7: Mouse lines and their description

Mouse line	**Description**
C57BL/6	Inbred wt and immunocompetent mice suitable as murine CLL recipient. (Janvier Labs)
R2b	C57BL/6N-*Rag2*^{TM1}-*IL2rg*$^{Tm1/CIPH}$: Immunodeficient mouse with a knock out in the *RAG2* gene on a C57BL/6 genetic background. RAG2 is critical for (V(D)J) recombination in the process of B- and T-cell maturation, therefore this lack interferes with the development of T and B cells and leads to complete absence of peripheral T and B lymphocyte cells. Suitable as human and murine CLL recipient. (Janvier Labs)
TCL1	Tg(Igh-V186.2-TCL1A)3Cro: Eμ-*TCL1* transgenic mice with *TCL1* under the control of a V_H promoter-IgH-Eμ enhancer to target *TCL1* expression in B cells on a C57BL/6 genetic background. After 12 - 16 months of age, mice show expansion of $CD5^+$ B cells resembling human B-CLL. Serves as murine CLL donor.[71]
MYCxTCL1xMb1CreERT2	C57BL/6N-*Gt(ROSA)26Sor*$^{tm13(CAG-MYC,-CD2*)Rsky}$ x Tg(Igh-V186.2-TCL1A)3Cro x B6.C-*Cd79a*$^{tm3(cre/ERT2)Reth}$: Eμ-*TCL1* transgenic mice crossed with R26StopFLMYC mice with tamoxifen-inducible Cre recombinase-mediated expression of human *MYC* and signaling deficient human *CD2* from the *Gt(ROSA)26Sor* locus from the endogenous promoter/enhancer elements of the Cd79a locus. When induced, Cre activity is only observed in the B-cell lineage. Serves as murine CLL / RT donor.
CARD11^{L225LI}xTCL1x Mb1CreERT2	C57BL/6N-*Gt(ROSA) 26Sor*$^{tm2(CARD11*L225LI)Jrld}$ x Tg(Igh-V186.2-TCL1A)3Cro x B6.C-*Cd79a*$^{tm3(cre/ERT2)Reth}$ Eμ-*TCL1* transgenic mice crossed with R26StopFLCARD11^{L225LI} mice with tamoxifen-inducible Cre recombinase-mediated expression of human CARD11 with the activating mutation L225LI and reporter protein GFP from the *Gt(ROSA)26Sor* locus from the endogenous promoter/enhancer elements of the Cd79a locus. When induced, Cre activity is only observed in the B-cell lineage. Serves as murine CLL donor.
AKT^{E17K}xTCL1xMb1CreERT2	C57BL/6N-*Gt(ROSA) 26Sor*^{AKTE17K} x Tg(Igh-V186.2-TCL1A)3Cro x B6.C-*Cd79a*$^{tm3(cre/ERT2)Reth}$ Eμ-*TCL1* transgenic mice crossed with R26StopFLAG-AKT^{E17K} mice with tamoxifen-inducible Cre recombinase-mediated expression of human FLAG-tagged AKT with the activating mutation E17K and reporter protein GFP from the *Gt(ROSA)26Sor* locus from the endogenous promoter/enhancer elements of the Cd79a locus. When induced, Cre activity is only observed in the B-cell lineage. Serves as murine CLL donor.

2.6. Cell lines

Table 8: Cell lines and their origin

Cell line	Origin
HEK293T	kindly provided by Jürgen Ruland
MEC-1	DSMZ, Braunschweig (Germany)
MEC-1 (Slc7a) Eco	generated through lentiviral transduction
OSU-CLL	kindly provided by Lukas Frenzel
OSU-CLL (Slc7a) Eco	generated through lentiviral transduction
EHEB	DSMZ, Braunschweig (Germany)
A5 hybridoma cells	kindly provided by Jürgen Ruland

2.7. Patient PBMC samples

Primary CLL patient samples were obtained from patients from the “Tumor Therapie Zentrum” (TTZ) of the MRI. The patients kindly donated peripheral blood (PB), from which peripheral blood mononuclear cells (PBMCs) were isolated. For that, the blood was diluted 1:2 with PBS, slowly pipetted on top of Ficoll solution, and spun at 400 x g for 30 min at room temperature, acceleration = 1, deceleration = 0. The PBMC layer was transferred into a fresh falcon tube, washed with PBS, and analyzed via flow cytometry. The responsible ethics committee approved the patient sampling and use of the obtained cells. All patients gave informed consent.

2.8. Mouse diets

Table 9: Mouse diets

Diet	Product	Company	Ordered
chow control diet	1310 M “Zuchtdiät für Mäuse”	Altromin Spezialfutter GmbH & Co. KG	03/2020
plant-based low fat diet	D19011501	Brogaarden	03/2020
Western diet	D12079B	Brogaarden	03/2020

It is important to consider that diet recipes have been altered by the companies since the ordering date in 2020 and could be further altered in the future. All diets were given as pellets. A detailed list of ingredients of the different diets is given in Suppl. Table 1. Figure 3 and Figure 4 depict the diet compositions and food energy values per gram.

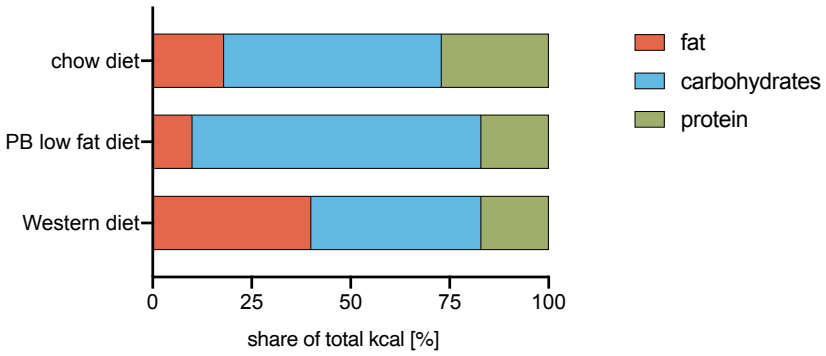

Figure 3: Share of nutrients in the different diets used in the experimental setup – Chow diet: 18% fat, 55% carbohydrates, 27% protein. Plant-based low fat diet: 10% fat, 73% carbohydrates, 17% protein. Western diet: 40% fat, 43% carbohydrates, 17% protein.

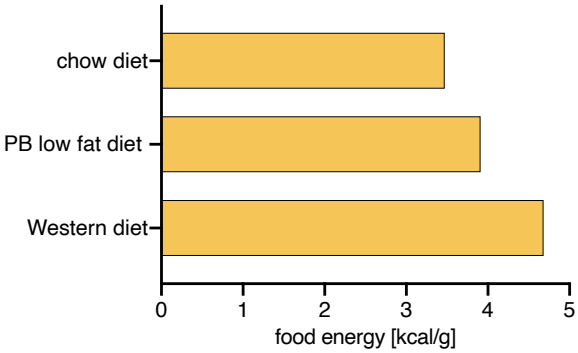

Figure 4: Food energy values per gram of chow diet, plant-based low fat diet, and Western diet.

3. Methods

3.1. Human blood lipid measurements

The voluntary donors were eating a strict whole food plant-based and primarily healthy diet for seven consecutive days followed by seven days on a Western diet consisting mainly of animal fats and carbohydrates (Figure 5). A calorie restriction was not given during the diet periods. Blood was drawn into serum tubes, which were given directly to the main laboratory of the Institute of Clinical Chemistry and Pathobiochemistry of the TUM for a small blood count, or were centrifuged at room temperature and the supernatant serum was collected and stored at -80°C.

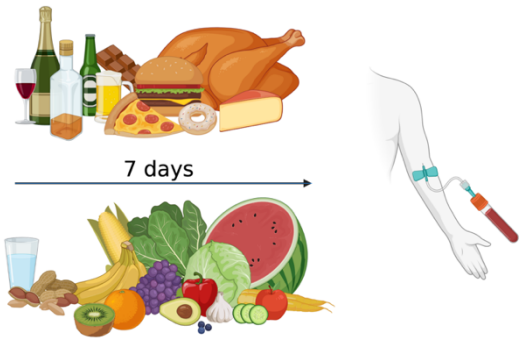

Figure 5: Schematic display of the diet plan before serum collection – Blood was drawn after 7 days on a Western orientated high fat diet or a whole food plant-based diet.

3.2. Murine plasma lipid measurements

Blood was drawn from the cheek of C57BL/6 mice after eleven weeks on different diets into lithium-heparin microvettes (SARSTEDT AG & Co. KG). The microvettes were centrifuged at 2000 x g for 5 min at room temperature and the supernatant plasma was collected. 120 µl of diluted plasma (1:4 dilution with dH_20) were transferred into measuring tubes and were analyzed at the main laboratory of the Institute of Clinical Chemistry and Pathobiochemistry of the TUM.

3.3. CLL transplantation model

To study CLL engraftment, development, and shift towards Richter transformation under different conditions in a system that resembles human CLL, we chose the transplantation model of Eμ-*TCL1* transgenic mice with *TCL1* under the control of a V_H promoter-IgH-Eμ enhancer to target *TCL1* expression in B cells on a C57BL/6 genetic background. After 12 to 16 months of age, these mice develop a population of $CD5^+$ $CD19^+$ B cells resembling human CLL, which is mainly found on the secondary lymphoid organs.[71] For the study of RT development, this mouse line was crossed with lines carrying inducible oncogenic mutations or overexpressions that were found in human RT cases.

For transplantations, enlarged spleens were extracted from mice with an advanced course of CLL detected in the peripheral blood (PB). Splenocytes were isolated and upon flow cytometric characterization injected intravenous (i.v.) or intraperitoneal (i.p.) in C57BL/6 or R2b recipient mouse strains. For the transfer of splenocytes into immunodeficient R2b mice, splenocyte suspensions were depleted of $CD8^+$ T cells to avoid graft-versus-host disease. Regular blood draws and flow cytometric analysis were performed to monitor engraftment and progression of CLL in the recipients. Treatments were planned according to CLL blood levels.

3.4. Bacterial transformation

TOP10 competent *E. coli* were used for plasmid replication. Bacteria were thawed on ice. 200 ng of plasmid DNA were added to 50 µl of *E. coli*. The suspension was mixed by gently snipping against the tube and incubated on ice for 30 min. The *E. coli* were “heat shocked” at 42°C for 30 sec and immediately put on ice for 2 min. 200 µl of SOC outgrowth medium were added to the suspension and incubated for at least 30 min at 37°C at 600 rpm. Next, the bacteria were added to 200 ml of LB Amp medium and incubated for 16 h overnight. The next day, plasmid DNA was extracted using the NucleoBond Xtra Maxi kit.

3.5. Retrovirus production and cell transduction

Replication-defective retroviruses are commonly used to insert a gene of interest into cells resulting in a stable integration into the target genome. Thereby, retroviruses depend on specific cell surface receptor binding. Murine and rat cells express the ecotropic receptor, therefore the most viral glycoprotein used to infect murine cells is the ecotropic type. Replication-defective retroviruses derive from proviruses and have most of their viral genome deleted to make room for the genes of interest. The remaining sequences include the Ψ packaging sequence, reverse transcription signals, integration signals, and viral promoter, enhancer, and polyadenylation sequences.

Generally, replication-defective retroviruses are produced by transiently transducing a packaging cell line, e.g. HEK293T, with plasmids encoding the necessary viral genes (*gag*, *pol*, *env*) and the gene of interest. The viral particles are generated inside the packaging cells, move into the supernatant through budding, and can be collected with the supernatant. Importantly, only proliferating cells can be transduced, as mitosis is required for the entry of the viral integration complex into the nucleus.[72,73]

For the production of retroviruses, $1*10^7$ HEK293T cells were plated in a 15 cm dish in DMEM (1% PenStrep, 10% FCS). After 18 hours, the cells were transfected with the plasmids pHIT60 (CMV-driven gag-pol expression plasmid), pHIT123 (CMV-driven ecotropic env expression plasmid), and target plasmid. For that, a master mix of 3 ml of plain DMEM with 80 µl Lipofectamine 2000 and a master mix of 3 ml of plain DMEM with 20 µg target plasmid DNA, 20 µg pHIT60, and 5 µg pHIT123 were prepared. Both master mixes were incubated for 5 min at RT. Subsequently, both master mixes were mixed, vortexed thoroughly, and again incubated for 20 min at RT. The current medium on the HEK293T cells was discarded and 6 ml plain DMEM were carefully added from the side of the dish to not detach the adherent cells. Then, the 6 ml of the master mix are added and incubated for 4 h at 37°C. Afterwards, 15 ml of DMEM (1% PenStrep, 10% FCS) were added and the cells were incubated overnight. The next day, the medium was decarded and 15 ml of fresh DMEM (1% PenStrep, 10% FCS) including 1.1 mg/ml sodium butyrate were added to the cells and incubated for 6 h at 37°C. Afterwards, the medium was discarded and 15 ml of fresh DMEM (1% PenStrep, 10% FCS), in which the final virus was produced for 24 h, was added. 3 ml of virus supernatant were pipetted in a 6-well plate (untreated plate, coated with RetroNektin ON and blocked with 2% BSA in TBST for 30 min) and spun for 2 h at 2000 x g at 32°C to attach the virus particles to the well's bottom. Then, $1*10^6$ target cells (OSU-CLL Eco, MEC-1 Eco, or murine splenocytes) in 2 ml of RPMI (1% PenStrep, 10% FCS) were added and spun for 30 min at 600 x g at 32°C. The cells were incubated at 37°C for at least 24 h. Afterwards, they were transferred to cell culture-treated dishes. The successfully transduced cells carried either GFP as reporter protein, which was used to track and sort the cells using optical flow cytometry, or puromycin resistance, which was used to positively select the cells.

3.6. Doxycycline-inducible gene expression using the Tet-On system

The Tet-On system is a genetic model in eukaryotic cells, which enables controlled gene expression *in vitro* and *in vivo* with the administration or withdrawal of tetracyclines. It is based on the tetracycline-resistance operon system found in gram-negative bacteria. There, tetracycline resistance is regulated by the tetracycline-responsive repressor protein TetR dimers. In gram-negative bacteria, TetR binds to $tetO_1$ and $tetO_2$ (operator sequences) in the absence of tetracyclines and prevents the expression of downstream resistance proteins. In the presence of tetracyclines, however, the TetR dimers undergo conformational changes, are released from the operator, and resistance-facilitating efflux proteins are expressed. In the Tet-On system, TetR is fused to an eukaryotic reversed regulatory domain (rtTA), that doesn't bind tetO sequences in the absence of tetracyclines.

The binding of a tetracyclines, e.g. doxycycline, to rtTA, triggers a conformational switch, which allows tetO binding. Subsequently, transcription of the downstream positioned genes, including our gene of interest *KRAS*^{G12D}, is initiated (Figure 6).[74,75]

OSU-CLL and MEC-1 CLL cell line cells were transduced lentivirally with the Tet-On-*KRAS*^{G12D}-*GFP* or Tet-On-*GFP* control construct. Positively transduced cells were selected via gained puromycin resistance (0.5 µg/ml puromycin). For induced gene expression, 5*10^5 cells were plated out in a 24-well plate and treated with 0.1 µg/ml doxycycline for 48 hours.

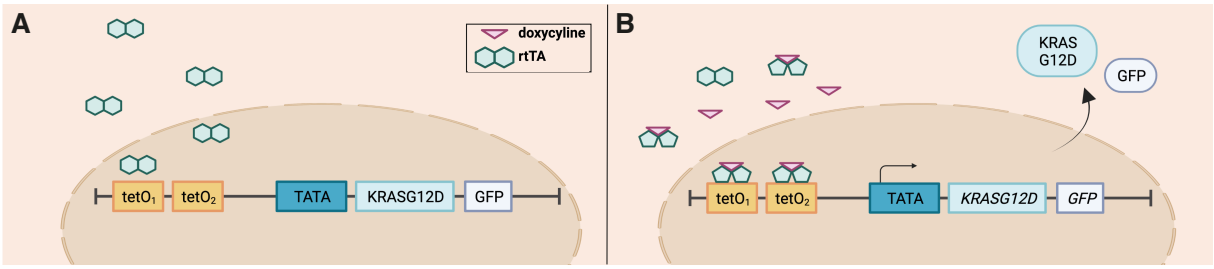

*Figure 6: Schematic illustration of the Tet-On systems for doxycycline-inducible gene expression – **A** In the absence of doxycycline, the regulatory domain rtTA doesn't bind to the operator sequences tetO$_1$ and tetO$_2$, hence no transcription of the gene of interest KRAS^{G12D} occurs. **B** In the presence of doxycycline, the regulatory domain rtTA undergoes a conformational change, binds the operator sequences tetO$_1$ and tetO$_2$, and enables the expression of the downstream proteins of interest.*

3.7. Tamoxifen-inducible Cre-ERT2 recombinase system

Genetically engineered mouse models are commonly used to examine human disease. Above all, the tamoxifen-inducible Cre-ERT2 recombinase system is widely used as a tool for generating tissue-specific conditional disease models. The Cre (cyclization recombinase) is a tyrosine site-specific recombinase originally found in the bacteriophage P1. It recognizes specific 34 bp long DNA sequences called *loxP* (locus of x-over, P1) and can remove sequences located between two *loxP* cassettes.[76] If the *Cre-ERT2* locus is placed following a tissue-specific promoter, e.g. *Mb1*, the recombinase is expressed exclusively in B lymphocytes. The recombinase is present in a fused form with the estrogen receptor ERT2 (triple mutant in ligand binding site) and remains in the cytoplasm due to HSP70 binding. In the presence of synthetic steroids, e.g. tamoxifen (TAM), HSP70 is released, and the Cre-ERT2-TAM complex is translocated into the nucleus.[77-79] There, the recombinase can remove either an exon of an unwanted gene, or a stop cassette, whose removal enables ligand-depended gene expression, as in our studies *CARD11*^{L225LI}, *MYC*, or *AKT*^{E17K} (Figure 7). For gene expression induction *in vivo*, tamoxifen (dissolved in EtOH, diluted in peanut oil) was given 4 days in a row with 1 mg/mouse per day via i.p. injections. *In vitro*, the hydrophilic analog 4-hydroxytamoxifen (4OHT) was used with 1µg/ml for 48 h.

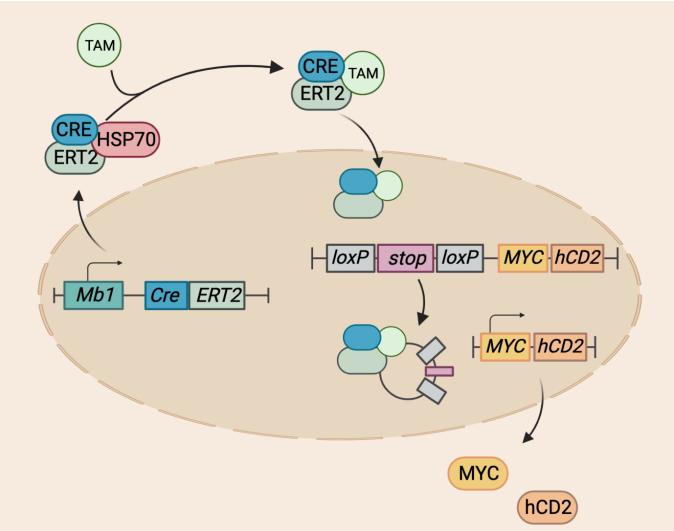

Figure 7: Schematic illustration of the tamoxifen-inducible Cre-ERT2 recombinase system in MYCxTCL1xMb1CreERT2 murine cells – Under the Mb1 promoter, the Cre-ERT2 fusion protein is expressed in B lymphocytes and kept in the cytoplasm through HSP70 binding. In the presence of tamoxifen (TAM), HSP70 is released and Cre-ERT2 can translocate into the nucleus, where the Cre recombinase excises a loxP-flanked stop cassette before our gene of interest MYC. This leads to MYC expression together with our reporter protein hCD2.

3.8. Western Blotting

Western blotting is an immunohistochemical technique to quantitatively detect specific denatured proteins in multi-cell samples. Complete protein denaturation is implemented through heat, reducing agents, and anionic detergents. The proteins are separated by polyacrylamide gel electrophoresis (PAGE) based solely on size, transferred and immobilization to a membrane, and selectively detected using an antibody-mediated reporter system inducing chemiluminescence.[80,81]

In the described experiments, cells were washed twice with ice-cold PBS, incubated in RIPA buffer (50X cOmpleteTM EDTA-free protease inhibitor cocktail, 50X phosphatase inhibitor cocktail) for 20 min on ice, and centrifuged for 15 min at 4°C on full speed. The protein-containing supernatant was mixed with 6X Leammli loading buffer and incubated for 5 min at 95°C. Protein concentrations were determined with Pierce® BCA Protein Assay Kit, 25 µg protein of each sample were separated using a 10% SDS-PAGE Gel and transferred onto a nitrocellulose membrane (for WB buffer see Table 6). The membranes were blocked for 30 min with 5% BSA in TBST, incubated in primary antibody (1:1000 in 5% BSA in TBST) ON, washed 3 times with TBST, incubated in secondary AB for 1 h (1:1000 in 5% BSA in TBST), and again washed 3 times with TBST (for Westen Blot AB see Table 2). Then, the membranes were developed using the ChemiDoc MP Imaging System (BioRad) and quantified using the ImageJ software.

3.9. Flow cytometry

Flow cytometry is a multi-parametric laser-based method to analyze intra- and extracellular features. The fluidics system of a flow cytometer creates single-cell droplets, whereas the optical system points lasers with different wavelengths on each particle generating visible and fluorescent light signals used to analyze the sample. With this, the size and granularity, as well as fluorescent signals (e.g. fluorescently conjugated antibodies, DNA binding dyes, proliferation and viability dyes, fluorescent expression proteins) of single cells can be detected. Spectral overlap limits the analysis of a maximum of 30 parameters at once. Flow cytometry sorters are additionally able to transfer a positive or negative charge to the generated single-cell droplet, which can subsequently be separated from other cells via a metal deflection plate.[82-84]

The experimental samples were measured with the BD FACSCanto™ Flow Cytometry System and analyzed using the FlowJo software (for flow cytometry antibodies see Table 1). Viable/dead cells were determined via DAPI or zombie aqua staining, afterwards, drug-specific cell death was calculated with the following equation: 100*(% dead cells – % baseline dead cells)/(100% – % baseline dead cells). For a general gating strategy see Figure 8.

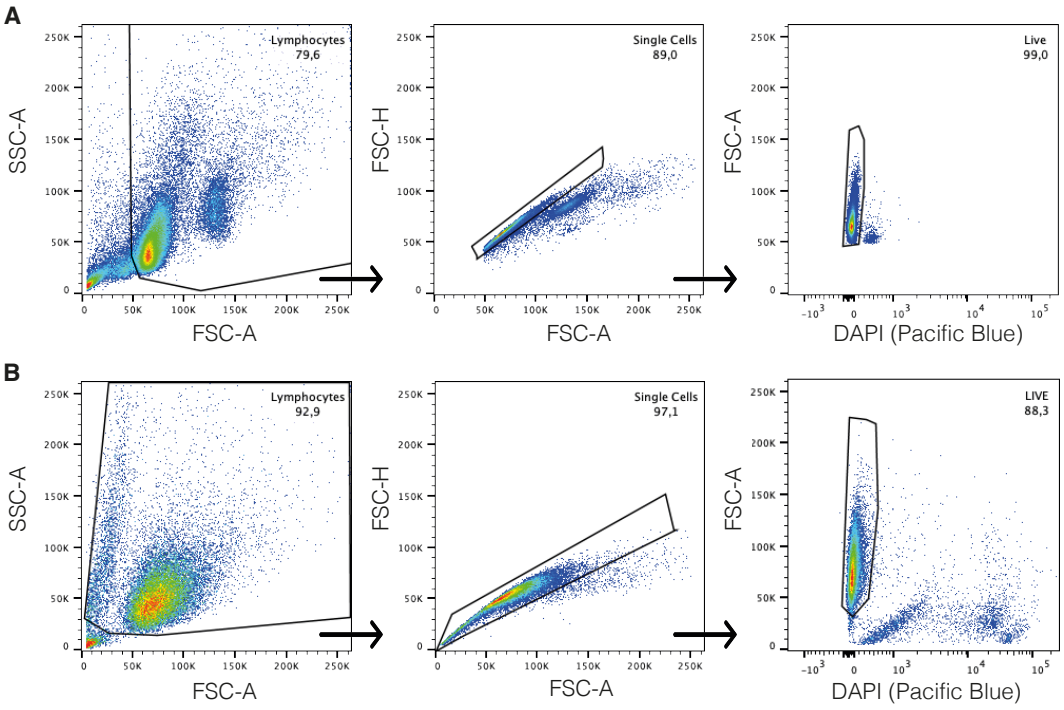

*Figure 8: Flow cytometry gating strategy for viable single cells of **A** human patient PBMCs and **B** the MEC-1 cell line – Lymphocytes are gated in a plot showing sideward-scatter-amplitude (SSC-A) vs. forward-scatter-amplitude (FSC-A) excluding small fragments of cell debris. Single cells are gated as a diagonal in a plot showing forward-scatter height (FSC-H) vs. forward-scatter amplitude (FSC-A). Viable cells are gated as a DAPI-negative population in a plot showing forward-scatter amplitude (FSC-A) vs. Pacific Blue intensity.*

3.10. Cytometry by time-of-flight

Cytometry by time-of-flight (CyTOF) enables single-cell-based immunophenotyping of complete tumor microenvironments, including rare cell populations, as up to 10^7 per sample can be analyzed. Samples are stained with antibodies against extra-, as well as intracellular antigens, which are tagged with unique heavy metal isotopes. Contrary to fluorescent labels in optical flow cytometry, isotopes don't generate spectral overlap, enabling an analysis of a maximum of 60 parameters simultaneously. During measurement, single-cell droplets are generated and subsequently nebulized. By passing through argon plasma, the single-cell samples are atomized and ionized. A high-pass optic removes biological low-mass ions (< 75 kDa) and the time-of-flight chamber separates the sample by mass-to-charge ratio. Finally, the detector amplifies ion counts and converts them into electrical signals.[85,86]

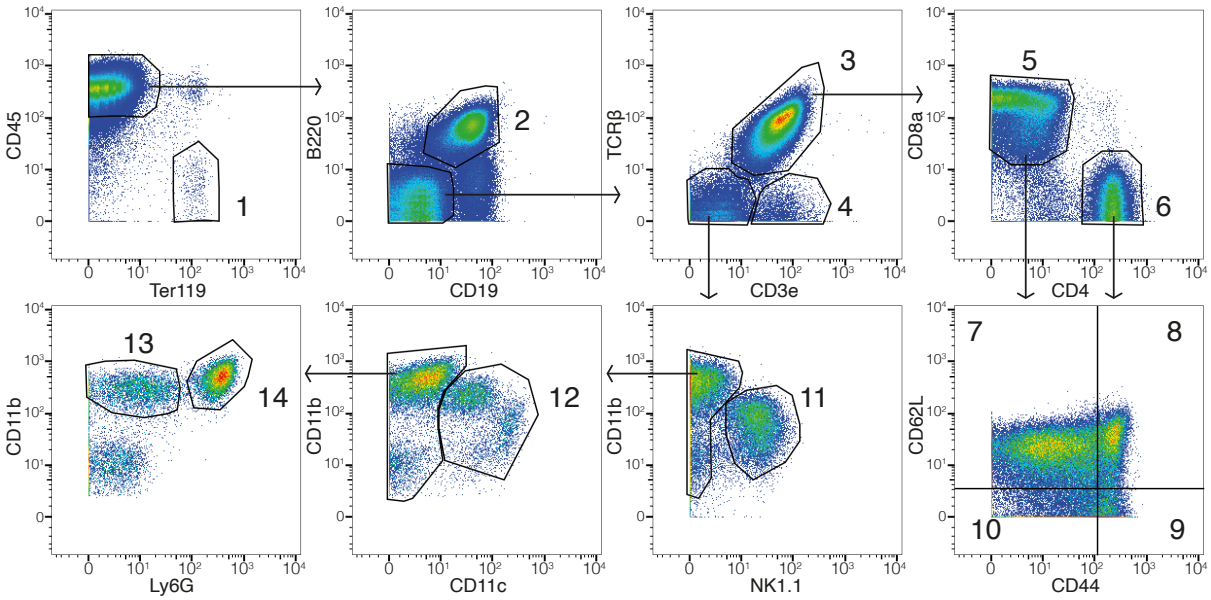

Figure 9: Gating strategy suggested for Maxpar® Mouse Sp/LN Phenotyping Panel Kit from Fluidigm – Erythrocytes (1), B cells (2), αβ T cells (3), γδ T cells (4), CD8 T cells (5), CD4 T cells (6), naive (7), central memory (8), effector (9), and effector memory T cells (10), NK cells (11), circulating DCs (12), monocytes/macrophages (13) and granulocytes (14) are identified by the numbered gates.

For our measurement, red blood cell lysis was performed on murine whole splenocytes. $3*10^6$ splenocytes were stained with Cell-ID cisplatin, followed by surface antibody staining. Subsequently, the cells were fixed with 1.6% formaldehyde. The stain with Cell-ID Intercalator-Ir was performed overnight and measurements were performed at the CyTOF system Helios on the following day. t-SNE analysis was performed with CYANUS (CYtometry ANalysis Using Shiny) software, and classical gating was performed with FlowJo software according to the manufacturer's suggested gating strategy (Figure 9).

3.11. Positron emission tomography (PET) and magnetic resonance imaging (MRI)

Positron emission tomography (PET) is a technique in nuclear medicine that results in cross sections of living organisms detecting gamma radiation after beta decay of radiotracers. A common radiotracer is ^{18}F, which is used in 2-[^{18}F]fluoro-2-deoxy-D-glucose (^{18}F-FDG) to track metabolic deviations in inflammation and cancer.[87] Commonly, PET imaging is paired with magnetic resonance imaging (MRI). MRI uses nuclear magnetic resonance (NMR) technology to image adjustable soft-tissue contrast for anatomical and functional assessment.[88] Together, both methods enable the visualization and location of altered glucose uptake levels *in vivo*.

For our experiments, mice were transferred into the imaging area of the ZPF. Food pellets were removed 3 h before imaging. Mice were anesthetized using isoflurane and injected with 2-[^{18}F]fluoro-2-deoxy-D-glucose and subsequently imaged individually by members of the Kossatz group. The mice were transferred back into our mouse facility after no more detection of gamma radiation was possible.

3.12. Seahorse real-time cell metabolic analysis

Measuring cellular metabolism is fundamental to grasping the cellular physiology of cancer cells. The Seahorse XF Analyzer series allows real-time measurement of pH and O_2 concentrations, providing information about cellular metabolism. The extracellular acidification rate (ECAR) is used as a measure of anaerobic glycolysis during the glycolysis stress test (GST), and the oxygen consumption rate (OCR) is used to determine levels of aerobic mitochondrial respiration during the mito stress test (MST). Through a maximum of four ports, various respiratory inhibitors are injected into the experimental wells at specific time points allowing the calculation of the baseline respiration rate and total aerobic and anaerobic ATP production (Figure 10).[89]

Wells of the Seahorse assay plate were coated with Cell-Tak at 22.3 µg/ml overnight at 4°C. 300.000 cells per well were plated out in 184 µl of GST (Seahorse XF RPMI medium, 2 mM glutamine, 1 mM pyruvate) or MST assay medium (Seahorse XF RPMI medium, 2 mM glutamine, 1 mM pyruvate, 25 mM D-glucose) and spun down before the assay run. Experiments were performed in quadruplicates. For the MST, D-glucose (port A, 100 mM, 20 µl), oligomycin (port B, 10 µM, 22 µl), and 2-DG (port C, 500 mM, 24 µl) were injected. For the GST, oligomycin (port A, 10 µM, 20 µl), FCCP (port B, 15 µM, 22 µl), and antimycin A + rotenone (port C, 10 µM + 1 µM, 24 µl) were injected. Measurements were performed with 3 cycles of 3 min “Mix”, 2 min “Wait”, and 3 min “Measure” each.

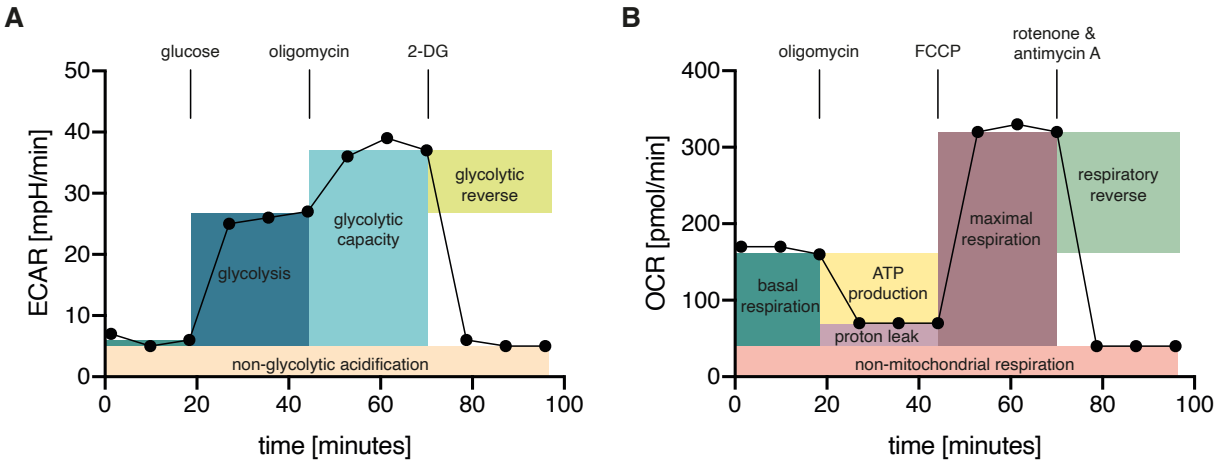

*Figure 10: Agilent Seahorse XF **A** glycolysis stress test profile and **B** mito stress test profile – Sequential compound injections measure glycolysis, glycolytic capacity, basal respiration, and maximal respiration and allow calculation of non-glycolytic acidification, ATP production, and non-mitochondrial consumption. Adapted from Agilent Technologies´ user guide.*

3.13. Murine 16S rRNA sequencing

16S rRNA sequencing is a next-generation sequencing technique used to perform microbiome analysis from native material. It is one of the most commonly used methods to determine the taxonomic distribution in bacterial communities such as the gut microbiome. The 16S rRNA gene, which encodes part of the bacterial ribosome, contains highly conserved and nine highly variable regions (V1-V9).[90] The variable regions can be used for taxonomic identification, as they provide specific information about genus and species.[91]

Sampling of cecal content was performed directly after the animal's death. The material was transferred into an Eppendorf tube, frozen in liquid nitrogen, and stored at -80°C. Content from the cecum is used for the analysis, as it contains the entire range of anaerobic bacteria. High-throughput sequencing of amplicons of the 16S rRNA gene (V3-V4) inclusive DNA isolation, library preparation, purification, and sequencing was performed in cooperation with the Core Facility Microbiome at ZIEL - Institute for Food & Health of the TUM.

3.14. scioDiscover - array-based protein expression analysis

This protein expression analysis was performed by the Sciomics GmbH. The scioDiscover service enables high-content, immuno-based protein profiling of various biological samples leading to a comprehensive overview of proteomic changes. Key pathways in various diseases such as cancer, neurological disorders, and organ failure are covered. The scioDiscover protein array-based service enables fast and targeted research while still offering a broad overview of potential changes in the protein level in your samples.

For this process, dry cell pellets of $1*10^7$ cells were sent to the company on dry ice, where proteins were extracted. The bulk protein concentration was determined, and proteins were labeled and analyzed in a dual-color approach using a reference-based design on 10 scioDiscover antibody microarrays targeting 1,470 different proteins with 1,929 antibodies. Each antibody is represented on the array in four replicates. Slide scanning was conducted using a Powerscanner (Tecan, Austria) with constant instrument laser power and PMT settings. Spot segmentation was performed with GenePix Pro 6.0 (Molecular Devices, Union City, CA, USA). Acquired raw data were analyzed using the linear models for the microarray data (LIMMA) package of R-Bioconductor after uploading the median signal intensities. For normalization, a specialized invariant Lowess method was applied. For analysis of the samples, a one-factorial linear model was fitted via least squares regression with LIMMA, resulting in a two-sided t-test or F-test based on moderated statistics. All presented p-values were adjusted for multiple testing by controlling the false discovery rate according to Benjamini and Hochberg. Proteins were defined as a differential for $|logFC| > 0.5$ and an adjusted p-value < 0.05. Differences in protein abundance between the sample groups are presented as log-fold changes (logFC) calculated for the basis 2. Therefore, a logFC = 1 means that the sample group had on average a $2^1 = 2$-fold higher signal than the control group. logFC = -1 stands for $2^{-1} = 1/2$ of the signal in the sample as compared to the control group.

4. Results

4.1. Effects of diets with different fat contents on blood parameters and CLL pathogenesis

4.1.1. Effects of Western diet and PB low fat diet on murine CLL pathogenesis in immunocompetent mice

Based on the high prevalence of CLL in Western countries, we hypothesized that in addition to genetic predispositions, the consumption of a Western diet contributes to the disease. To study whether diet affects murine CLL engraftment and progression, we performed *in vivo* transplantation experiments on immunocompetent C57Bl6/J wt mice. To do this, we collected splenocytes of aged Eμ-*TCL1* donor mice and confirmed CLL development in the donor mouse by determining the percentage of CD5 CD19 double-positive cells of lymphocytes. The CLL splenocytes were i.v. injected equally into the experimental recipient mice, which were randomly divided into the experimental groups.

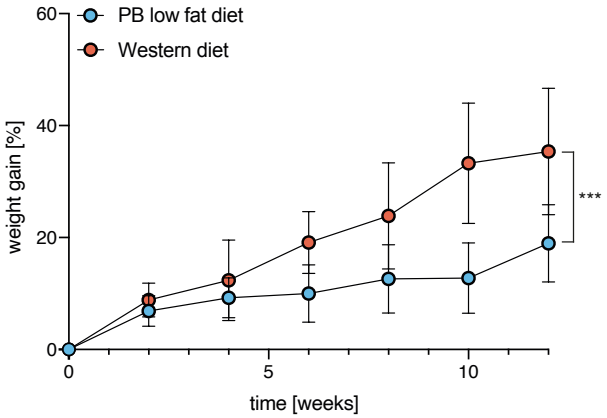

*Figure 11: Weight gain of mice on different diets – Weight gain of C57Bl6/J mice on the plant-based low fat diet (n=12) (blue) and the Western diet (n=12) (red). For statistical analysis, a two-tailed unpaired Student's t-test was performed. ***, p=0.0004. Representative result for 3 independent experiments is shown. All data is presented as mean values ± SD.*

First, to investigate the effects of different diets on CLL progression, C57Bl6/J wt mice were randomly divided into two different groups at the age of 10 weeks. One group was fed a Western high fat diet, the other group was fed a plant-based low fat diet before CLL injection. We confirmed an increase in weight gain in C57Bl6/J wt mice on the Western diet as compared to mice on the PB low fat diet (Figure 11).

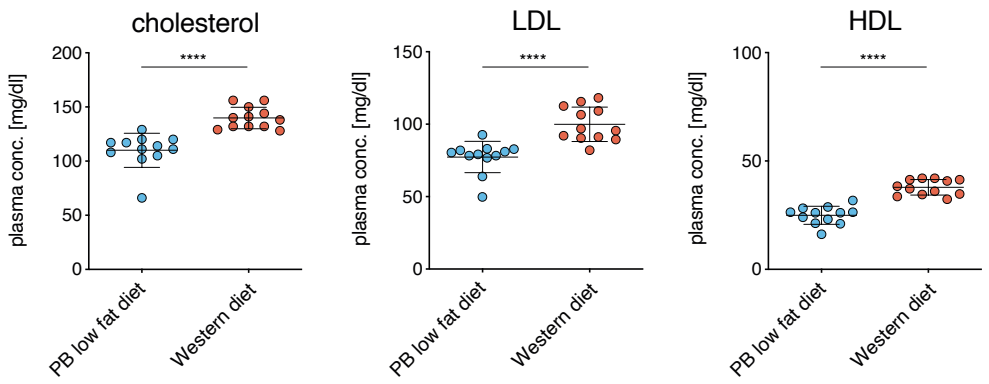

*Figure 12: Plasma lipid levels of C57Bl6/J mice on different diets – Plasma lipid levels of C57Bl6/J mice after eleven weeks on diet. Mice were given the plant-based low fat diet (blue) or the Western diet (red) (n=12 each). For statistical analysis, a two-tailed unpaired Student's t-test was performed. Cholesterol: ****, p<0.0001; LDL: ****, p<0.0001; HDL: ****, p<0.0001. Data is presented as mean values ± SD.*

To further assess the effects of the diets, we next analyzed murine lipid plasma contents after 11 weeks of diet (Figure 12). In C57Bl6/J mice, the intake of the Western diet increased the blood lipids cholesterol, LDL, and HDL significantly compared to the uptake of the PB low fat diet.

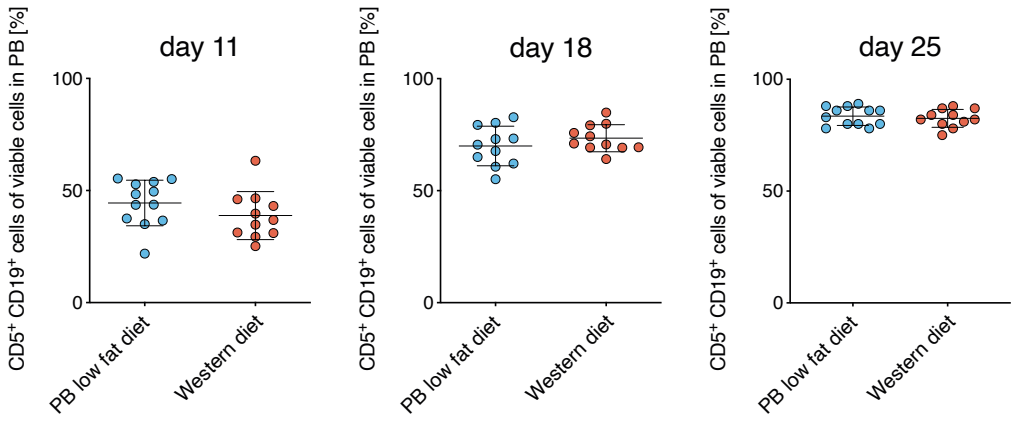

*Figure 13: CLL engraftment of C57Bl6/J mice on different diets – Content of CD5⁺ CD19⁺ CLL cells in the PB of C57Bl6/J mice transplanted with 1*10⁷ Eμ-TCL1 splenocytes per mouse after 20 weeks on diet. The mice were given the plant-based low fat diet (n=12) (blue) or the Western diet (n=12) (red) (pooled regardless of the access of a running wheel). For statistical analysis, a two-tailed unpaired Student's t-test was performed, no significant differences were detected. Data is presented as mean values ± SD.*

When transplanted with donor CLL splenocytes, we tracked the engraftment of the CLL cells via flow cytometry-based analysis of CD5 CD19 double-positive cells in the peripheral blood of C57Bl6/J mice. The mice were 20 weeks old and 10 weeks fed with the specific diets at the time of transplantation. The cells engrafted fairly aggressively, as the CLL content in the PB almost exceeded 50% at day 11 in both groups. We continued tracking the CLL progression and could not detect a differentiated engraftment of CLL in mice fed with PB low fat diet or Western diet (Figure 13).

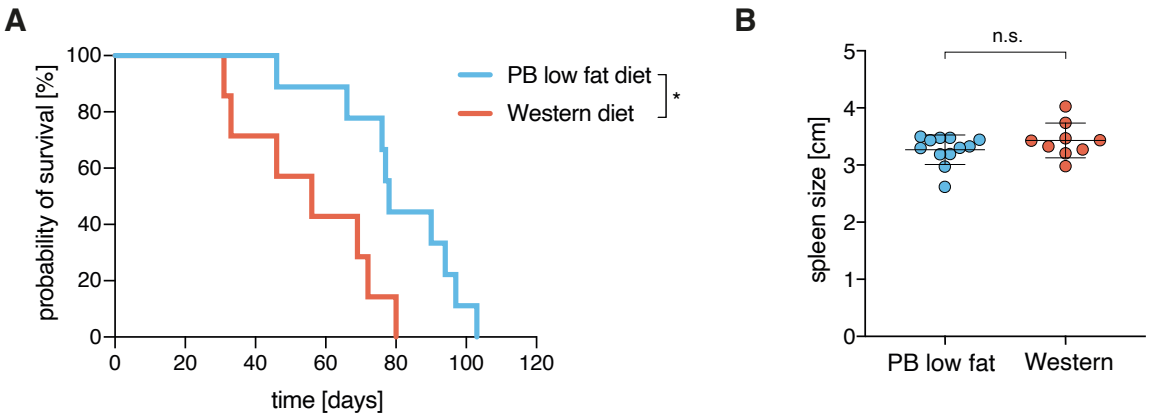

*Figure 14: Survival and end analysis of C57Bl6/J mice on different diets – **A** Kaplan-Meier survival analysis of C57Bl6/J mice transplanted with 1*10^7 Eμ-TCL1 splenocytes per mouse. The mice were given the plant-based low fat diet (blue) (n=12) or the Western diet (red) (n=12). For statistical analysis, Log-Rank (Mantel-Cox) analysis was performed. *, p=0.0139. **B** Analysis of the spleen sizes of C57Bl6/J mice transplanted with 1*10^7 Eμ-TCL1 splenocytes per mouse after death. For statistical analysis, a two-tailed unpaired Student's t-test was performed, no significant differences were detected. Data is presented as mean values ± SD.*

While we did not see affected CLL engraftment by different diets in C57Bl6/J wt mice, CLL-bearing mice fed a Western diet showed a significantly decreased survival as compared to a PB low fat diet (Figure 14A). In this survival analysis, the experimental animals' health was evaluated using a predetermined scoring system and the mice were euthanized after reaching the endpoint criteria. We confirmed CLL as the leading cause of death in all experimental mice. After death, the spleens were removed and their measured. No difference in spleen size was detected between the two different diet groups. (Figure 14B).

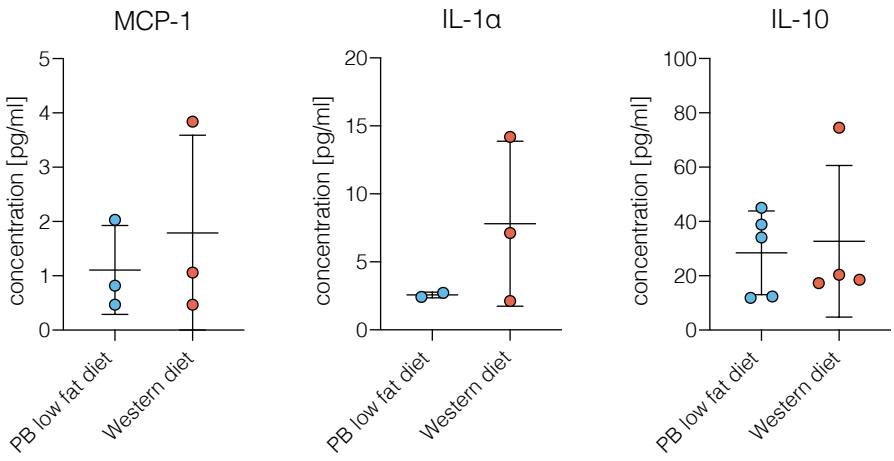

Figure 15: Cytokine levels of C57Bl6/J mice on different diets – Final plasma cytokine levels of C57Bl6/J mice analyzed with the LEGENDplex™ Mouse Inflammation Panel Standard Kit after 26 weeks on diet and 18 weeks after CLL transplantation. Data is presented as mean values ± SD.

We analyzed plasma cytokine levels of C57Bl6/J wt mice after 26 weeks on the specific diets and 18 weeks after CLL transplantation with the LEGENDplex™ Mouse Inflammation Panel Kit, which can detect IL-1α, IL-1β, IL-6, IL-10, IL-12p70, IL-23, IL-27, IFN-β, IL-17A, MCP-1, TNF-α, IFN-γ, and GM-CSF. Only MCP-1, IL-1α, and IL-10 were detected with concentrations above the minimal threshold (Figure 15). We could not detect significant differences between the cytokine levels of mice on the PB low fat diet and the Western diet (using a two-tailed unpaired Student's t-test), but a small trend may indicate an upregulation of the detected cytokines in mice on the Western diet.

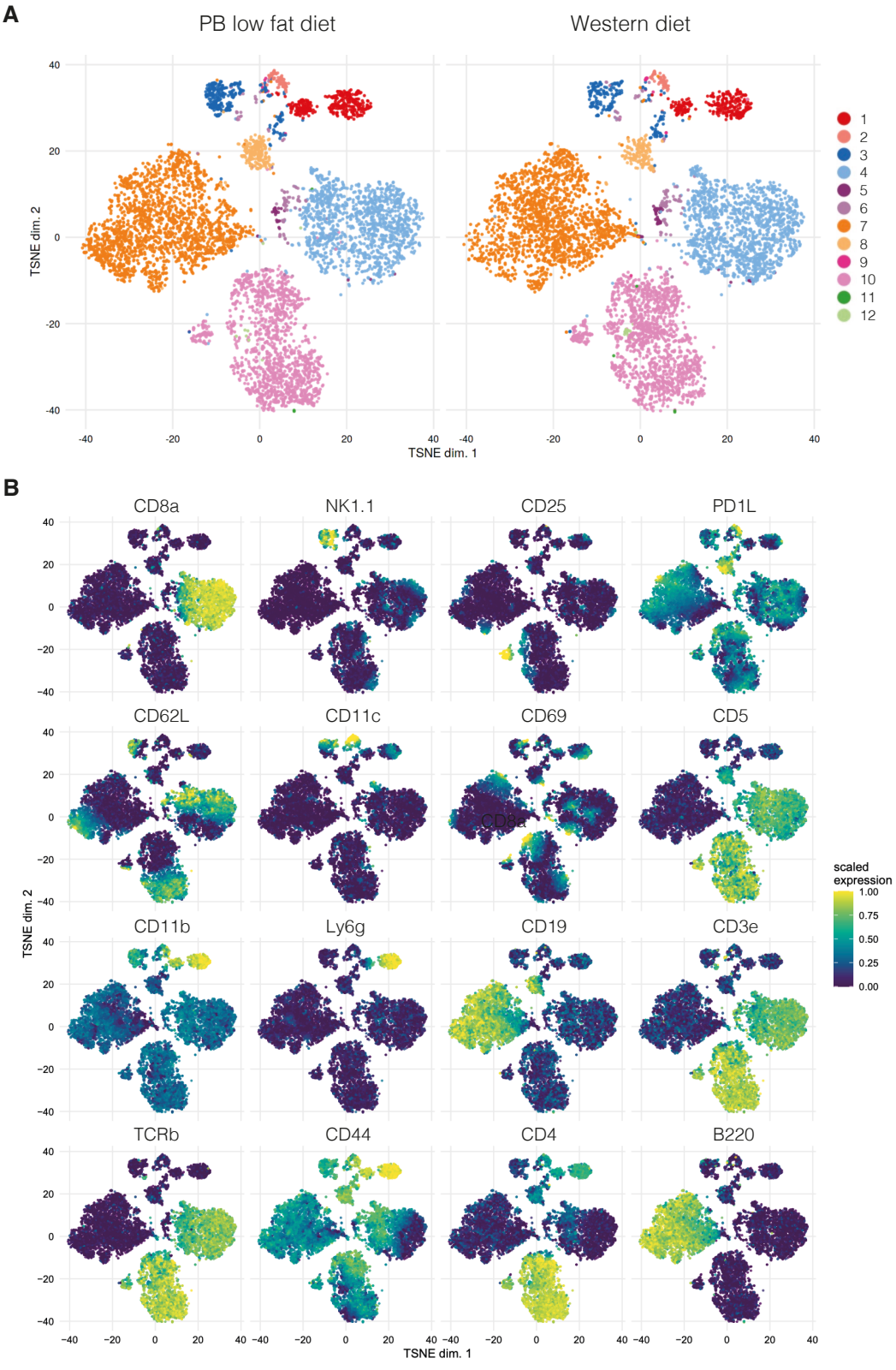

Figure 16: Immune cell population of C57Bl6/J mice on different diets – TSNE projection of whole splenocytes of C57Bl6/J mice (11 weeks on diet, 11 days after CLL transplantation) clustered using sixteen extracellular markers. The analysis was performed with CYANUS (CYtometry ANalysis Using Shiny) software. The samples were gated for CD45⁺ expression before analysis. ***A*** *Comparison of plant-based low fat diet and Western diet splenocytes with an classification into twelve clusters (meta12) defined by the extracellular markers CD8a, NK1.1, CD15, PD1L, CD62L, CD11c, CD69, CD5, CD11b, Ly6g, CD19, CD3e, TCRβ, CD44, CD4, and B220.* ***B*** *Localization of the different sixteen extracellular markers inside the TSNE projection.*

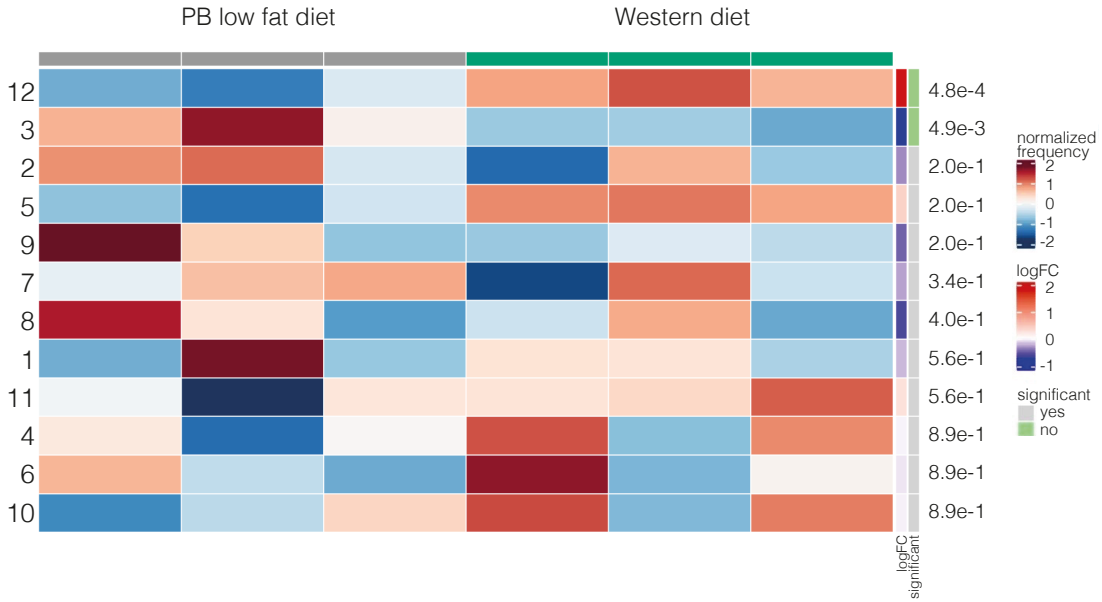

Figure 17: Differential expression analysis heatmap of immune cell population of C57Bl6/J mice on different diets – Differential expression analysis using differential cluster abundance testing of TSNE clusters. Depicted are the twelve (1-12) defined clusters (meta12) vs. the six experimental mice (1-6). Cluster 12 and 3 are significantly differentially expressed (marked in light green). For statistical analysis: method: edgeR, comparison: condition, cluster: meta12, trend method: none, normalized: yes, FDR threshold: 0.05, sorted by: p-adjusted, z-score normalization: yes.

We further analyzed immune cell populations of the spleens of C57Bl6/J mice on the Western diet and PB low fat diet using CyTOF and the software CYANUS (CYtometry ANalysis Using Shiny). The mice were fed with specific diets for 11 weeks and were transplanted with CLL 11 days before the analysis. Figure 16A shows a comparing TSNE projection of the different cell populations clustered using sixteen extracellular markers depicted in Figure 16B. The associated differential expression analysis (Figure 17) identified clusters 3 and 12 as significantly deregulated. With the specific marker localization within the TSNE projection (Figure 16B), we could match cluster 3 with the NK1.1-positive population, which is downregulated in Western diet mice, and cluster 12 with a subpopulation that is TCRβ, CD3, CD5, and CD4-positive, and is upregulated in Western diet mice.

The same data set was analyzed manually with the software FlowJo (Figure 18). The applied gating strategy is shown in Figure 9. As the CLL transplantation was performed 11 days before the analysis the CLL content in the spleens range between 3% and 14%. We could not detect a significant difference in CLL engraftment between both groups. Manual gating validates the significantly lower percentage of NK1.1-positive NK cells in the spleen of Western diet-fed mice. Interestingly, CD11b-positive macrophages were also found to be less frequent in the spleens of Western diet mice. DCs were also detected with a slightly lower frequency in Western diet splenocytes, whereas this difference was not significant.

The population of γδ T cells was significantly enhanced in Western diet spleens, as well as CD25 CD4 double-positive T cells. This population could include regulatory T cells but also activated T cells. Interestingly, a lower amount of naive and a higher amount of effector memory T cells in the spleens of mice fed with the Western diet was found. We observed no differences in CD4/CD8 T cell ratio (data not shown). This experiment was purposely performed 11 days after murine CLL transplantation to detect the effects of the different diets on the immune cell compartments with minimized influence of the CLL engraftment.

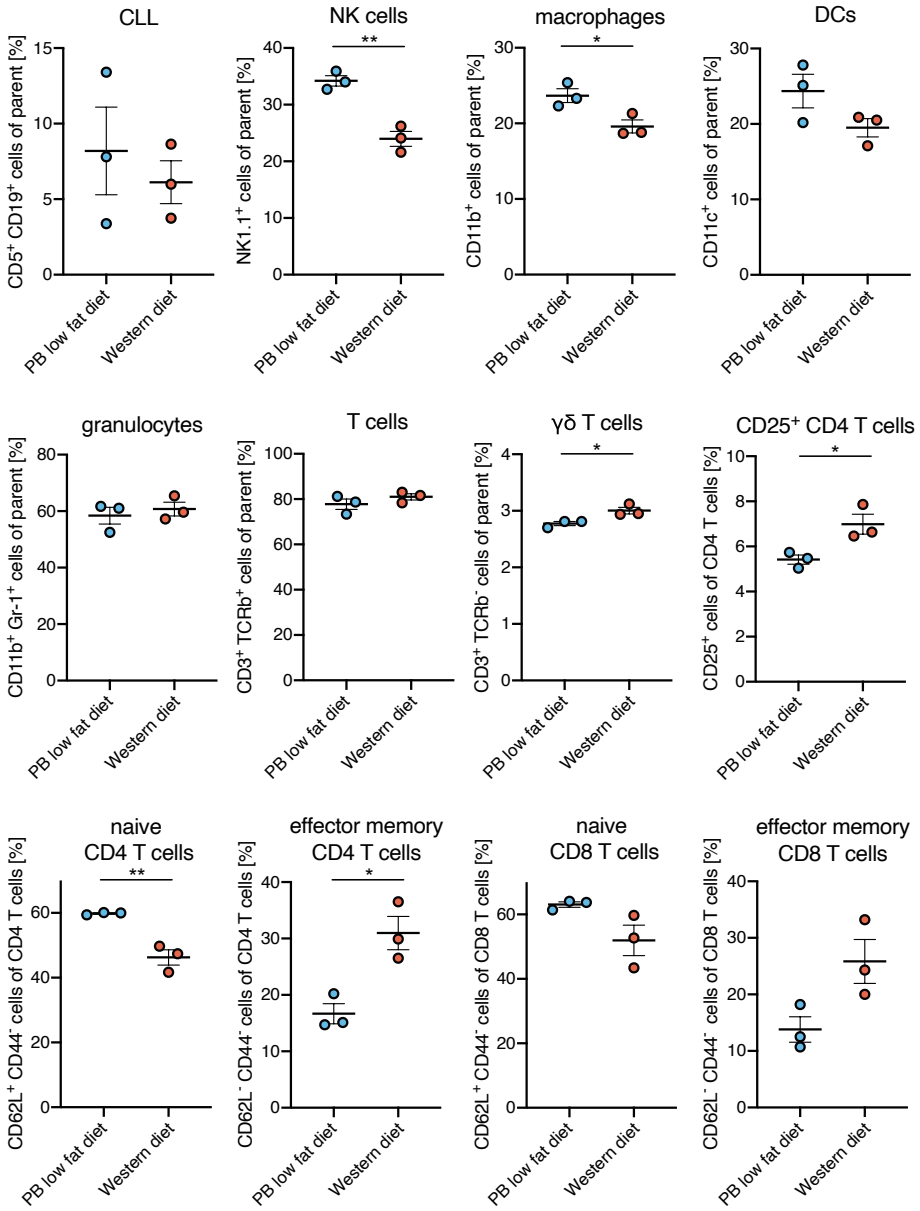

*Figure 18: Manual gating of immune cell populations of whole splenocytes of C57Bl6/J mice (11 weeks on diet, 11 days after CLL transplantation) measured with the CyTOF system Helios using FlowJo software. The gating was performed according to the manufacturer's suggested gating strategy (see Figure 9). For statistical analysis, a two-tailed unpaired Student's t-test was performed. NK cells: **, p=0.0032; macrophages: *, p=0.0311; γδ T cells: *, p=0.0290; CD25⁺ CD4 T cells: *, p= 0.0317; naive CD4 T cells: **, p= 0.0047; effector memory CD4 T cells: *, p=0.0140. Data in graphs without statistical labels were not significant. Data is presented as mean values ± SD.*

We performed an identical analysis of whole splenocytes of mice at the end of a CLL course using CyTOF and the software CYANUS (Suppl. Figure 1+2) and observed no significant difference in any cell population between the different dietary groups. There, the immune cell environment adjusted to the engrafting CLL, and possible effects occurring from dietary differences could not be seen, even though CD19-positive cells were depleted for the CyTOF measurement, indicating that these differences occur early upon engraftment and are less pronounced in late disease stages.

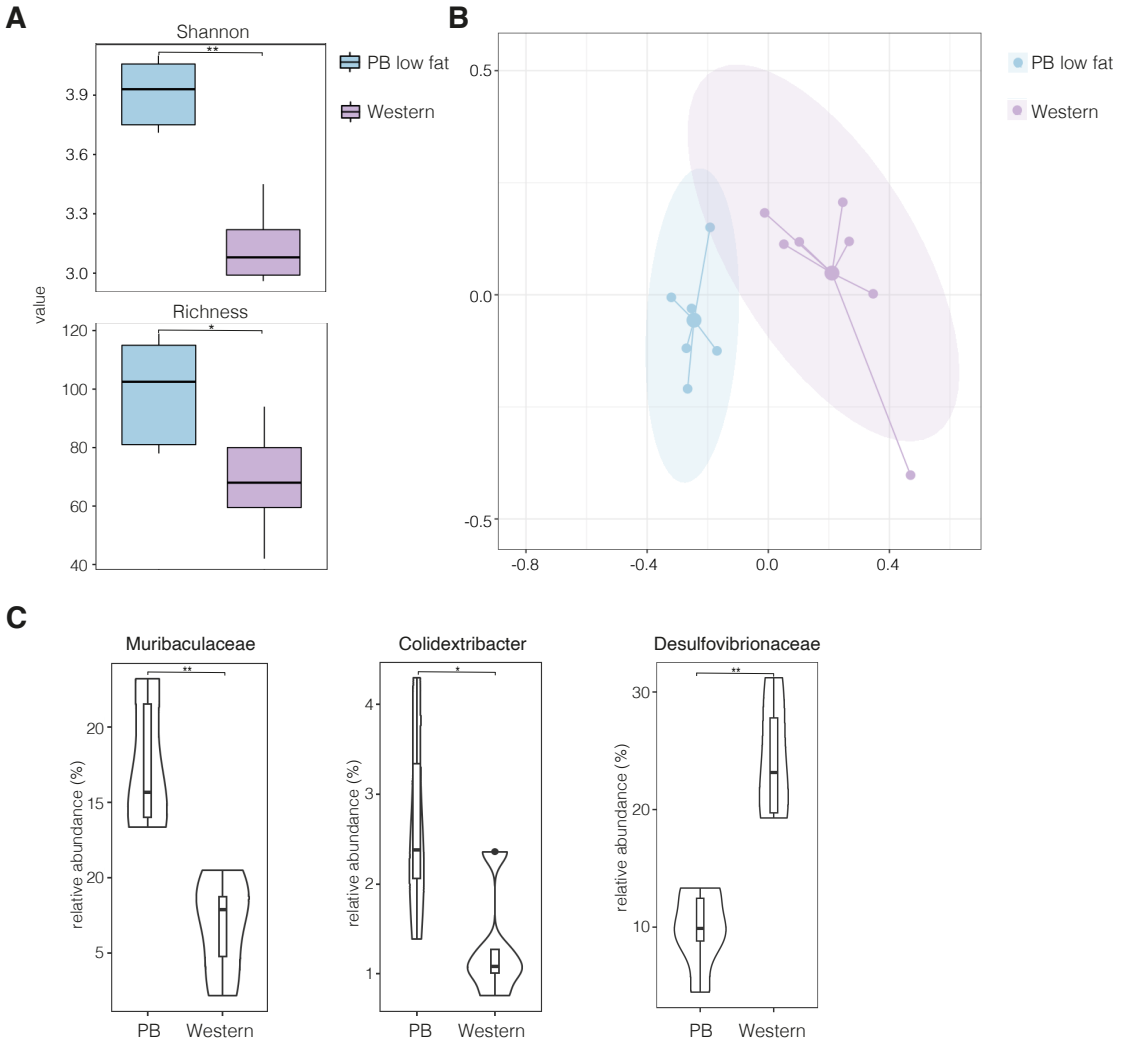

Figure 19: 16S rRNA sequencing analysis of C57Bl6/J mice on different diets – Analysis of 16S rRNA sequencing results from cecal content of CLL-burdened C57Bl6/J mice on Western diet (n=7) or PB low fat diet (n=6). ***A*** *Alpha diversity is depicted by the Shannon index and Richness index. Shannon, **, p=0.0034; Richness, *, p=0.026* ***B*** *Beta diversity depicted by Bray-Curtis Dissimilarity. For statistical analysis, a permutational multivariate analysis of variance (PERMANOVA) was performed. p=0.002.* **C** *Group comparison of taxonomic families. For statistical analysis, a pairwise Wilcoxon Rank Sum test was performed with Western diet n=5 and PB low fat diet n=6. Muribaculaceae: p=0.0043, Colidextribacter: p=0.0303, Desulfovibrionaceae p=0.0043*

Finally, we analyzed cecal content 16s rRNA sequencing data from mice on the Western diet and the PB low fat diet. The analyzed mice were part of the shown survival analysis (Figure 14) and the cecal content was collected after the individual death of each experimental mouse. A Shannon-index and Richness analysis revealed a significant reduction of alpha diversity within mice on the Western diet (Figure 19A). A comparison of the two diet groups' microbiomes revealed a clear distinction between the bacteria compositions. Using the Bray-Curtis dissimilarity, a statistic used to quantify the compositional dissimilarity between two different sites, we were able to determine the significance of this difference (Figure 19B). A deeper taxonomic analysis showed a reduced relative abundance of gut bacteria belonging to the Muribaculaceae and Colidextribacter family in mice on Western diet. On the contrary, the relative abundance of gut microbiota of the Desulfovibrionaceae family was significantly increased in mice on the Western diet (Figure 19C).

In summary, we could show that the consumption of a Western diet in immunocompetent C57Bl6/J mice leads to increased weight gain, increased blood lipids, and a reduced lifespan after CLL disease, while the development of CLL was not affected. In addition, we observed slightly elevated plasma levels of the pro-inflammatory cytokines MCP-1 and IL-1α and altered immune cell populations in the spleen in mice on Western diet. Finally, a 16S rRNA sequencing analysis revealed a significant demarcation between the intestinal flora of both groups with greatly reduced diversity within Western diet samples.

4.1.2. Effects of Western diet and WFPB diet on human blood values *in vivo*

To test, whether we can mimic the effects of the Western diet observed in our preclinical animal model in humans, we performed experiments with voluntary participants. The participants were asked to eat a strict whole food plant-based (WFPB) diet for one week, followed by a Western diet consisting mainly of animal fats and carbohydrates and processed food (Figure 5). Blood was drawn after 7 consecutive days on diet and analyzed regarding blood lipid concentrations.

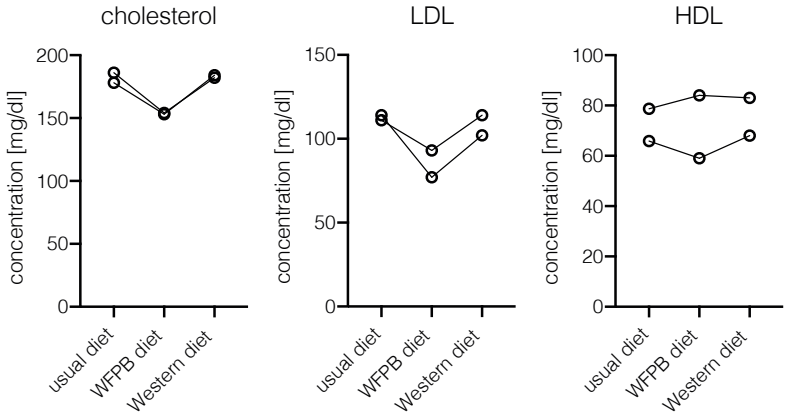

Figure 20: Human blood lipid levels in different diets – Blood lipid levels of two participants seven days on their regular diet, whole food plant-based diet (WFPB), and Western diet.

Two participants were also donating blood before the beginning of the diet periods while eating their usual diet (Figure 20). Compared to their usual diet, cholesterol and LDL decreased strongly after one week on the WFPB diet in the blood of both participants, whereas HDL decreased in the blood of one participant. After the following week on the Western diet, the cholesterol and LDL concentration in the serum increased again clearly. Interestingly, the serum lipid concentration after the Western diet resembles the concentrations of the usual diets of the volunteers. Notably, switching to a WFPB diet decreased serum lipids in humans within a week in both volunteers.

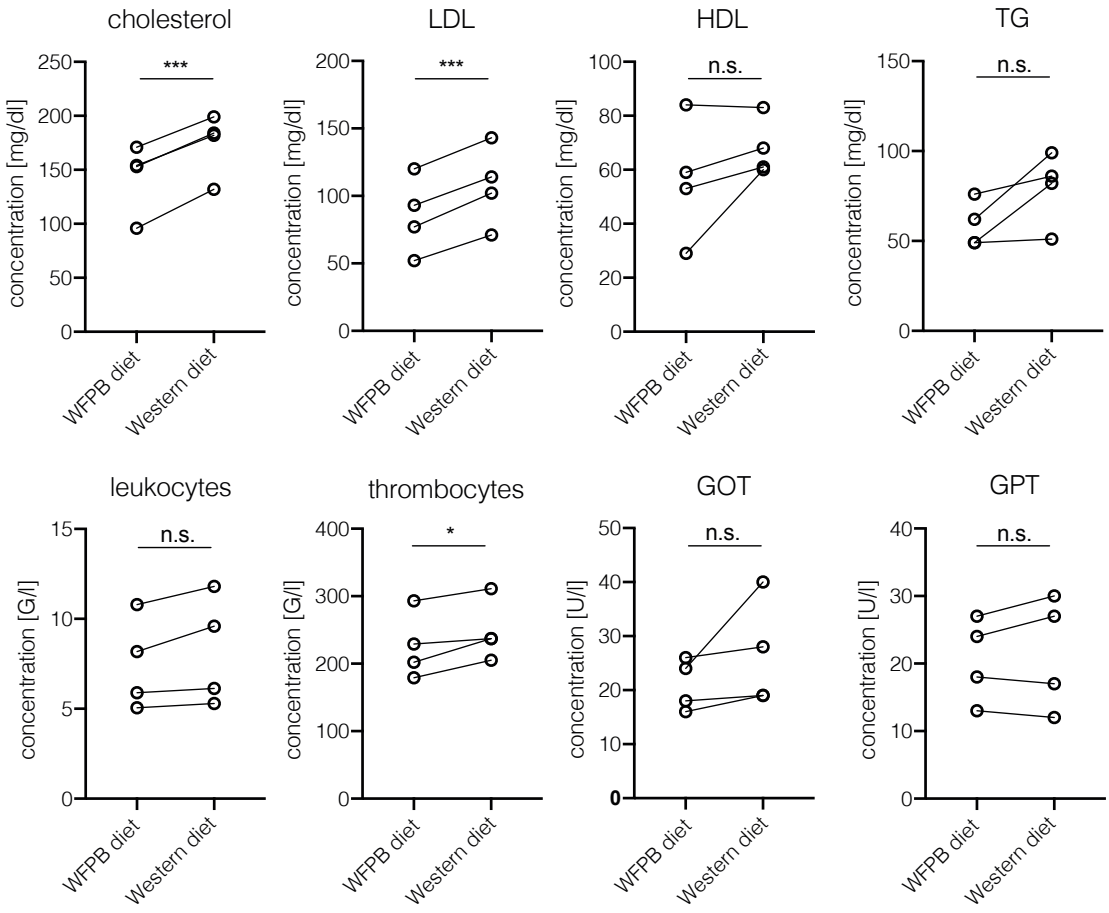

*Figure 21: Blood analysis and small blood count of four participants after seven days on the whole food plant-based diet and Western diet – For statistical analysis, a two-tailed paired Student's t-test was performed. Cholesterol: ***, p=0.0005. LDL: ***, p=0.004. HDL: n.s., p=0.1824. TG: n.s., p=0.0965. Leukocytes: n.s., p=0.0911. Thrombocytes: *, p= 0.0324. GOT: n.s., p=0.2165. GPT: n.s., p=0.4502.*

In total 4 volunteers participated in the diet experiments and donated their blood after a WFPB and Western diet. Their serum lipid concentrations and small blood count are shown in Figure 21. While changes in cholesterol and LDL were significant, the increase of serum HDL was not, presumably due to one out layer. We could also detect an increase in triglycerides, leukocytes, thrombocytes, and glutamic oxaloacetic transaminase (GOT, also known as aspartate aminotransferase (AST)), with only a significant difference in thrombocytes. We could not detect differences in glutamic pyruvic transaminase (GPT, also known as alanine aminotransferase (ALT)) levels between both diets.

4.1.3. Effects of high lipid concentrations on human CLL cells *in vitro*

Not only did we want to analyze the changes of serum lipid concentrations in different diets in humans *in vivo*, but we also used this experiment to collect the human serum with the different lipid concentrations to perform *in vitro* experiments together with primary patient CLL cells and human-derived CLL cell lines.

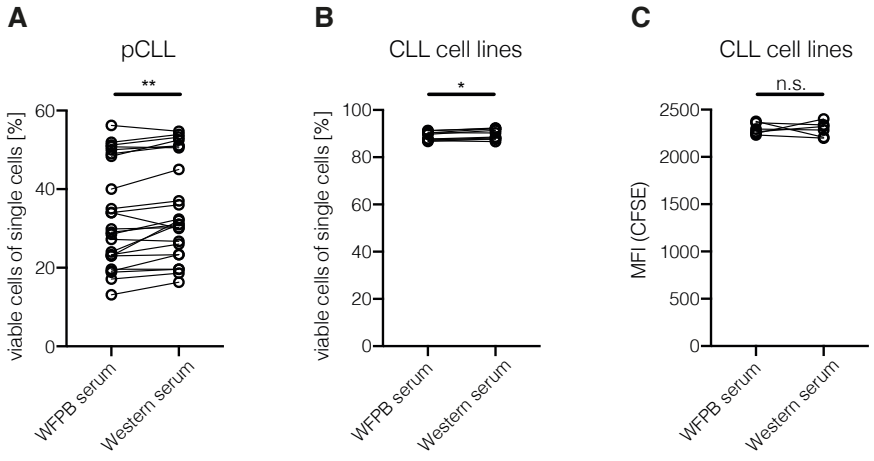

Figure 22: Viability and proliferation of CLL cells incubated with human whole food plant-based diet or Western diet serum – Each patient CLL and cell line, was cultured with paired serum from 3-5 donors and analyzed via flow cytometry regarding viability (A+B) and cell proliferation (C) after 24 h. For statistical analysis, a two-tailed paired Student's t-test was performed. ***A****: **, p=0.0013 (n=6 patients, n=5 plasma donors).* ***B****: *, p=0.0104 (n=2 cell lines, n=5 plasma donors).* ***C****: n.s., p=0.9190 (n=2 cell lines, n=3 plasma donors)*

First, we evaluated the survival of CLL cells in a medium supplemented with 5% WFPB serum compared to Western serum. Therefore, the cells were incubated in their specific medium for 24 hours and analyzed using flow cytometry and DAPI staining to assess cell viability. Although the effects were small, both patient CLL cells and CLL cell lines showed significantly higher viability when incubated in Western diet serum compared to WFPB serum (Figure 22A+B). Additionally, we investigated whether the increased cell viability is due to increased cell proliferation.

When staining CLL cell lines with the proliferation dye CFSE, we could not detect a difference in proliferation after 24 hours between the two groups (Figure 22C). This indicates the elevated cell viability might be due to a reduction in cell death in Western serum rather than increased turnover, which is in line with the result obtained in primary CLL that does not proliferate in standard culture conditions. Together these analyses show that serum obtained from healthy donors after the Western diet increases CLL cell viability *in vitro* as compared to matched serum samples harvested after the WFPB diet.

To gain further insight into potential mechanisms behind the observed increase in viability, we performed *in vitro* experiments using different concentrations of soluble cholesterol in the medium and analyzed signaling processes and metabolic enzymes in CLL cells.

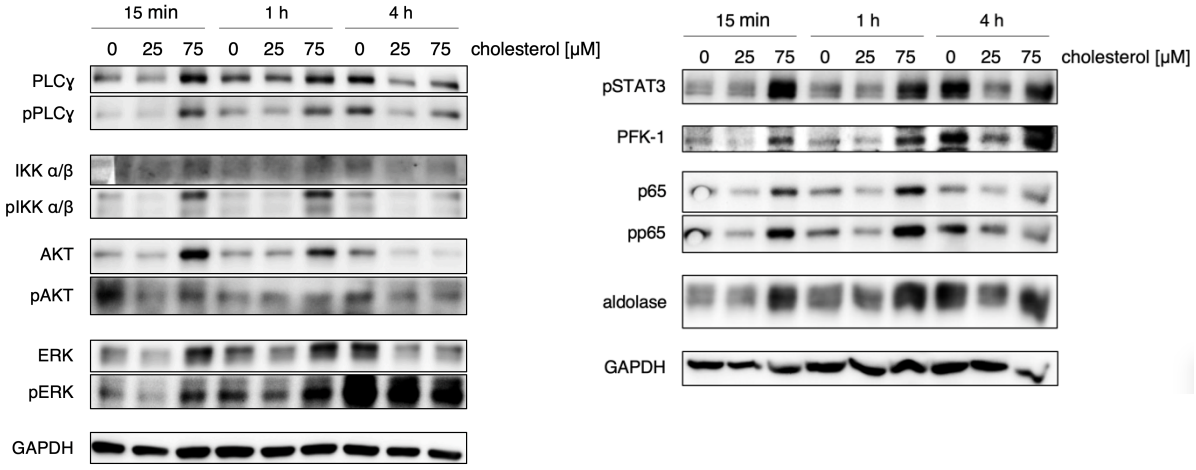

*Figure 23: Intracellular signaling in MEC-1 cells after cholesterol stimulation – Western blot of 5*10⁶ MEC-1 cells seeded out in 2 ml media in 6-well plates. The cells were stimulated with 0, 25, or 75 µM cholesterol for 15 min, 1 hour, and 4 hours.*

With 75 μM but not 25 μM of cholesterol in the medium, we detected an increase in signaling molecules and their phosphorylation already after 15 min of incubation and in expression of the glycolytic enzymes phosphofructokinase-1 (PFK1) and aldolase (Figure 23). That indicates that not only signaling cascades are activated through kinase activity but also upregulation of protein anabolism and cell metabolism takes place. We saw the same effects after a 1 h incubation time but reduced signals after 4 h.

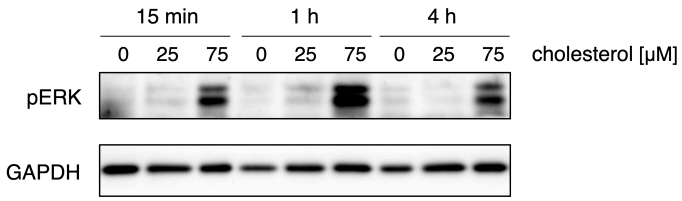

*Figure 24: Intracellular signaling in patient CLL cells after cholesterol stimulation – Western blot of 1*10^7 patient PBMCs seeded out in 2 ml media in 6-well plates. The cells were stimulated with 0, 25, or 75 µM cholesterol for 15 min, 1 hour, and 4 hours. Representative result for 3 independent experiments is shown.*

In human primary CLL cells, we could detect increased phosho-ERK with 75 µM but not 25 µM of cholesterol after already 15 min, but with the highest signal after 1 hour of incubation. Again, the signal decreased after 4 hours of incubation with cholesterol (Figure 24)

In summary, we observed a significant difference in serum LDL and cholesterol levels in participants after one week on the WFPB diet or Western diet. Also, we could detect an increase in thrombocytes on a Western diet, whereas, we did not detect changes in the quantity of the metabolic proteins GOT and GPT. When utilizing said serum *in vitro* experiments, we detected increased cell viability of human primary CLL cells and human CLL cell lines after incubation in Western diet serum. For the analysis of intracellular signaling, when performed *in vitro* experiments with added soluble cholesterol and detected increased phosphorylation events already after 15 min of incubation, which decreased after 4 h, only in high concentrations of cholesterol, which warrants further investigation.

4.2. Negative feedback regulation of MAPK signaling in CLL

In previous studies, we could show that hyperactivating intracellular signaling pathways in CLL is lethal. In particular, we could show that genetic hyperactivation of PI3K/AKT-signaling induces acute cell death in CLL cells.[92] In this project, we focused on negative feedback regulation in CLL cells, especially in the MAPK signaling pathway, with DUSP1 and DUSP6 as critical negative regulators in this pathway. This project was initially conducted by a former PhD student, Veronika Ecker, and continued until accepted for publication by myself.

In collaboration with Junyan Lu,[93] it was discovered that DUSP6 mRNA levels were upregulated in patients with an unmutated IGVH status, which have a more aggressive disease course than patients with mutated IGHV.[94,95] Also, high levels of DUSP6 mRNA were correlated with a decreased overall survival of CLL patients. Taken together, this suggests that the expression of the negative regulator of MAPK signaling DUSP6 is linked to a poor disease prognosis in CLL. Additionally, DUSP6 mRNA levels were increased in patients who carry mutations in BRAF and KRAS genes, which cause enhanced MAPK signaling. Therefore, we hypothesize that the expression levels of DUSP6 are linked to the activation status of the MAPK pathway.

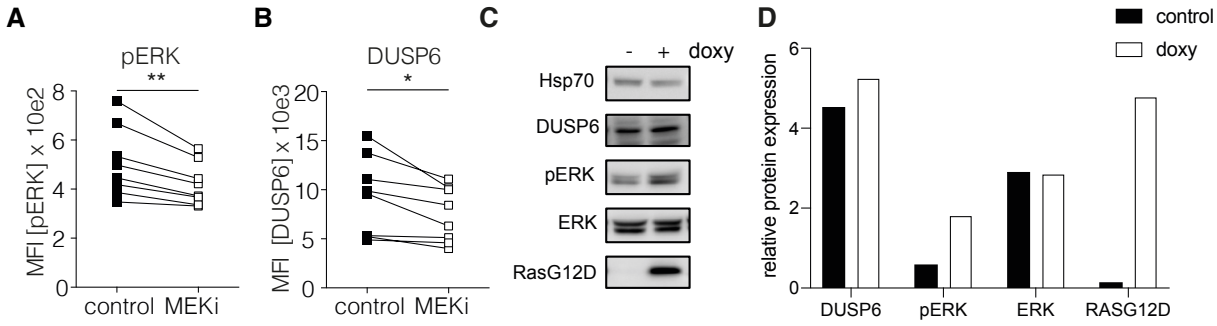

*Figure 25: DUSP6 and pERK levels are tightly linked in CLL – **A** Analysis of the phospho-ERK and **B** associated DUSP6 mean fluorescence intensity (MFI) of CLL-derived cell lines (n=8, pooled data from 2 independent experiments) treated with 5 µM MEK1/2 inhibitor (PD901) for 24 hours. For statistical analysis, a two-tailed paired Student's t-test was performed. **A**: *, p=0.0155; **B**: **, p=0.0033. **C** Western blot and **D** quantification of OSU-CLL RAS^{G12D} cells after doxycycline activation. Cells were treated with 0.1 µg/ml doxycycline for 48 h before lysis with RIPA buffer. Representative result for 2 independent experiments is shown.*

To test this, we analyzed DUSP6 protein levels in conjugation with phosphorylation levels of the downstream MAP kinases ERK1/2. By inhibiting the upstream MAP kinase kinase MEK1/2 for 24 hours with the specific small molecule inhibitor PD0325901 (PD901), we decrease phospho-ERK and DUSP6 levels simultaneously in CLL cell lines, confirming our hypothesis of coregulation (Figure 25A+B).

Inversely, when activating MAPK signaling in CLL cell lines transduced with a doxycycline-inducible constitutively active RAS^{G12D} mutant, we saw an increase in ERK phosphorylation that went in hand with an increase in DUSP6 protein levels (Figure 25C+D).

Previous work in the lab could show that the inhibition of the negative MAPK regulators DUSP1 and DUSP6 results in cell death especially in CLL cells. When incubating healthy donor B cells and patient CLL cells with the DUSP1/6 inhibitor BCI, a strong induction of specific cell death was detected in the patient CLL samples, whereas healthy donor B cells remained mainly unaffected.

Next, we wanted to prove that the induced cell death in CLL cells is directly linked to unrestricted MAPK signaling due to the inhibition of the negative regulators DUSP1/6. Therefore, we inhibited MAPK pathway activation upstream of DUSP1/6 using MEK1/2 inhibitors. We saw decreased drug-specific cell death in human primary CLL cells (Figure 26A), as well as in human CLL cell lines (Figure 26B), after a co-treatment with the MEK1/2 inhibitor PD901. To rule out that this impact is caused due to off-target effects, we also tested additional MEK1/2 inhibitors PD98059 (PD059) (Figure 26C) and Trametinib (Tram) (Figure 26D) and detected a similar reduction in drug-specific cell death. This data supports the hypothesis that excessive MAPK signaling drives CLL cells towards cell death.

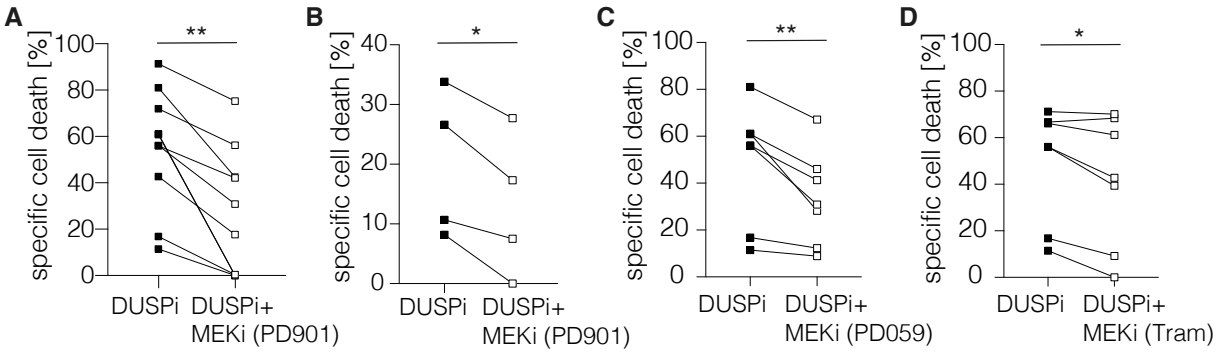

*Figure 26: MEK1/2 inhibition can prevent DUSP1/6 inhibition-induced cell death – **A**-**D** Specific cell death was calculated after flow cytometric viability analysis by DAPI staining. **A** Patient CLL cells (n=6, pooled data from 2 independent experiments; **, p=0.0010) and **B** CLL-derived cell lines (n=4, pooled data from 2 independent experiments; *, p=0.0159) were pre-treated for 1 hour with 5 µM of the MEK1/2 inhibitor (PD901) followed by DUSP1/6 inhibitor treatment (BCI; 1.25 µM) or control treatment for 48 hours. **C**+**D** Patient CLL cells were pre-treated for 1 hour with 5 µM MEK1/2 inhibitor PD059 (**C**: **, p=0.0085) or 1 µM MEK1/2 inhibitor Trametinib (**D**: *, p=0.0232) followed by DUSP1/6 inhibitor treatment (BCI; 1.25 µM) or control treatment for 48 hours (n=7, pooled data from 2 independent experiments).*

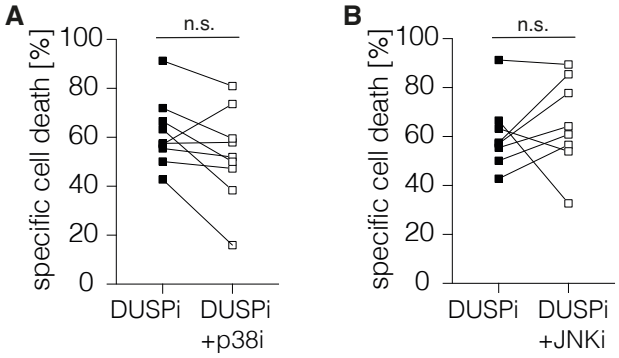

*Figure 27: p38 inhibition and JNK inhibition contribute to DUSP1/6 inhibition-induced cell death – **A** Patient CLL cells (n=9, pooled data from 3 independent experiments; n.s., p=0.0813) were pre-treated for 1 hour with 10 µM of the p38 inhibitor (SB 202190) followed by DUSP1/6 inhibitor treatment (BCI; 1.25 µM) or control treatment for 48 hours. **B** Patient CLL cells (n=8, pooled data from 3 independent experiments; n.s, p=0.5247) were pre-treated for 1 hour with 5 µM of the JNK inhibitor (SP600125) followed by DUSP1/6 inhibitor treatment (BCI; 1.25 µM) or control treatment for 48 hours. For statistical analysis, a two-tailed paired Student's t-test was performed*

As described previously, p38 and JNK are MAP kinases besides ERK1/2 and are negatively regulated by DUSP1 (Figure 1).[13] We were interested in the effects of DUSP inhibitions together with the inhibition of p38 and JNK on CLL cells. We could not detect a significant amplification, nor a reduction in cell death (Figure 27A+B), which implies additional MAPK inhibition does not contribute to DUSP1/6 inhibitor-mediated cell death.

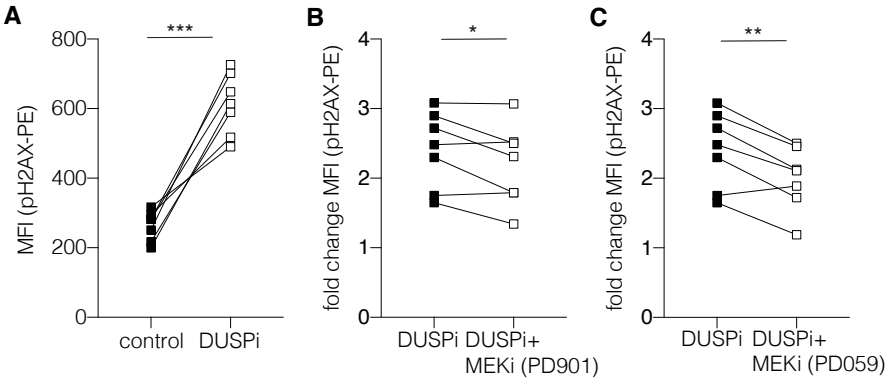

*Figure 28: MEK1/2 inhibition rescues DUSP1/6 inhibition-induced DNA damage partially in patient CLL cells. **A** Phospho-H2AX mean fluorescence intensity (MFI) of primary human CLL cells after incubation with DUSP1/6 inhibitor BCI (2.5 µM) for 24 h. **B+C** Fold change of phospho-H2AX MFI of primary human CLL cells after pre-treatment for 1 hour with 5 µM of MEK1/2 inhibitor (PD901) or 10 µM of MEK1/2 inhibitor (PD059) followed by DUSP1/6 inhibition for 24 h (BCI; 2.5 µM). n=7, pooled data from 2 independent experiments. For statistical analysis, a two-tailed paired Student's t-test was performed. **A:** ***, p=0.0002; **B:** *, p=0.0480; **C**: **, p=0.005*

Subsequently, we discovered that increased MAPK signaling due to DUSP1/6 inhibition induces DNA damage in primary CLL cells. The phosphorylation of the histone γH2AX is a marker for DNA damage after DNA double-strand breaks.[96] We detected a significant increase in γH2AX phosphorylation after 24 hours of treatment with the DUSP1/6 inhibitor BCI (Figure 28A). MEK1/2 inhibition alone also resulted in DNA damage traceable with the phospho-γH2AX staining. Therefore, we further analyzed the fold change in γH2AX phosphorylation and showed that a co-treatment of MEK1/2 and DUSP1/6 inhibitor reduces DNA double-strand breakage in patient CLL cells (Figure 28C+D).

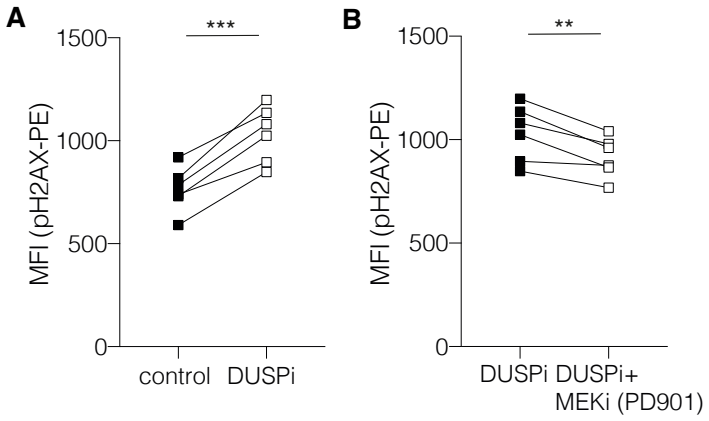

*Figure 29: MEK1/2 inhibition rescues DUSP1/6 inhibition-induced DNA damage partially in CLL cell lines – **A+B** Phospho-γH2AX mean fluorescence intensity (MFI) of CLL cell lines (MEC-1, OSU-CLL, and EHEB) (n=6, pooled data from 2 independent experiments) were pre-treated for 1 hour with 5 µM of MEK inhibitor (PD901) or control followed by DUSP1/6 inhibition (BCI; 5 µM). For statistical analysis, a two-tailed paired Student's t-test was performed. **A:** ***, p=0.0004 **B:** **, p=0.0051*

We were also able to show that MEK1/2 inhibition caused a reduction of DUSP1/6 inhibition-induced DNA damage in human CLL cell lines, already after 4 hours of inhibitor treatment (Figure 29A+B). This data suggests that hyperactivation of MAPK signaling due to the inhibition of the main negative regulators DUSP1/6 leads to severe DNA double-strand breaks, which contribute to the induction of cell death in CLL cells.

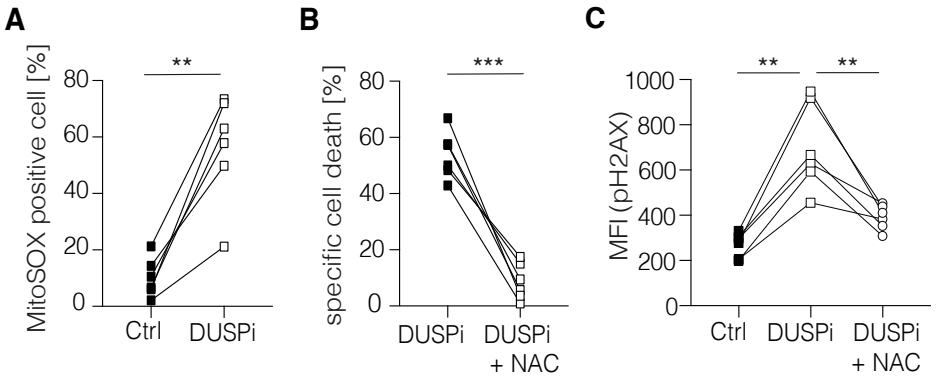

Figure 30: DUSP1/6 inhibition induces mitochondrial ROS production – The antioxidant NAC prevents ROS-induced cell death and DNA damage. ***A*** *Flow cytometry analysis of MitoSOX™-positive primary CLL cells treated with BCI (1.25 µM) or control treatment for 24 hours.* ***B*** *Specific cell death was calculated after flow cytometric viability analysis by DAPI staining. Primary CLL cells were pre-treated for 1 hour with 50 µM N–acetylcysteine (NAC) followed by DUSP1/6 inhibitor treatment (BCI; 1.25 µM) or control treatment for 24 hours.* ***C*** *Analysis of the phosphorylation of γH2AX MFI of primary CLL cells pre-treated for 1 hour with 50 µM NAC followed by DUSP1/6 inhibitor treatment (BCI; 2.5 µM) or control treatment for 24 hours. For statistical analysis, a two-tailed paired Student's t-test was performed. (n=6, pooled data from 2 independent experiments)* ***A:*** ***, p=0.0011* ***B:*** ****, p=0.0002* ***C****: **, p=0.0012, **, p=0.007.*

To assess potential causes for the observed cell death and DNA damage, we further considered mitochondrial respiration and collateral production of mitochondrial reactive oxygen species (ROS). The MAPK/ERK signaling pathway is known to alter mitochondrial functions and activities,[97,98] influencing mitochondrial ROS levels. ROS oxidize the elements of DNA, nitrogenous bases, and deoxyribose, causing strand damage and excisions.[99] Upon DUSP1/6 inhibition, we could detect a strong upregulation of mitochondrial ROS levels in primary CLL cells (Figure 30A). Notably, N-acetylcysteine (NAC) treatment rescues CLL cells from DUSP inhibition-induced cell death due to its antioxidant properties, confirming the correlation between ROS and DUSP inhibitor-mediated cell death (Figure 30B). Additionally, NAC partially reduced DUSP inhibitor-induced DNA damage measured via phosphorylation of γH2AX (Figure 30C).

Taken together, we show that targeting the negative regulators of the MAPK pathway DUSP1/6 induces excessive intracellular signaling, causing harmful mitochondrial ROS accumulation in CLL cells. This leads to DNA damage and CLL cell death, proposing DUSP1/6 inhibition as a potential treatment strategy for CLL including cases with drug resistance. This collaborative work has now been published in Cell Report.

4.3. Mutations and their potential to drive lymphoma towards Richter transformation

In addition to drug resistance, Richter's transformation remains a significant clinical challenge. To gain insight into the transformation process, we used different mouse models and cell line-based approaches to study the effect of potentially activated pathways in RT. To analyze the effects on human CLL cells *in vitro*, we performed experiments with the human CLL cell lines MEC-1 and OSU-CLL after retroviral induction of the respective mutations. For more physiologically accurate studies of the development of RT *in vivo* and *in vitro*, we utilized the Eμ-*TCL1* transgene mouse model, in which mice develop CLL after 12 - 16 months of age.[71] These mice were crossed with the tamoxifen-inducible Cre recombinase-mediated expression of selected mutations (described below) in combination with the endogenous promoter/enhancer elements of the Cd79a locus (Mb1). Therefore, Cre activity is only observed in the B-cell lineage after induction. With this genetic mouse model, it is possible to induce specific transgenes/mutations in mature primary CLL cells at a selected point in time.

4.3.1. Constitutively active CARD11 expression in murine and human CLL *in vitro*

First, we utilized the human CLL cell lines MEC-1 and OSU-CLL as a model system for human CLL and retrovirally transduced the cells with a vector encoding the constitutive active CARD11 mutation CARD11^{L225LI}. Enhanced expression of CARD11 in transduced cell lines was validated via immunoblotting and related quantification (Figure 31A+B).

It is described that CLL cells have immunosuppressive characteristics, which favors CLL development and evasion of immune responses. Major alterations are found in T-cell populations, with inhibition of CD8 and CD4 T cells.[100] Therefore, we established a T-cell activation assay with the T-cell line A5, a T-cell hybridoma cell line that contains an NFAT-GFP expression cassette.[101,102] We confirmed the effectiveness of our coculture model by testing the T-cell activation after coculture with B cells of healthy donors compared to human primary CLL cells. There, we detected a significant reduction in the activation of A5 when cocultured with CLL cells (Figure 31C). Vice versa, we saw an enhanced T-cell activation on coculture experiments with the CLL cell lines transduced with CARD11^{L225LI}, compared to the cells carrying the empty vector (Figure 31D).

Further, we performed coculture experiments with human pan T cells, representing all human T-cell subsets extracted from the PB. With a ratio of 1:1 at the beginning of the experiments, MEC-1 cells with and without CARD11^{L225LI} expression represented less than 10% after 48 h (Figure 31E), indicating a strong activation and expansion of T cells. The viability of MEC-1 cells is equal in both conditions (about 80%) at this time point (Figure 31F).

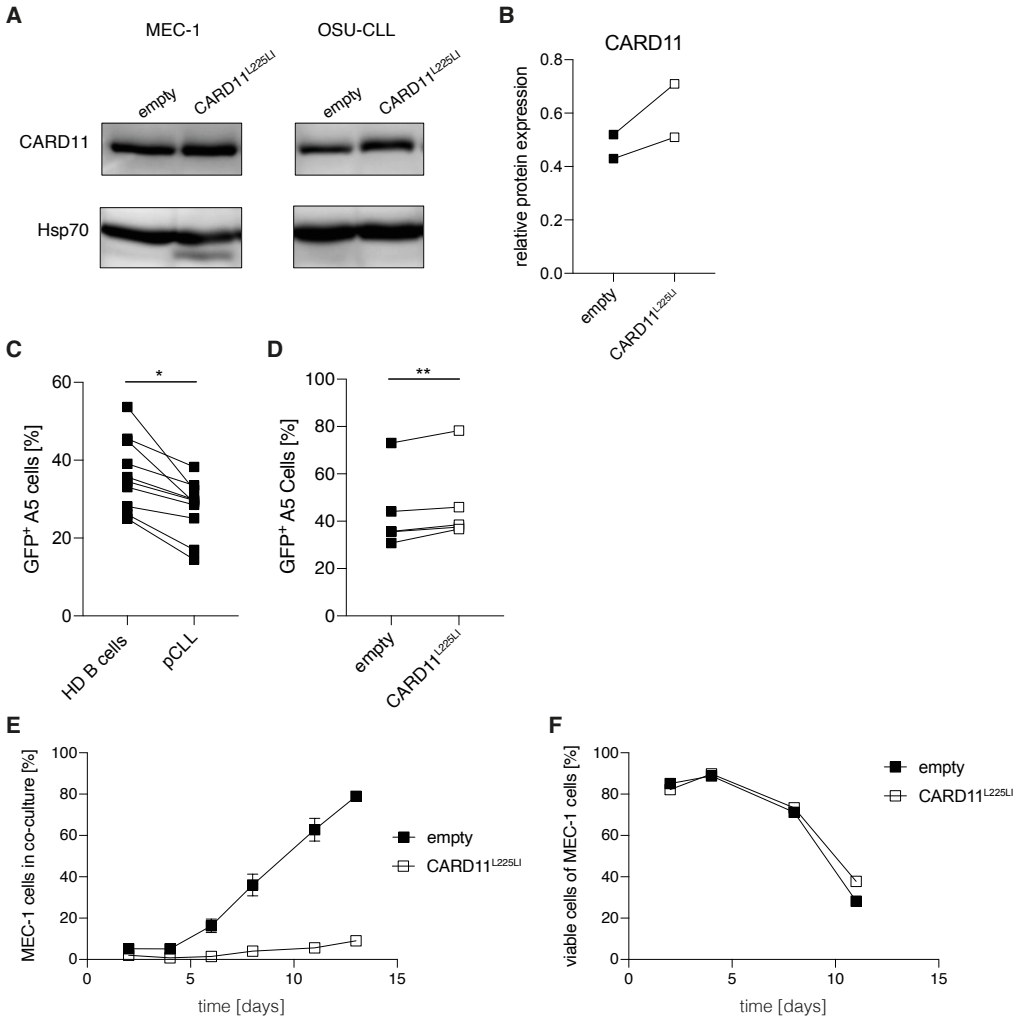

*Figure 31: Human CLL cell lines MEC-1 and OSU-CLL transduced with the pMIG empty and pMIG Card11^{L225LI} plasmid – **A+B** Western blot with associated quantification of CARD11 protein expression. **C+D** T-cell activation assay with the T-cell hybridoma cell line A5. **C** Immunosuppressive potential of healthy donor (HD) B cells compared to human CLL cells. For statistical analysis, a two-tailed paired Student's t-test was performed. *, p=0.0306 (n=10, pooled data from 2 independent experiments). **D** Immunosuppressive potential of control CLL cell lines compared to cell lines expressing CARD11^{L225LI}. For statistical analysis, a two-tailed paired Student's t-test was performed. **, p=0.0142 (n=5, pooled data from 4 independent experiments). **E** Killing assay with human pan T cells in a ratio of 1:1 with control CLL cell lines compared to cell lines expressing CARD11^{L225LI}. Data from 1 experiment with three technical replicates is shown **F** Associated viability of used cell lines in a control setting without T cells.*

Over the time course of the experiment, MEC-1 control cells proliferate in culture and represent about 80% of all cells in culture after 13 days. In parallel, MEC-1 CARD11^{L225LI} expansion in coculture with pan T cells is suppressed with a maximum of about 10% representation. The amount of viable MEC-1 cells remained mostly identical. This suggests that MEC-1 empty control cells suppress T-cell function, prohibiting further T-cell expansion, while multiplying themselves. However, MEC-1 CARD11^{L225LI} cells appear to lose the CLL's immunosuppressive capacities. We would like to stress that for a reliable statement, this experiment needs to be repeated with a starting ratio of 1:1. A parallel experimental approach with a starting ratio of 1:10 supports the seen results.

Additionally, we performed *in vitro* experiments with murine CARD11^{L225LI}xTCL1xMb1CreERT2 splenocytes after the development of a CLL phenotype in the donor mice. CARD11^{L225LI} expression is induced after the application of the tamoxifen *in vitro* analog 4-hydroxytamoxifen (4OHT).

As the CARD11^{L225LI} expression is genetically linked to the expression of GFP, we could detect an increasing GFP signal over time (Figure 32A). In parallel, we saw decreasing cell viability, which is commonly seen in cultured primary CLL splenocytes. But when comparing the 4OHT-treated cells to control cells treated with DMSO, we detected even stronger decreased viability in CARD11^{L225LI} expressing CLL cells after 48 h, suggesting toxicity of either CARD11 activation or 4OHT itself (Figure 32B).

To further characterize the CARD11^{L225LI} expressing CLL cells, we performed flow cytometry-based analyses and detected increased cell size, proliferation, expression of the surface markers CXCR4 and CXCR5, expression of the metabolic proteins glucose transporter 1 (GLUT1) and hexokinase 1 (HK1), and expression of the signaling molecule MYC (Figure 32C-I). Additionally, we analyzed metabolic characteristics of CARD11^{L225LI} expressing CLL cells with the Seahorse glycolysis stress test from Agilent. There, we measured increased ECAR values in CARD11^{L225LI} expressing CLL cells, suggesting elevated glycolytic processes (Figure 32J).

In summary, we could show that *in vitro* overexpression of CARD11^{L225LI} in CLL cells leads to a reduction in CLL's immunosuppressive capacities, while they increase in size, upregulate glycolysis, and show enhanced signs of MYC signaling.

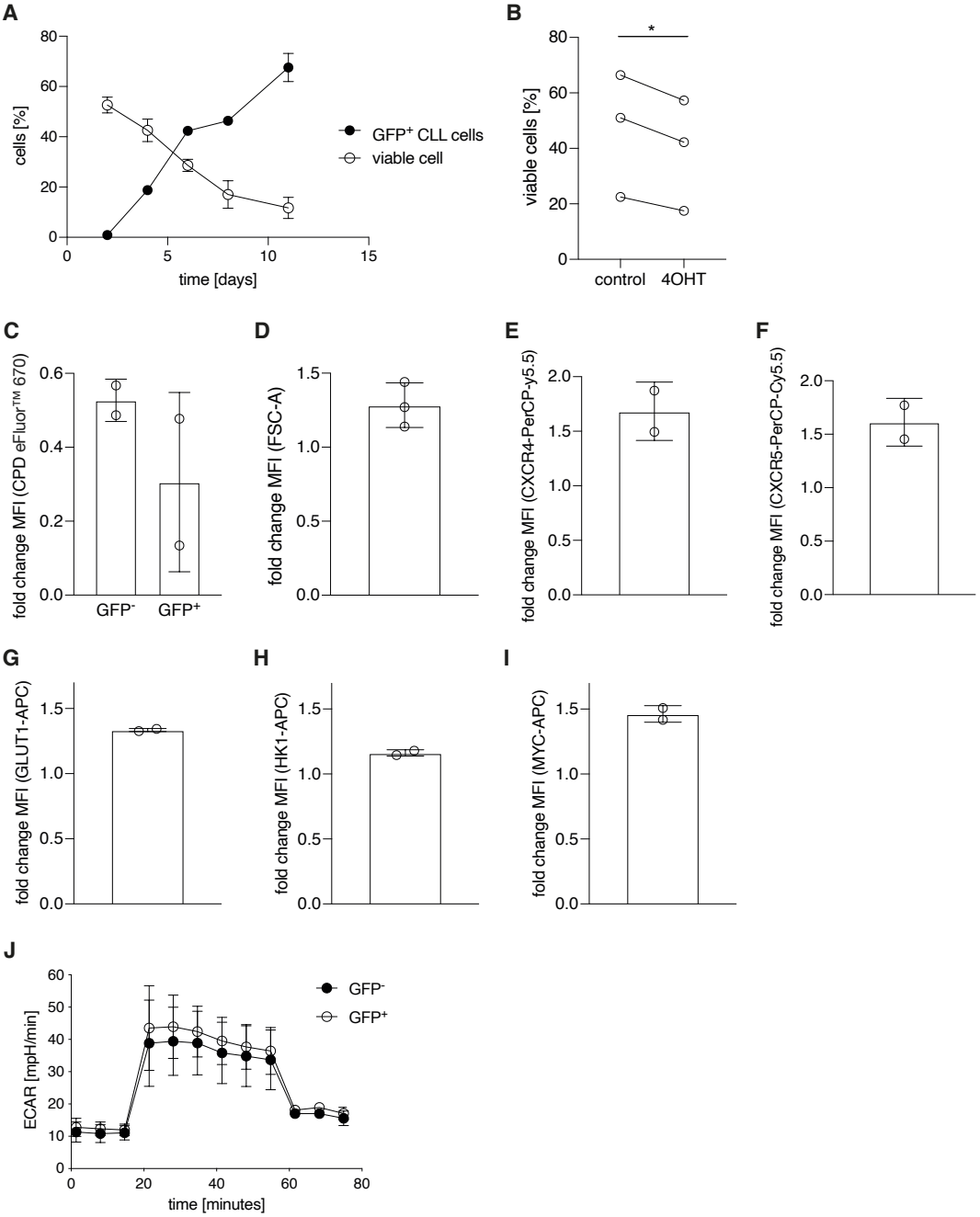

Figure 32: Flow cytometry analysis and Seahorse metabolism analysis of CARD11^{L225LI}xTCL1xMb1CreERT2 splenocytes – Expression of constitutively active CARD11 following 0.5 µg/ml 4OHT or DMSO ethanol (control) treatment for 48 h. ***A*** *Time course of reporter GFP expression and cell viability after 4OHT treatment. Representative result for 3 independent experiments is shown* ***B*** *Comparison of cell viability after 4OHT or DMSO treatment on day 4. For statistical analysis, a two-tailed paired Student's t-test was performed. *, p=0.0286 (pooled data from 3 independent experiments).* ***C*** *Fold change in cell size of GFP-positive cells after 4OHT treatment on day 4 (pooled data from 2 independent experiments).* ***D*** *Fold change in proliferation after 4OHT treatment measured via the MFI of cell proliferation dye eFlour™ 670 after 48 h (pooled data from 2 independent experiments).* ***E-I*** *Fold change in the expression of extracellular and intracellular proteins after 4OHT treatment on day 6 (pooled data from 2 independent experiments). The ratio of the measurements (GFP$^+$/GFP$^-$) is depicted as fold change* ***J*** *Glycolysis stress test of FACS-sorted CARD11^{L225LI}xTCL1xMb1CreERT2 splenocytes after 4OHT treatment on day 5 (pooled data from 2 independent experiments).*

4.3.2. Constitutively active CARD11 expression in murine CLL *in vivo*

Additionally, we performed *in vivo* experiments with murine CARD11^{L225LI}xTCL1xMb1CreERT2 splenocytes. After CLL development in donor mice, splenocytes were harvested and transplanted into several immunocompetent C57Bl6/J wt mice. The engraftment of CLL was monitored via regular blood drawings followed by flow cytometry-based analysis of CD5 CD19 double-positive lymphocytes. After CLL engraftment in the experimental mice, CARD11^{L225LI} expression was induced with daily applications of tamoxifen (TAM) for 4 consecutive days (marked with black arrows). The control group was treated similarly with ethanol (Figure 33A). After the first application cycle, we detected a drop in CLL amount in the PB of TAM-treated mice, whereas no reduction of CLL cells was seen in the control group. In parallel, we could not detect the CARD11^{L225LI} reporter GFP in TAM-treated mice, suggesting that the CARD11-expressing cells have either died or were depleted by T-cell responses. After a recovery of CLL cells in the blood of the TAM group after 25 days, a second cycle of TAM/ethanol was applied. This led to another minor reduction of CLL content in the PB of TAM-treated mice. Again, no GFP signal could be detected in CLL cells. A Kaplan-Meier survival analysis shows that mice on tamoxifen treatment showed a prolonged survival, compared to the control group (Figure 33B)

To find a possible explanation for why the CLL cells were depleted from the PB, we analyzed T-cell populations at day 38 after CLL transplantation (Figure 33C+D). We found that the group of TAM-treated mice could be split into two groups. Group “TAM CLL high” received two tamoxifen cycles and showed at least 50% in the PB at day 38, whereas group “TAM CLL low” showed less than 25% of CLL cells in the PB. Due to high or low CLL percentages in the PB, T-cell ratios were represented oppositely. Interestingly, the CD4/CD8 ratio is not influenced by the complete percentage of CLL in the PB, as TAM-treated mice with high levels of CLL showed the lowest CD4/CD8 ratio. This means this group showed low numbers of CD4 helper T cells compared to CD8 cytotoxic T cells (Figure 33C). Further analysis of the surface markers CD44 and CD62L provided information about the activation stages of studied T cells. Especially in the CD8 T-cell subset, it became clear that “TAM CLL high” mice had the lowest percentage of naive (CD62L^{+} CD44^{-}) and the highest percentage of effector memory (CD62L^{-} CD44^{-}) T cells (Figure 33D). The group of “TAM CLL low” mice shows the lowest amount of CLL cells in the PB, but the highest percentage of CD8 effector T cells.

After the individual death of the mice, CLL contents in the spleen and inguinal lymph nodes (iLN) were analyzed (Figure 33E). We saw no significant difference in the CLL amount in the spleen between both groups and a trend towards reduced CLL cells in the LNs of TAM-treated mice. Notable, we could not detect GFP reporter-positive CLL cells in any of the organs.

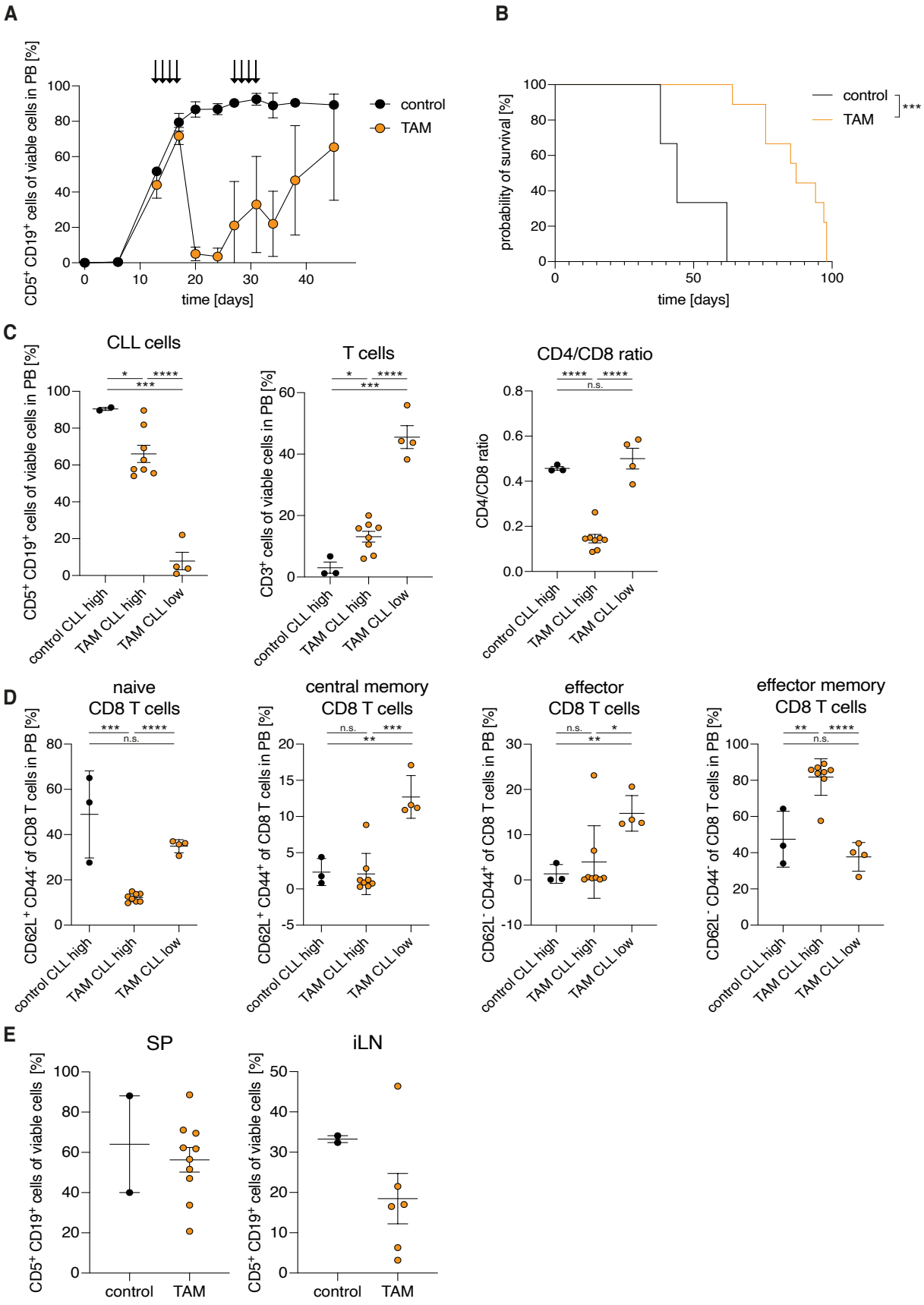
A
CD5+ CD19+ cells of viable cells in PB [%]
time [days]
control
TAM
B
probability of survival [%]
time [days]
control
TAM
***
C
CLL cells
T cells
CD4/CD8 ratio
CD5+ CD19+ cells of viable cells in PB [%]
CD3+ cells of viable cells in PB [%]
CD4/CD8 ratio
control CLL high
TAM CLL high
TAM CLL low
D
naive CD8 T cells
central memory CD8 T cells
effector CD8 T cells
effector memory CD8 T cells
CD62L+ CD44- of CD8 T cells in PB [%]
CD62L+ CD44+ of CD8 T cells in PB [%]
CD62L- CD44+ of CD8 T cells in PB [%]
CD62L- CD44- of CD8 T cells in PB [%]
n.s.
E
SP
iLN
CD5+ CD19+ cells of viable cells [%]
control
TAM

*Figure 33: In vivo experiments with CLL cells expressing constitutively active CARD11 in C57Bl6/J mice – **A** Tracking of CD5+ CD19+ CLL cells in PB after i.v. transplantation of 2*10^7 murine CARD11^{L225LI}xTCL1xMb1CreERT2 CLL cells per mouse with following induction of CARD11 ^{L225LI} expression through tamoxifen (n=3) or ethanol (control) (n=12) application. Application dates are marked with black arrows. **B** Corresponding Kaplan-Meier survival analysis. p=0.0002 **C+D** Analysis of immune cell populations in the PB of the experimental mice on day 38 after transplantation (seven days after TAM application). For statistical analysis, a two-tailed paired Student's t-test was performed. **C** CLL: p=0.0373, p<0.0001, p=0.0003; T cells: p=0.0107, p<0.0001, p=0.0003; CD4/CD8: p<0.0001, p<0.0001, p=0.4673 **D** naive: p=0.0002, p<0.0001, p=0.1972; cen. memory: p=0.8868, p=0.0001, p=0.0032; effector: p=0.5996, p=0.0319, p=0.0033; eff. memory: p=0.0017, p<0.0001, p=0.3184 **E** Pooled analysis of CLL cell populations in SP and iLN on the day of death of each animal. Data is presented as mean values ± SD.*

As we could not detect any GFP reporter signal for the expression of CARD11^{L225LI} in vivo, we repeated the transplantation of CARD11^{L225LI}xTCL1xMb1CreERT2 splenocytes, but induced CARD11^{L225LI} expression beforehand *in vitro*. Figure 34A shows flow cytometry data of the splenocytes after 4OHT-mediated induction of the CARD11^{L225LI} reporter GFP expression in approximately 15% of all CLL cells. After three days, the mice and their spleens (SP), inguinal lymph nodes (iLN), and peritoneal cavities (PC) were analyzed (Figure 34B). We could barely detect any CLL cells in these organs, and again could not detect GFP-positive CLL cells. Analyses of T cells showed increased effector CD4 and CD8 T-cell populations (CD62L$^-$ CD44$^+$) in the spleen and peripheral blood (Figure 34C+D)

As we discovered that the T-cell response might affect the outgrowth of CARD11^{L225LI} in immunocompetent wildtype C57Bl6/J mice, we performed transplantation experiments in R2b. This immunodeficient mouse line carries a knockout in the *RAG2* gene on a C57BL/6 genetic background. RAG2 is critical for (V(D)J) recombination in the process of B- and T-cell maturation, therefore this lack interferes with the development of T and B cells and leads to the complete absence of peripheral T and B cells. In contrast to the immunocompetent NSG mice, R2b mice possess NK cells.

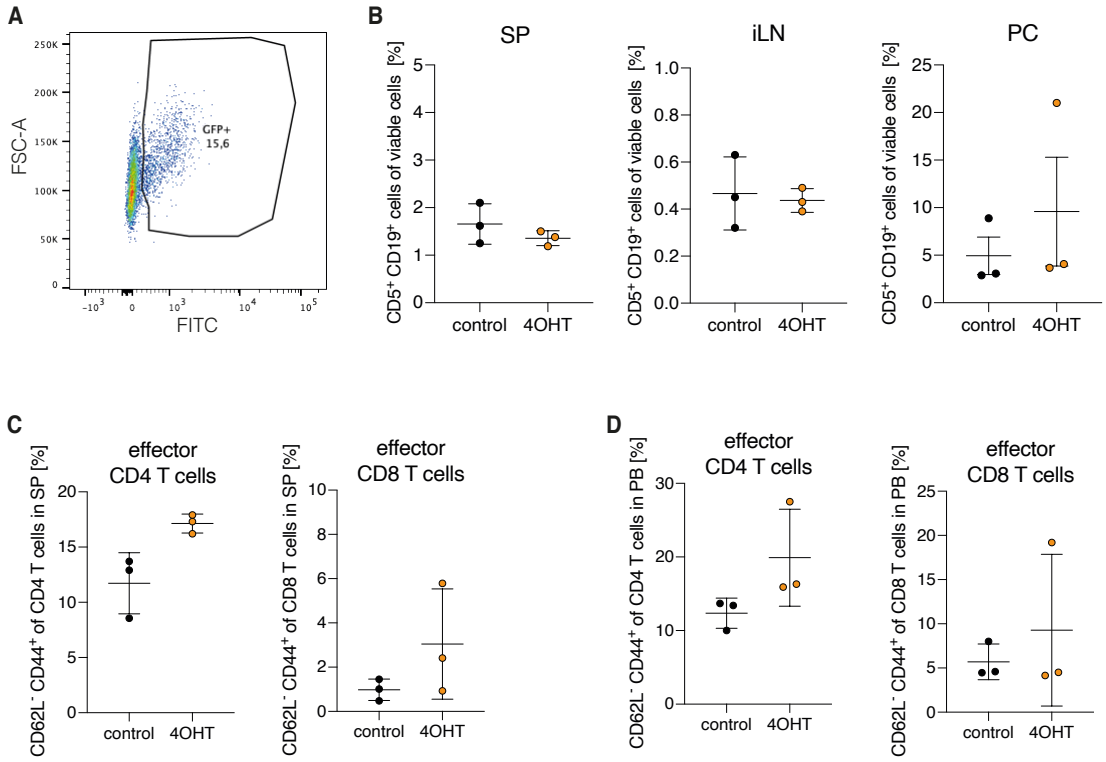

*Figure 34: In vivo experiments with CLL cells expressing constitutively active CARD11 in C57Bl6/J mice after gene expression in vitro – **A** Flow cytometry plot depicting CARD11^{L225LI} -GFP expressing CD5^{+} CD19^{+} CARD11^{L225LI}xTCL1xMb1CreERT2 cells after treatment with 1µg/ml 4OHT for 72 h in vitro. Corresponding control cells were treated equally with DMSO. **B-D** 5*10^{6} of 4OHT (n=3) or DMSO (n=3) treated cells were i.v. transplanted in C57Bl6/J mice. After three days immune cell populations in different organs were analyzed. **B** Analysis of CD5^{+} CD19^{+} CLL populations in SP, iLN, and PC. **C+D** Analysis of T-cell populations in SP and PB. Data is presented as mean values ± SD.*

As previously described, donor CARD11^{L225LI}xTCL1xMb1CreERT2 splenocytes were transplanted into experimental mice, and after the detected engraftment of CLL cells, tamoxifen, or ethanol as control, were applied (marked by black arrows) (Figure 35A). Again, we could detect a decrease of CLL cells in the PB of TAM-treated mice after the first treatment cycle. Nevertheless, at day 45 after CLL transplantation, there was no difference in CLL amounts between both groups.

During the time course of the experiment, again, we could not detect GFP-positive CLL cells in the PB. We performed an end analysis of the mice on day 51 after transplantation and could not find any GFP-positive cells in SP, PB, PC, BM, or iLN, either. We detected by trend reduced amounts of CD5^{+} CD19^{+} CLL cells in all analyzed organs without reaching statistical significance. Results for SP and iLN are shown in Figure 35B. The mixed splenocytes transplanted into the R2b mice consisted of approx. 60% CLL cells and 23% T cells. During CLL progression in the mice, it became clear that T cells were engrafted together with the CLL cells (Figure 35C). Therefore, it is unclear whether the decreased amount of CLL cells after tamoxifen application is induced by cytotoxic CD8 T cells, or due to CLL intrinsic cell death processes.

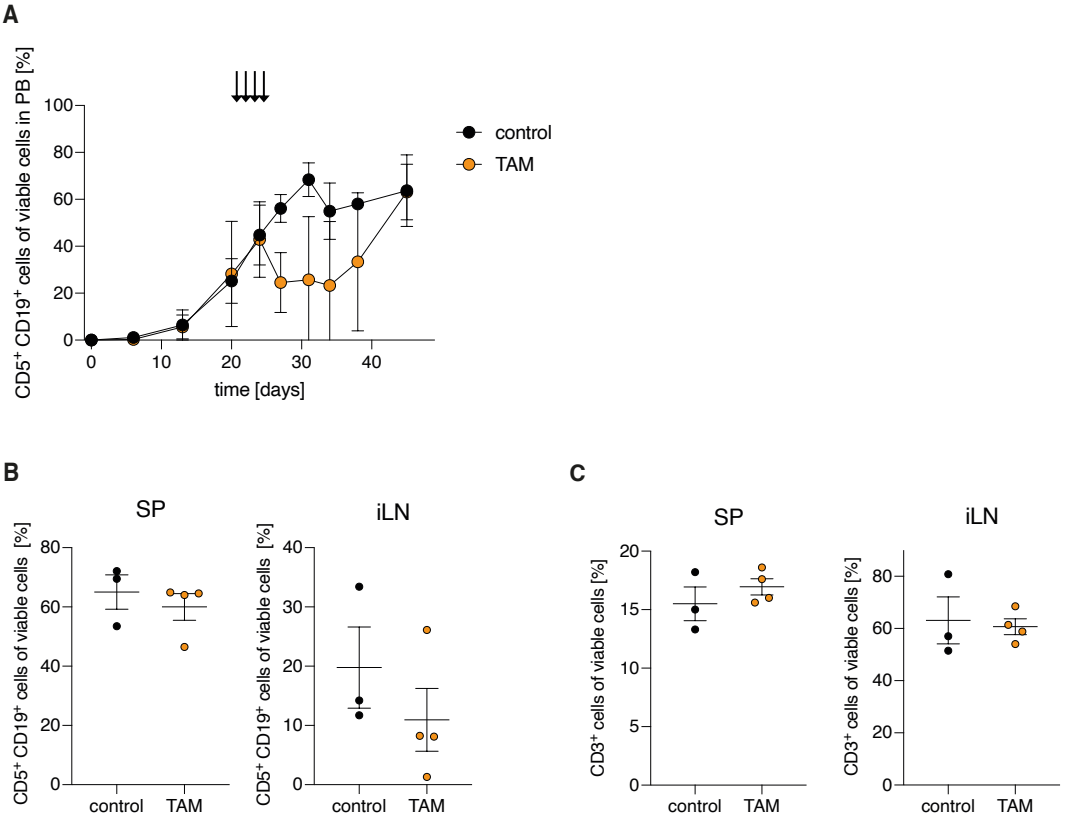

Figure 35: In vivo experiments with CLL cells expressing constitutively active CARD11 in R2b mice. ***A*** *Tracking of CD5+ CD19+ CLL cells in PB after i.v. transplantation of 2*10⁷ murine CARD11^{L225LI}xTCL1xMb1CreERT2 CLL cells per mouse with following induction of CARD11^{L225LI} expression through tamoxifen (n=4) or ethanol (control) (n=3) application. Application dates are marked with black arrows.* ***B+C*** *Collective analysis of immune cell populations (****B*** *CD5+ CD19+ CLL cells) (****C*** *CD3+ T cells) in the SP and iLN of experimental mice at the defined end of the experiment. Data is presented as mean values ± SD.*

In summary, we observed that CARD11^{L225LI} expression in human CLL cell lines increased cell proliferation and amplified the T-cell response in coculture experiments. *In vitro*, constitutive active CARD11 signaling also resulted in increased proliferation and cell size, but also enhanced cell death in murine CLL splenocytes. Additionally, we saw elevated metabolic processes and increased expression of extracellular receptors and signaling molecules. *In vivo*, the induction of CARD11^{L225LI} expression in murine CLL splenocytes led to the depletion of CLL cells in the PB, without the detection of GFP reporter-positive CLL cells. Further, tamoxifen treatment led to increased overall survival in C57Bl6/J mice, suggesting that either T cell-dependent or cell-intrinsic CLL cell death significantly reduced disease burden. In addition, in TAM-treated mice, activation of CD8 T cells was shown to be dependent on CLL content, as mice with high CLL levels had a high proportion of effector memory T cells. Aside from that, T-cell activation was elevated in TAM-treated mice compared to control mice with equal CLL levels. Furthermore, we could neither detect GFP reporter-positive CLL cells in immunocompetent wt C57Bl6/J mice after prior *in vitro* CARD11^{L225LI} induction, nor in immunocompetent R2b mice.

4.3.3. Constitutively active AKT expression in murine CLL *in vivo*

Yet another inducible mouse line we worked with was the AKT^{E17K}xTCL1xMb1CreERT2 strain, which enables the expression of constitutively active AKT^{E17K} after tamoxifen application. Additionally, we generated primary murine CLL cells expressing myrAKT through retroviral transduction. Phosphorylation of AKT (Thr308/Ser473) occurs at the cell membrane after translocation due to stimulation. Therefore, membrane-associated AKT is catalytically active. MyrAKT carries a myristylation signal at its N-terminus, which causes permanent association with the cell membrane, resulting in constitutively AKT phosphorylation and enzymatic activity.[103] The used myrAKT plasmid (pMIG) and its empty vector control carry the reporter protein GFP.

As primary CLL cells show limited proliferation and survival in culture, the transduced splenocytes were i.v. transplanted 48 h after first contact with the retroviral particles in low cell numbers into immunoincompetent R2b cells. The engraftment of GFP-positive CLL cells was monitored via regular blood drawings followed by flow cytometry-based analysis. As only low numbers of CLL cells were transplanted, slow engraftment of CLL cells with no visible difference between both groups was observed (Figure 36A). In parallel, the percentage of GFP reporter-positive CLL cells was monitored. There, we detected a steady increase of GFP-positive empty vector cells, but no occurrence of myrAKT-GFP CLL cells in the PB (Figure 36B).

To generate a potentially better environment for the engraftment of myrAKT transduced splenocytes, we tested the injection of cells into the peritoneal cavity (i.p.) simultaneously to i.v. injections in R2b mice. Again, we detected a slow engraftment in both approaches, but with an observable faster engraftment after i.v. injections (Figure 36C). Finally, it was possible to detect myrAKT-GFP CLL cells in the PB of both groups, however, no more than 5% of all CLL cells expressed the constitutively active AKT (Figure 36D). Analyses of the secondary lymphoid organs resulted in insufficient amounts of myrAKT-GFP CLL to perform further experiments.

In parallel, we performed i.v. transplantation experiments with tamoxifen-inducible AKT^{E17K}xTCL1xMb1CreERT2 splenocytes after prior CLL development in donor mice in R2b and C57BL/6 mice. After the first detection of CLL populations in the PB in experimental mice, AKT^{E17K} expression was induced with daily applications of tamoxifen (TAM) for 4 consecutive days (marked with black arrows) (Figure 36E+G). In wt and immunoincompetent mice, CLL engrafted similarly in control and TAM-treated mice, without a visible drop in CLL counts. In our model, GFP expression is induced together with the expression of AKT^{E17K} and was therefore used as a reporter for constitutively active AKT signaling in CLL cells. We detected AKT^{E17K}-GFP CLL cells in the PB of R2B mice after tamoxifen treatment with no more than 0.5% of all CLL cells even decreasing after the second treatment cycle (Figure 36F). In immunocompetent C57BL/6 mice, we could not detect AKT ^{E17K}-GFP-positive cells in the PB or secondary lymphoid organs upon tamoxifen induction (Figure 36H).

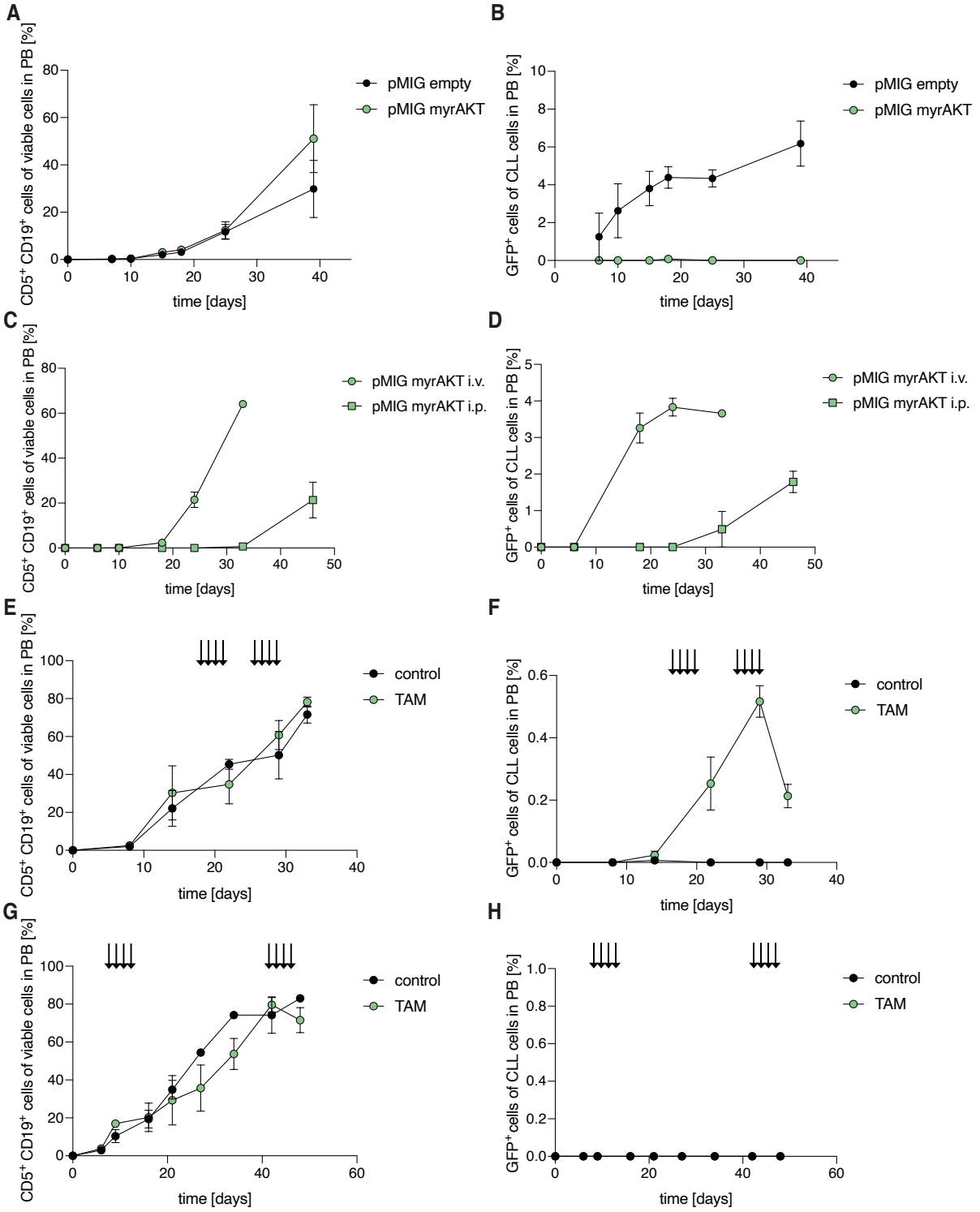

*Figure 36: In vivo experiments with CLL cells expressing constitutively active AKT – **A**+**B** Tracking of CD5⁺ CD19⁺ CLL cells and their GFP-reporter protein expression in PB of R2b mice after i.v. transplantation of murine CLL cells transduced with the pMIG myrAKT (n=4) or the pMIG empty vector (n=4). **C**+**D** Tracking of CD5⁺ CD19⁺ CLL cells and their GFP-reporter protein expression in PB of R2b mice after i.v. (n=3) and i.p. (n=3) transplantation of murine CLL cells transduced with the pMIG myrAKT. **E**-**H** Tracking of CD5⁺ CD19⁺ CLL cells and their GFP-reporter protein expression in PB of R2b (**E**+**F**) mice and C57Bl6/J mice (**G**+**H**) after i.v. transplantation of murine AKT^{E17K}xTCL1xMb1CreERT2 CLL cells with the following induction of AKT^{E17K} expression through tamoxifen (n=3) or ethanol (control) (n=3) application. Representative result for 2 independent experiments is shown. Application dates are marked with black arrows.*

In summary, we were not able to detect induced constitutive AKT signaling in transplanted CLL cells *in vivo*. The induced overexpression of myrAKT or AKT^{E17K} led to a significant survival disadvantage in CLL cells, as control and reporter-negative CLL engrafted unimpeded in experimental mice, whereas AKT-GFP-positive cells were not found with ratios above 5% of all CLL cells.

4.3.4. MYC overexpression in murine and human lymphoma *in vitro*

MYC is part of a highly conserved super-family of related basic-helix-loop-helix-zipper proteins that integrate extracellular and intracellular signals and modulate global gene expression. Notably, the MYC network is reported to be acutely involved in an extensive variety of human cancers.[104] Further, one of the most frequent pathway alterations in RT is associated with MYC abnormalities. Depending on the source, MYC alterations are described in 30% to 70% of all cases.[22,23,30] Hence, we also tested the induced overexpression of MYC as a possible model for RT.

First, we retrovirally transduced the human CLL cell lines MEC-1 and OSU-CLL with a MYC-GFP expressing plasmid or empty vector control plasmid. Figure 37A shows a representative quantification of MYC levels in the GFP-negative population compared to the GFP-positive population of cells transduced with the MYC plasmid using a flow cytometry-based analysis. Visibly, GFP-positive cells express elevated protein levels of MYC. In parallel, we analyzed the proliferative properties of GFP-positive control cells and MYC-transduced cells using the cell proliferation dye eFlour™ 670. MYC-GFP cells show slightly reduced intensities of the proliferation day after 24 h, indicating somewhat increased proliferation *in vitro* (Figure 37B). However, this trend is not significant. Lastly, we analyzed the immunosuppressive capacities of MYC-expressing lymphoma cells. In coculture experiments with the A5 T-cells line, which expresses GFP after CD3 stimulation,[101,102] we detected increased CD3-mediated T-cell activation in the presence of MYC-expressing cells suggesting that MYC expression partially reverses CLL-mediated reduction in TCR signaling capacity (Figure 37C).

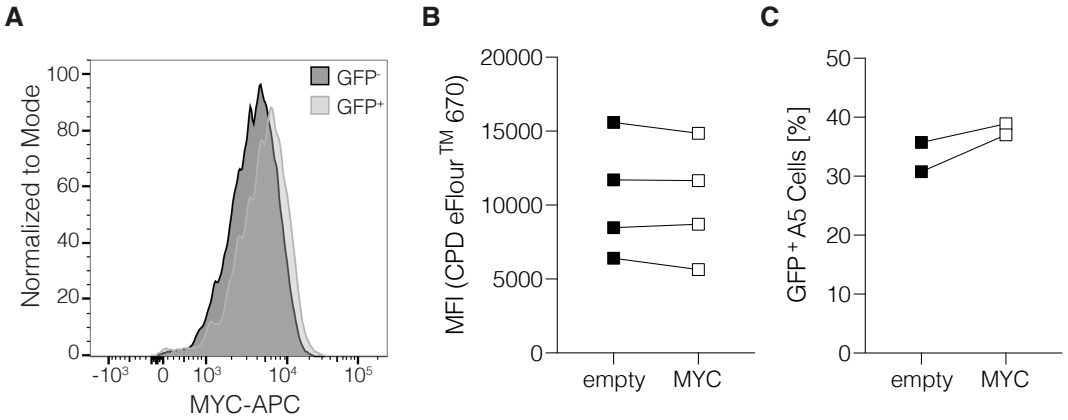

*Figure 37: Human CLL cell lines MEC-1 and OSU-CLL transduced with the pMIG empty and pMIG MYC plasmid – **A** Flow cytometry-based quantification of MYC protein expression. **B** Cell proliferation measured via the MFI of cell proliferation dye eFlour™ 670 after 24 h (n=4, pooled data from 3 independent experiments). For statistical analysis, a two-tailed paired Student's t-test was performed p=0.2777 **C** T-cell activation assay with the T-cell hybridoma cell line A5. Immunosuppressive potential of control CLL cell lines compared to cell lines expressing MYC (pooled data from 2 independent experiments).*

Additionally, we analyzed the overexpression of MYC in murine MYCxTCL1xMb1CreERT2 splenocytes after 4OHT treatment *in vitro*. Tamoxifen-inducible MYC expression under the promoter/enhancer elements of the Cd79a locus (Mb1) in *TCL1* transgene mice enables controlled MYC overexpression in mature lymphoma cells. As a reporter for MYC expression, human CD2 is co-expressed on the murine cell surface and can be detected with an antibody staining in flow cytometry-based analyses.

4OHT treatment induced MYC-CD2 expression in up to 30% of all splenocytes (Figure 38A). The observed cell death is not caused by MYC expression, as no decrease in viable cells was detected when comparing 4OHT treatment with control conditions (Figure 38B). MYC expression *in vitro* did not lead to increased cell size, did not increase proliferation, or increased expression of the glycolysis-controlling glucose transporter GLUT1 (Figure 38D-E). To be able to make the most precise statement about the changes in MYC-overexpressing cells, we compared the CD2-positive cells to their sample internal control, the CD2-negative population. The ratio of the measurements ($CD2^-/CD2^+$) is depicted as a fold change.

However, we did observe a reduction in the amount of CD2-positive cells after incubation in glucose-free media conditions, simultaneously with 4OHT exposure. This suggests enhanced dependency on glycolysis upon induced MYC expression (Figure 38F). Nonetheless, co-treatments with the metabolic inhibitors 2-DG (glycolysis) or Telaglenastat (glutamine metabolism) in combination with 4OHT, did not lead to alterations in the amounts of CD2-positive cells *in vitro* at the tested concentrations and time point (Figure 38G+H).

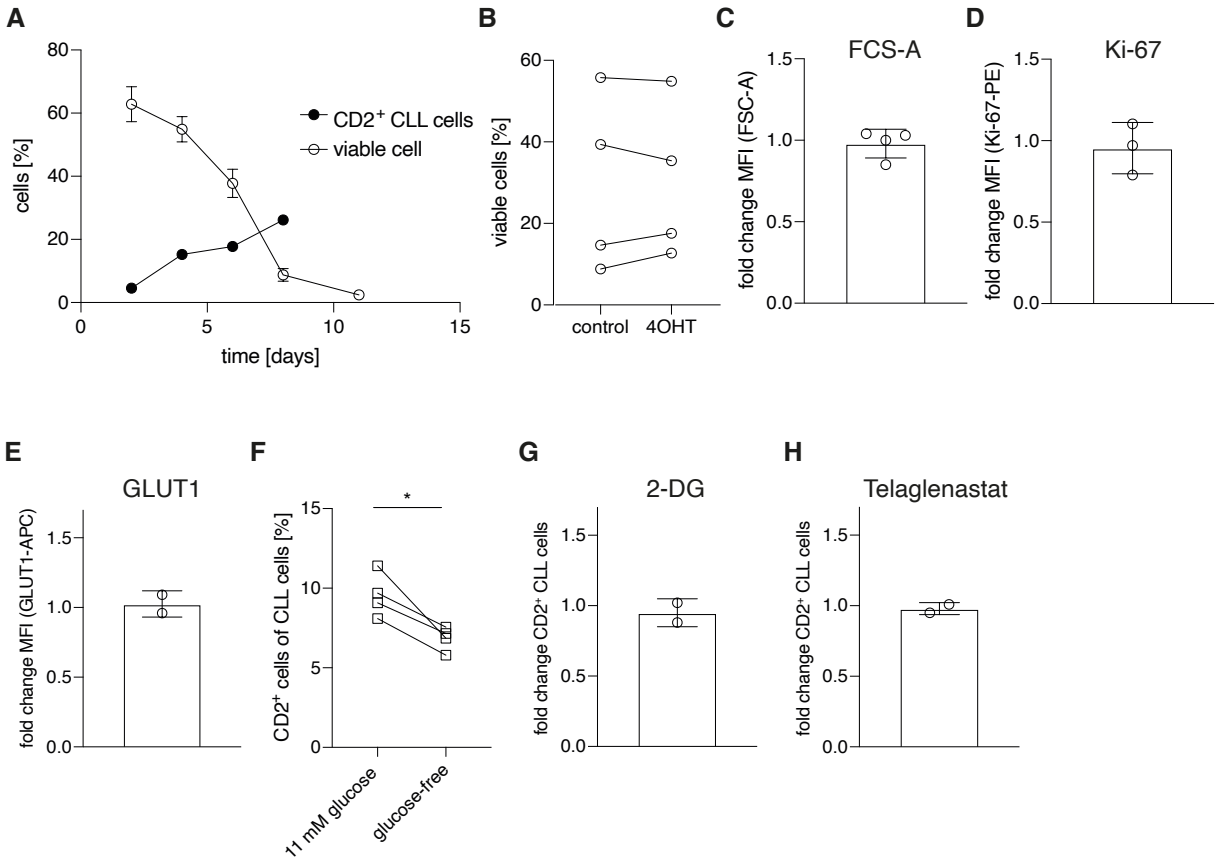

Figure 38: Flow cytometry analysis of MYCxTCL1xMb1CreERT2 splenocytes – Expression of MYC following 0.5 µg/ml 4OHT or DMSO ethanol (control) treatment for 48 h. ***A*** *Time course of reporter GFP expression and cell viability after 4OHT treatment. Representative result for 4 independent experiments is shown* ***B*** *Comparison of cell viability after 4OHT or DMSO treatment on day 4 (pooled data from 4 independent experiments).* ***C*** *Fold change in cell size of GFP-positive cells after 4OHT treatment on day 4 (pooled data from 4 independent experiments).* ***D*** *Fold change in proliferation after MYC expression measured via Ki-67 staining on day 4 (pooled data from 3 independent experiments).* ***E*** *Fold change in the expression of GLUT1 after MYC expression on day 6 (pooled data from 2 independent experiments).* ***F*** *Measurement of CD2-reporter expression in the presence or absence of glucose in the medium during 4OHT treatment after 48 h. For statistical analysis, a two-tailed paired Student's t-test was performed. *, p=0.0210 (n=4, pooled data from 2 independent experiments).* ***G+H*** *Fold change of CD2-reporter-positive cells in the presence of metabolic inhibitors 2-DG (0.625 µM) and Telaglenastat (25 µM) during 4OHT treatment after 24 h. (pooled data from 2 independent experiments).*

In summary, it was observed that MYC expression *in vitro* is tolerated by lymphoma cells, while proliferation, cell size, and metabolic processes were not affected by MYC overexpression. However, we show that the absence of glucose impairs the formation or survival of MYC-positive cells.

4.3.5. MYC overexpression in murine lymphoma *in vivo*

Consistently with the previously described experimental procedure, we performed transplantation experiments with MYCxTCL1xMb1CreERT2 splenocytes in C57Bl6/J recipient mice and subsequent tamoxifen treatment. Tamoxifen was again administered for 4 consecutive days after the first detection of lymphoma cells in the peripheral blood (marked with black arrows). We continued to track cell engraftment and CD2 reporter expression in the PB over time (Figure 39A+B). Interestingly, we detected a strong reduction of lymphoma cells in the PB of TAM-treated mice, even though MYC expression *in vitro* did not result in cell death. This implies that the expression of MYC leads to cell death only in the nutrient-restricted conditions *in vivo*, and/or that immune cell control reduces the amount of MYC-overexpressing cells. After the first treatment circle, we could not detect $CD2^+$ MYC-expressing cells. Therefore, we started a second treatment interval almost 70 days after the original cell transplantation. Then, two mice started to progress quickly with very high proportions of CD2-positive cells while 2 others within the TAM group did not reveal any CD2 expression. In the following, these two groups will be referred to as "TAM $CD2^-$" and "TAM $CD2^+$". This suggests that in 2 of 4 TAM-treated mice, additional events enabled the full transformation of MYC-expressing lymphoma.

When the individual health endpoint of the animals was reached, an analysis of lymphoid organs revealed no significant differences in lymphoma cell content in the spleen, peritoneal cavity, or inguinal lymph nodes (Figure 39C). We also analyzed the presence of CD2-positive lymphoma cells in the examined organs (Figure 39D). We could detect high ratios of CD2-positive MYC-expressing cells in all organs of TAM $CD2^+$ mice. A very interesting finding is a small percentage of CD2-positive cells in the inguinal lymph nodes of only one TAM $CD2^-$ mouse, which did not show reporter-positive cells in the spleen, peritoneal cavity, or peripheral blood. This discovery suggests that the LNs are the starting point for MYC-positive cell outgrowth and transformation.

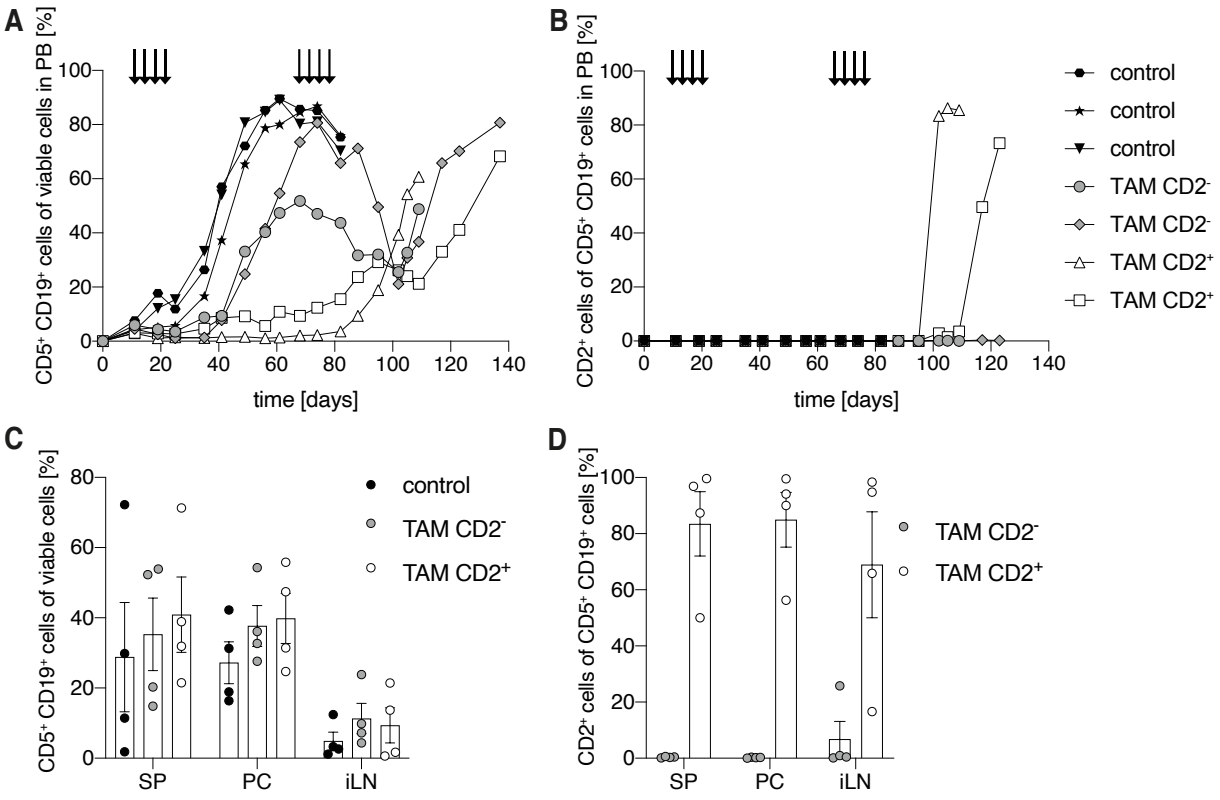

*Figure 39: In vivo experiments with lymphoma cells overexpressing MYC after tamoxifen application – **A+B** Tracking of CD5+ CD19+ cells and their CD2-reporter expression in PB of C57Bl6/J mice after i.v. transplantation of 2*10^7 murine MYCxTCL1xMb1CreERT2 splenocytes per mouse with the following induction of MYC expression through tamoxifen (n=4) or ethanol (control) (n=3) application. Application dates are marked with black arrows. Representative result for 4 independent experiments is shown. **C+D** Flow cytometry analysis of CD5+ CD19+ cells and their CD2-reporter expression in different organs. Pooled data of 2 independent experiments is shown, control: n=4, tamoxifen: n=8.*

To study the influence of the adaptive immune system in MYC-positive lymphoma outgrowth, we also performed the described transplantation experiments in immunoincompetent R2b mice. We carefully checked that all T cells were depleted from the splenocyte mix before transplantation. Even though, the transplanted cells engrafted slowly in the recipient mice, we detected a slow and linear increase in CD2 expression since the beginning of tamoxifen treatment (Figure 40A+B). T cells are known to support the progression of engraftment, suggesting the slow progression may be due to a lack of T-cell support in this model. This suggests that T-cell control contributes to the clearance of MYC+ lymphoma cells in the wt model. However, as we did not detect an increase in disease progression or exponential progression of MYC+ cells, we assume that they have not yet transformed despite transgene expression.

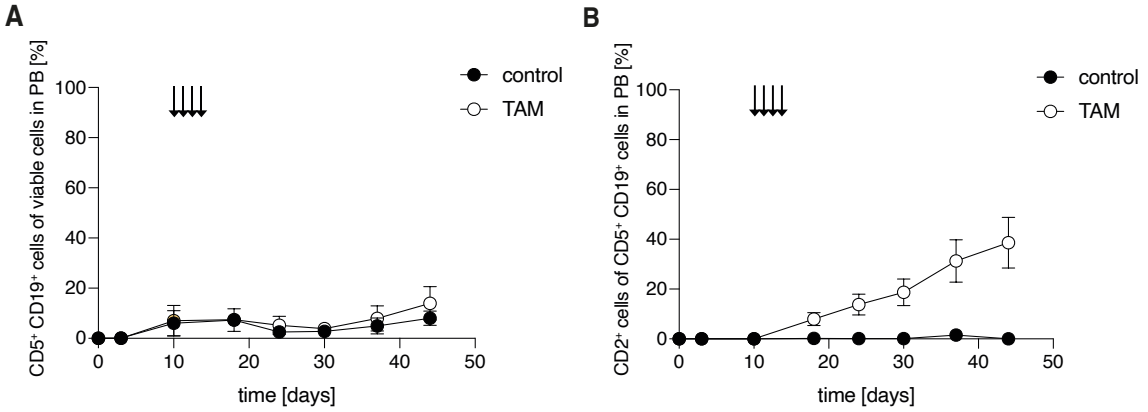

Figure 40: ***A+B*** *Tracking of CD5+ CD19+ cells and their CD2-reporter expression in PB of R2b mice after i.v. transplantation of 2*10^6 murine MYCxTCL1xMb1CreERT2 cells per mouse with the following induction of MYC expression through tamoxifen (n=3) or ethanol (control) (n=3) application. Application dates are marked with black arrows.*

To expand the transformed and outgrown cells of interest seen in Figure 39, we decided to re-transplant the harvested splenocytes that included MYC-CD2-positive lymphoma cells into another set of recipient mice. After simultaneous i.v. transplantations of T cell-depleted splenocytes into R2b and C57Bl6/J mice, which partially express MYC after previous tamoxifen induction in a donor mouse, we could see that the cells would engraft faster in R2b mice and indicated a strong progression of MYC-positive lymphoma cells that remained CD2-positive over time. In C57Bl6/J mice, however, MYC-positive cells showed reduced engraftment from the beginning as well as repetitive cycles of clearing and reappearing in the PB (Figure 41A+B). Endpoint organ analyses revealed MYC-CD2-positive lymphoma cells in approximately 50% of all re-transplanted C57Bl6/J mice (data not shown).

Figures 41C and 41D show data from a re-transplantation experiment in R2b mice with successful depletion of CD8 T cells in the transplanted splenocyte mix. The mice were collectively euthanized at a set endpoint. We detected high amounts of lymphoma cells in the spleen and PC, but only a low percentage of lymphoma cells in the iLN (Figure 41C). CD2-positive lymphoma cells were detected in all mice in all analyzed organs, with the highest ratio in the PC (Figure 41D). In another independent experiment (Figure 41E-G), CD8 T cells were depleted from the splenocyte mix similarly, nevertheless, we detected the engraftment of CD8 T cells in one out of three mice. This outlier is indicated with a grey symbol (Figure 41E). This single R2b mouse with engrafted CD8 T cells showed decreased lymphoma cell amounts in SP and iLN (Figure 41F), and slightly decreased levels of CD2-positive cells in the spleen, but not in the lymph nodes (Figure 41G). Again, the mice were collectively analyzed at a set endpoint.

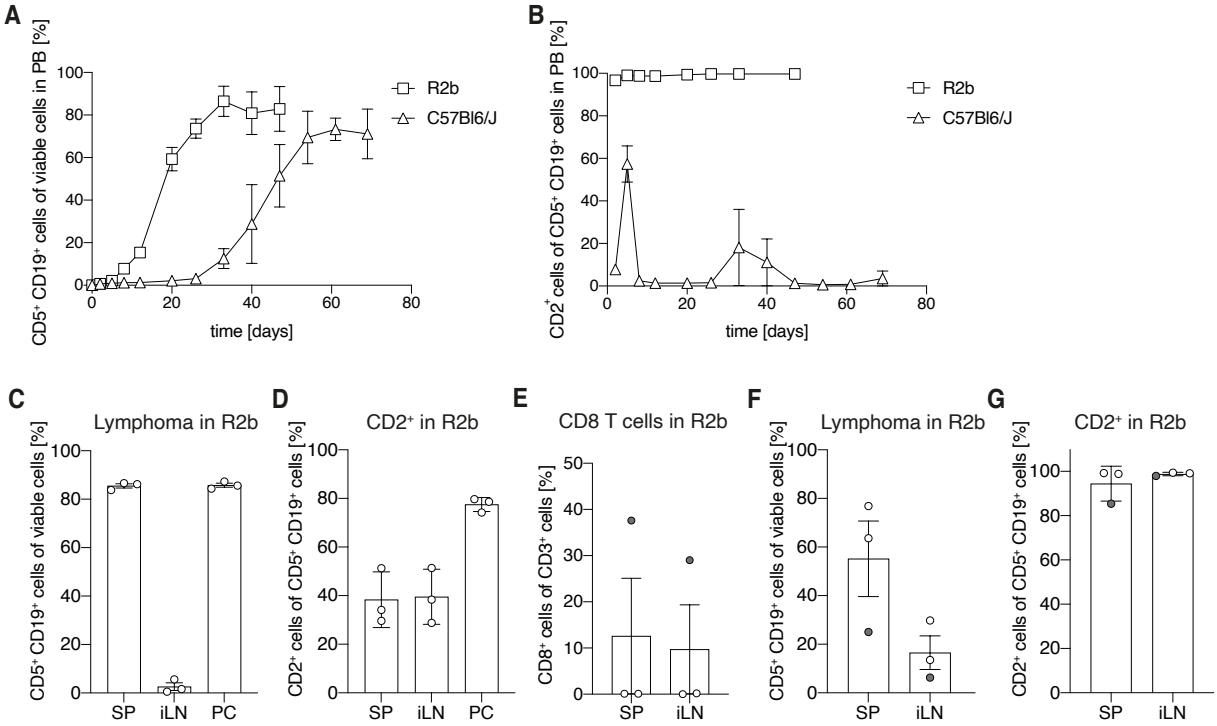

*Figure 41: Re-transplantation of MYC-CD2⁺ cells in R2b and C57Bl6/J mice – **A+B** Tracking of CD5⁺ CD19⁺ cells and their CD2-reporter expression in PB after i.v. transplantation of 2*10⁷ MYCxTCL1xMb1CreERT2 splenocytes per mouse after previous tamoxifen induction (see Figure 39) after CD8 T-cell depletion in C57Bl6/J (n=3) and R2b (n=3) mice. Representative result for 3 independent experiments with three different donors is shown. Lymphoma cells from 3 different donors with 97% (I), 50% (II), and 87% (III) MYC-positive cells were transplanted. A+B show experiments with donor I. **C-G** Analysis of immune cell populations of R2b mice at the end of experiments. (C+D show experiments with donor II. E-G show experiments with donor I.) Data is presented as mean values ± SD*

Therefore, the presented analyses of the lymphoid organs of the re-transplanted mice support the hypothesis that the cytotoxic response of CD8 T cells is largely responsible for the depletion of MYC-expressing lymphoma cells *in vivo.* Furthermore, we provide some evidence that CD8 T cells preferably target CD2-positive lymphoma cells in the spleen while LN-derived CD2-positive cells are less affected. However, additional experiments are required to confirm this assumption. Furthermore, we detected very high ratios of CD2-positive lymphoma cells in the PC, suggesting that the PC provides a protective niche.

Re-transplanting induced cells resulted in more opportunities for analyzing MYC overexpressing lymphoma cells *in vivo*. Unfortunately, with every additional transplantation passage, the re-transplanted cells become more aggressive and lose original phenotypical properties, potentially by gaining intrinsic MYC amplification.[105] To generate an additional model that does not express human CD2, we used primary mouse CLL cells transduced with the plasmids pMIG myc or pMIG empty as control, both expressing GFP as a reporter protein. As before, the splenocytes were transplanted into R2b mice 48 h after retroviral transduction.

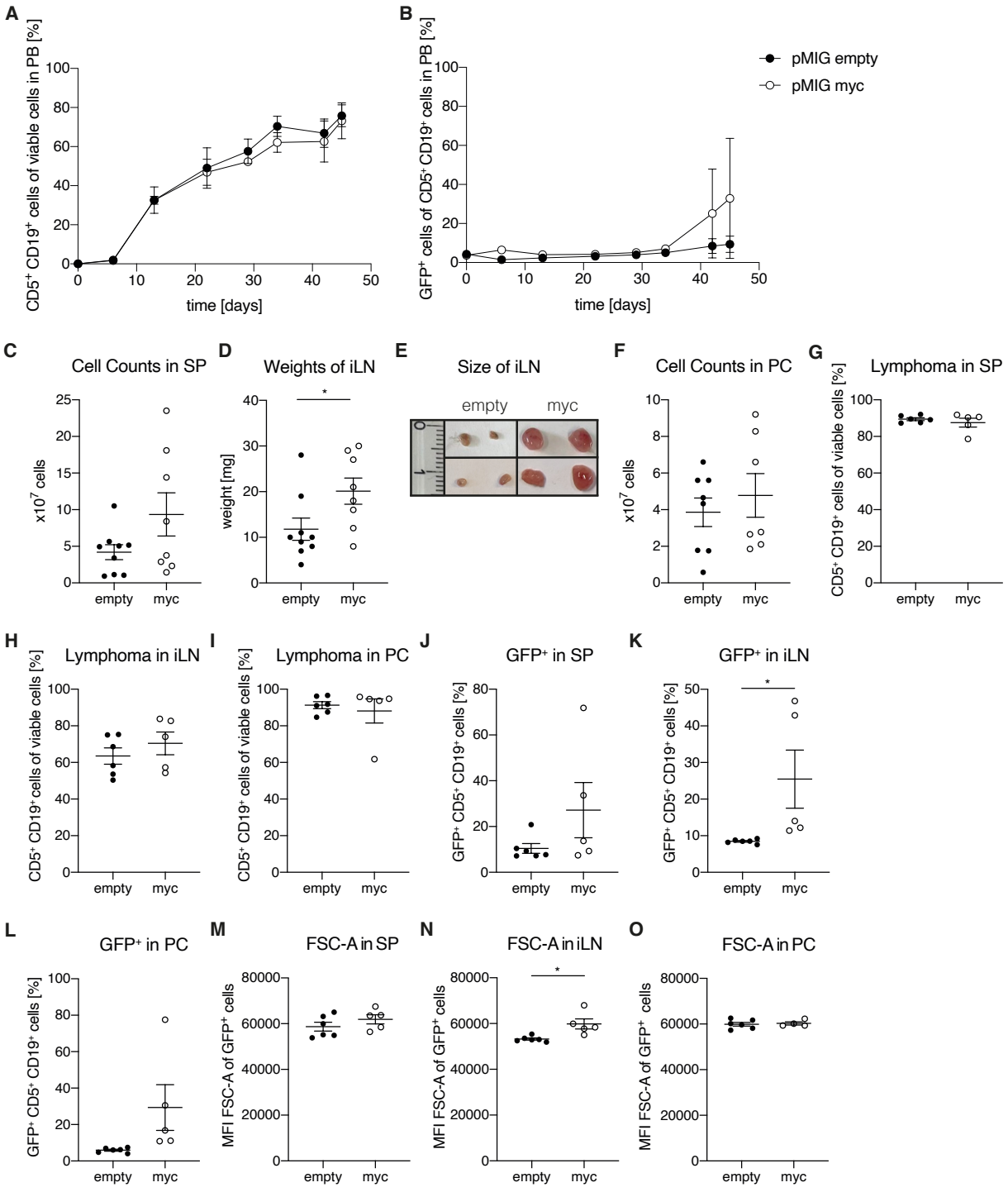

*Figure 42: In vivo experiments with lymphoma cells expressing MYC after retroviral transduction – **A**-**B** Tracking of CD5+ CD19+ cells and their GFP-reporter expression in PB of R2b mice after i.v. transplantation of 2*10⁶, which were retrovirally transduced with the pMIG empty (n=3) or pMIG myc vector (n=3), per mouse. Representative result for 3 independent experiments is shown. **C**-**O** Analysis of cell counts, organ weight, lymphoma cell content, GFP+ reporter pos. Lymphoma cells and cell size in spleen (SP), peritoneal cavity (PC), and inguinal lymph nodes (iLN). Pooled data from 3 independent experiments. Data is presented as mean values ± SD. For each statistical analysis, a two-tailed unpaired Student's t-test was performed. **D**: p=0.0411, **K**: p=0.0421, **N**: p=0.0105.*

Monitoring the lymphoma contents in the PB during the experimental time course of the first performed experiment revealed no significant differences between the MYC-expressing group and the control group (Figure 42A). Also, we did not see an expression of GFP in either of both groups until day 33 after transplantation. Then, one mouse showed an outgrowth of GFP-positive lymphoma cells in the PB (Figure 42B). This was repeated with similar results in later experiments (data not shown). As each lymphoma transplant shows different engraftment patterns, it is not possible to pool all collected data of MYC-positive lymphoma outgrowth in the PB. However, the following graphs depict pooled data of the final analyses after the animals' individual endpoint was reached of all performed transplantation experiments with retrovirally transduced cells, characterizing the distribution of MYC-expressing cells in the different immune compartments.

We counted the total cell numbers of spleens and flushes of the peritoneal cavity and weighed the harvested iLN (Figure 42C-F). While we detected a trend in increasing cell numbers in SP and PC, iLN weights of mice transplanted with pMIG myc transduced cells were significantly enhanced. An illustration of the enlarged lymph nodes is shown in Figure 42F. Using flow cytometry-based analyses, we could not find any significant differences in the percentage of lymphoma cells in the different organs (Figure 42G-I). While we observed a non-significant trend for higher amounts of GFP-positive lymphoma cells in SP and PC, the percentage of reporter-positive lymphoma cells was statically increased only in the iLN (Figure 42J-L). Finally, we studied the flow cytometric forward scatter intensities of GFP-reporter-positive lymphoma cells in the analyzed organs, which represent cell size (Figure 42M-O). The size of GFP-positive lymphoma cells in the PC did not vary noticeably between the two groups. MYC-expressing GFP-positive lymphoma cells showed a trend towards increased cell size in the spleen, but only in the inguinal lymph nodes of the myc group, the reporter-positive cells were significantly increased.

After expanding pMIG myc transduced cells in R2b mice, we harvested splenocytes (72% GFP-positive lymphoma cells) and transplanted them in immunocompetent C57Bl6/J mice. Monitoring the engraftment of cells and their reporter expression in the PB, we saw a slight decrease in lymphoma cell content after the first engraftment, followed by an outgrowth of MYC-positive lymphoma cells after approximately 20 days (Figure 43A). The percentage of GFP-positive lymphoma cells quickly rose to almost 100% and stayed constant thereafter. In contrast, GFP^+ empty vector cells were lost over 2-3 weeks (Figure 43B). After the set collective endpoint analysis of the lymphoid organs of the experimental mice, we detected two GFP-positive lymphoma populations (“GFP low” and “GFP high”), besides the reporter-negative cells (Figure 43C).

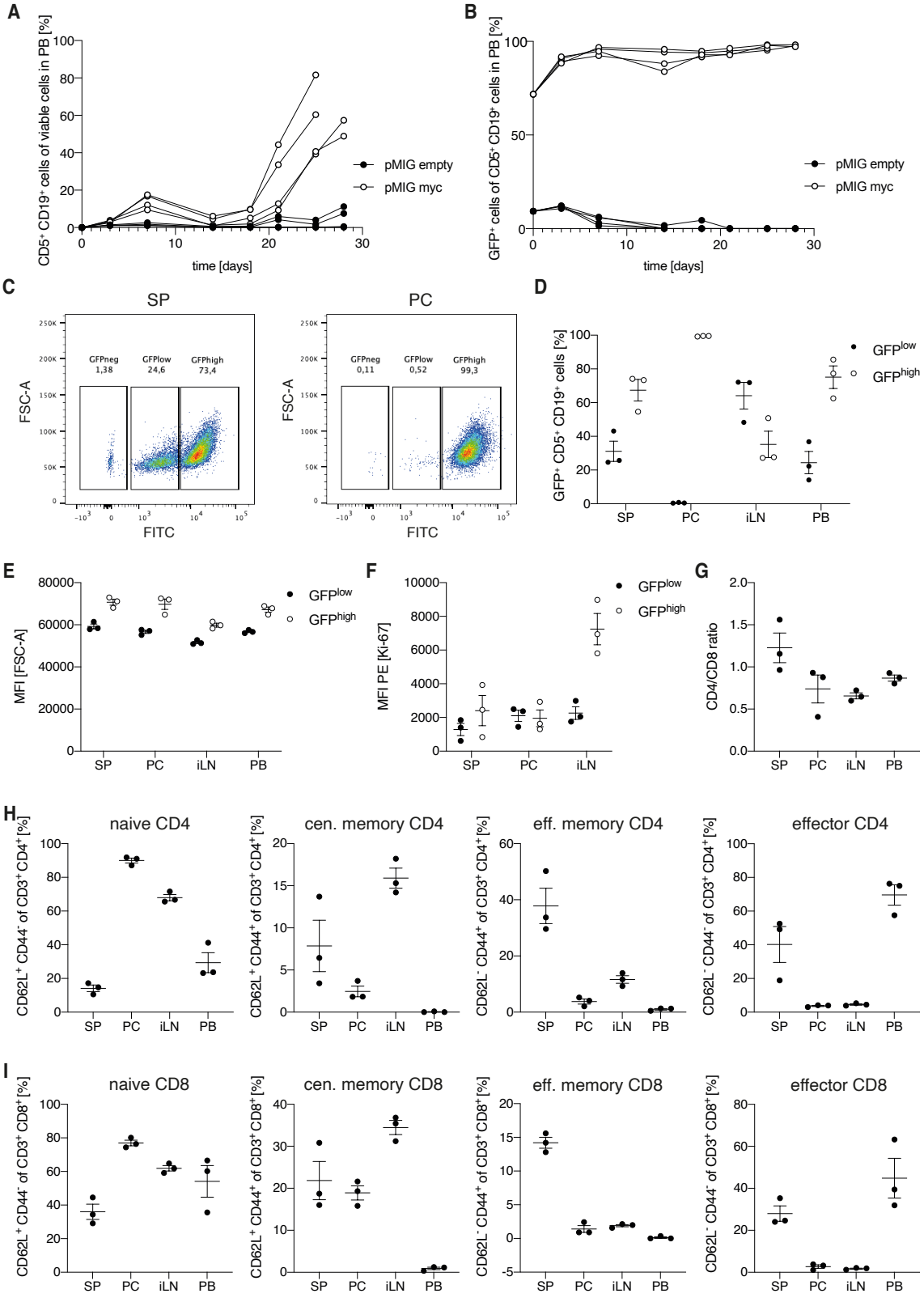

*Figure 43: In vivo experiments with lymphoma cells expressing MYC after retroviral transduction – **A**+**B** Tracking of CD5+ CD19+ cells and their GFP-reporter expression in PB of C57Bl6/J mice after i.v. re-transplantation of 2*10^7 murine lymphoma cells, which were retrovirally transduced with the pMIG empty (n=4) or pMIG myc vector (n=4) per mouse. **C**-**F** Flow cytometry analysis of cell characteristics at the end of the experiment in different organs of C57Bl6/J with re-transplanted pMIG myc cells **G**-**I** Flow cytometry analysis of T-cell characteristics at the end of the experiment in different organs of C57Bl6/J with re-transplanted pMIG myc cells.*

While comparing data from the different organs, we discovered that only GFP high lymphoma cells were found in the PC. The PB also obtained a high percentage of GFP high cells, whereas we found the lowest percentage of GFP high cells in the iLN (Figure 43D). In addition to different GFP intensities, the two GFP-expressing populations also differed in their cell size, with an increased FSC-A in the GFP high population (Figure 43E). A flow cytometry-based analysis of the proliferative capacitates of the GFP high and low populations showed that GFP high lymphoma cells in the iLN proliferate strongly compared to the GFP low cells, whereas only slight differences were visible in the SP and PC (Figure 43F).

Analyses of T-cell subgroups revealed a small percentage of naive CD4 and CD8 T cells in the spleen, and a high ratio of naive CD4 and CD8 T cells in the PC (Figure 43G-I). Further, the highest amount of central memory T cells was found in the iLN. Inside the spleen, we detected the most effector memory T cells and the second most effector T cells, while these populations were hardly represented in the PC and iLN.

Since we detected an almost 100% GFP high lymphoma population in the PC, which however has no survival advantage due to increased proliferation, there must be other benefits that reinforce this phenomenon. We did not find large numbers of activated T cells that could deplete MYC-expressing cells in the PC, but hardly any GFP-negative cells were found in this compartment, which speaks for a targeted migration or selective survival advantage of the GFP high population in(to) the PC. Therefore, we decided to conduct further studies to investigate the influence of PC on MYC-expressing lymphoma cells.

To test whether the PC creates a beneficial microenvironment for MYC-expressing lymphoma cells, we transplanted cells carrying pMIG myc/empty directly into the PC (i.p. injections) in direct comparison to i.v. injections. While tracking the cell engraftment, we found that i.v. injected lymphoma cells were naturally found at earlier time points in the PB of the mice (Figure 44A). Interestingly, we found that when transplanting mixed splenocytes including MYC-expressing lymphoma cells i.v. or i.p., the percentage of MYC-positive cells was strongly increased in the PB of mice transplanted via i.p. injections (Figure 44B). Additionally, we could show again that MYC-expressing lymphoma cells need a certain time to adjust to their environment before they outgrow MYC-negative cells in R2b mice after i.v. injection.

After both injection techniques, MYC overexpression led to increased cell numbers in the spleen, with the most cell numbers after i.v. injections of pMIG myc cells (Figure 44C). Organs were analyzed simultaneously after a set endpoint. Naturally, we detected more cells in the PC after i.p. compared to i.v. injections with significantly increased cell numbers under MYC overexpressing conditions (Figure 44D). Analyzing lymph nodes, i.p. injections with MYC-positive lymphoma cells significantly increased lymph node weight compared to i.p. injections with MYC-negative cells. After i.v. injections this trend is also visible, but it is not significant. (Figure 44E). Cell amounts in iLN reflected iLN weights (data not shown).

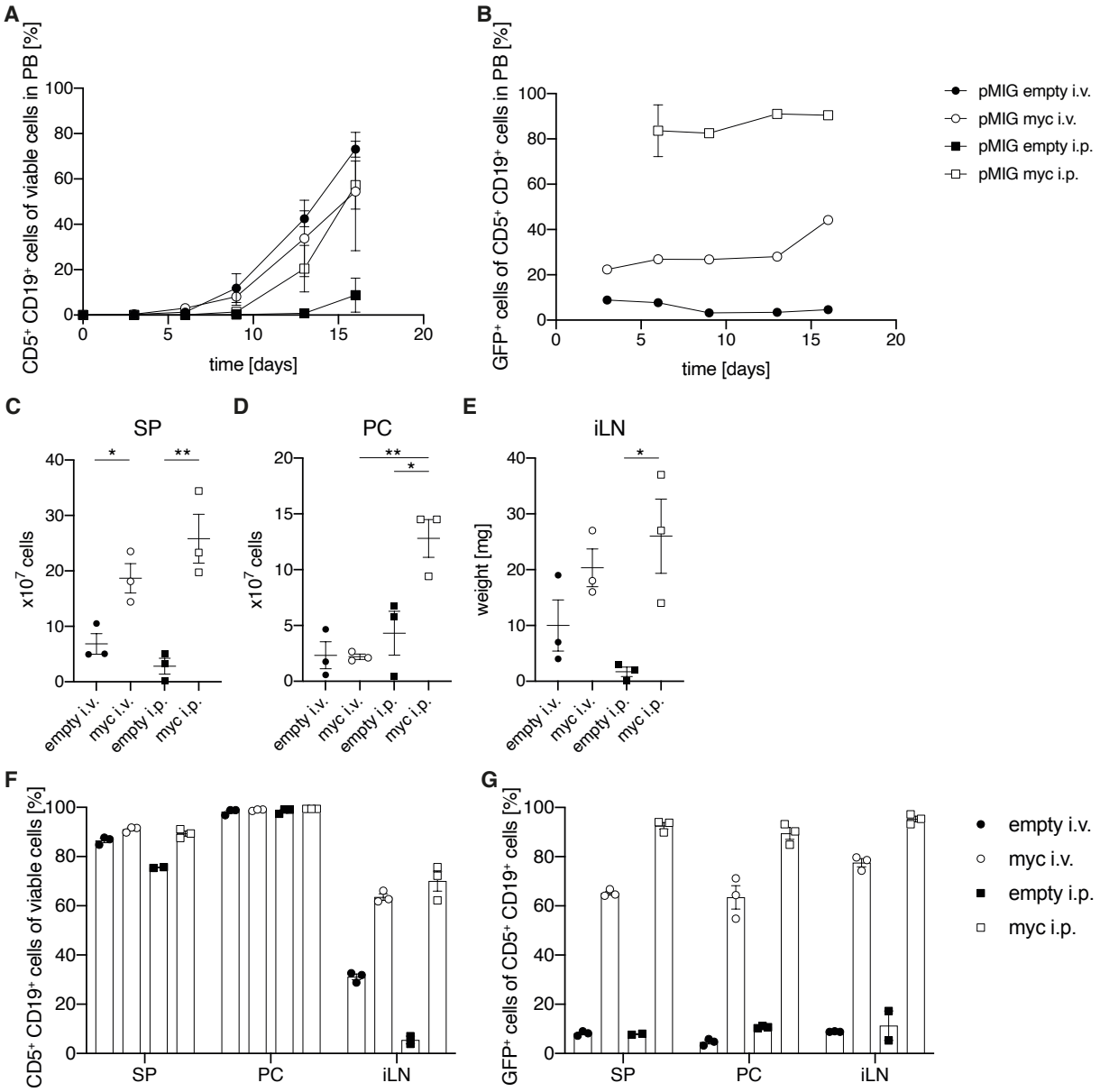

*Figure 44: Comparison of the engraftment of lymphoma cells transduced with pMIG empty and pMIG myc after i.v. and i.p. injections – **A+B** Tracking of CD5+ CD19+ cells and their GFP-reporter protein expression in PB of R2b mice after i.v. or i.p. re-transplantation of 2*10^6 murine cells per mouse, which were retrovirally transduced with the pMIG empty or pMIG myc vector (each n=3). One out of two representative experiments is shown **C-G** Analysis of cell counts, organ weight, cell content, and GFP+ reporter pos. lymphoma cells in the spleen (SP), peritoneal cavity (PC), and inguinal lymph nodes (iLN). All data is presented as mean values±SD. For each statistical analysis, a two-tailed unpaired Student's t-test was performed. **C**: p=0.0212, p=0.0077; **D**: p=0.0035, p=0.0308, **E**: p=0.0224.*

Peritoneal injections with MYC-expressing lymphoma cells led to the highest ratio of lymphoma cells in the iLN, although similar injections with control cells resulted in less than 10% of lymphoma cells in the iLN (Figure 44F). Further analyses showed that i.p. injections resulted in higher MYC-GFP levels in every examined organ compared to i.v. injections (Figure 44G).

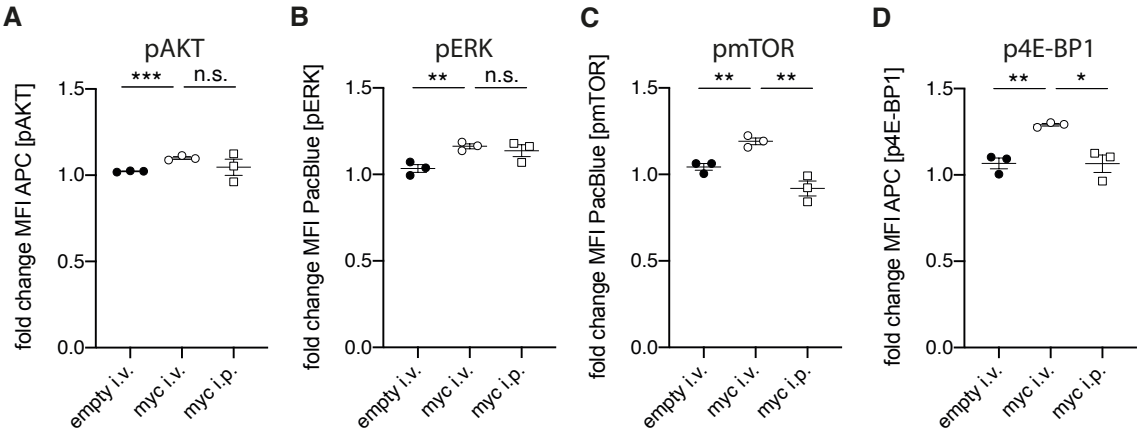

Figure 45: Intracellular signaling of lymphoma cells transduced with pMIG empty and pMIG myc after i.v. and i.p. injections ***A-D*** *Phosphorylation analyses of signaling pathway proteins AKT, ERK, mTOR, and 4E-BP1 in lymphoma cells transduced with pMIG empty or pMIG myc vector (each n=3).* ***E****: p=0.0007, p=0.3259;* ***F****: p=0.0086, p=0.5295;* ***G****: p=0.0057, p=00.45;* ***H****: p=0.0023, p=0.0115. All data is presented as mean values±SD. For each statistical analysis, a two-tailed unpaired Student's t-test was performed.*

In parallel, signaling pathway analyses showed increased phosphorylation of AKT and ERK in MYC-expressing cells compared to their control cells after i.v. transplantation. Injections into the peritoneal cavity did not result in differentiated activation of AKT or ERK in MYC-expressing lymphoma cells (Figure 45A+B). Phosphorylation of mTOR and 4E-BP1 was also upregulated in pMIG myc lymphoma cells compared to pMIG empty cells after i.v. transplantation. However, the activation of mTOR and 4E-BP1 was significantly decreased in MYC-positive lymphoma cells, after i.p. transplantations (Figure 45C+D).

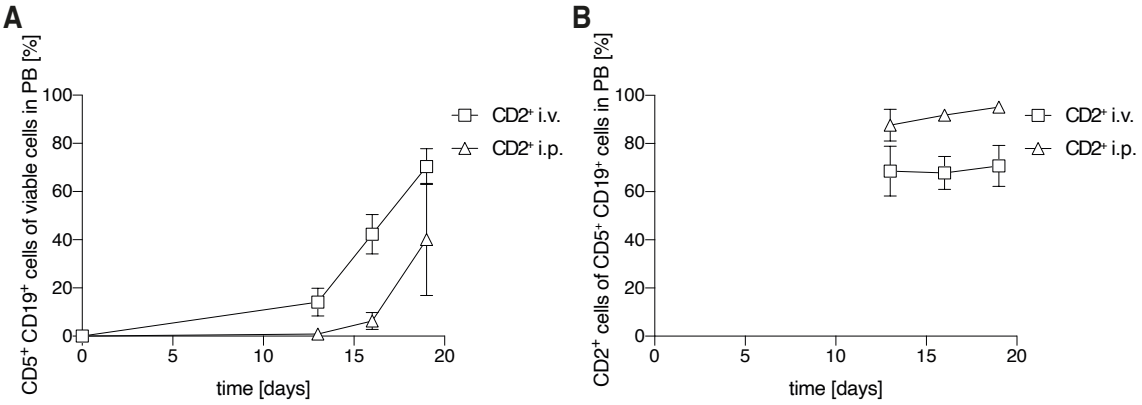

Figure 46: Comparison of MYC expressing MYCxTCL1xMb1CreERT2 cells after i.v. and i.p. injections. – ***A+B*** *Tracking of CD5+ CD19+ cells and their CD2-reporter expression in PB of R2b mice after i.v. or i.p. re-transplantation of 5*10^6^ cells per mouse, in which myc expression was induced due to prior tamoxifen application (each n=3).*

When re-transplanting MYCxTCL1xMb1CreERT2 splenocytes with active MYC-CD2 expression due to prior tamoxifen treatment into R2b mice via i.v. and i.p. injections, we were able to validate the observed engraftment patterns seen in Figure 44. Lymphoma cells were detected earlier in the PB of the i.v. injected group compared to the i.p. injected mice (Figure 46A). Simultaneously with the first detection, i.p. injected mice contain higher ratios of CD2-reporter-positive lymphoma cells (Figure 46B).

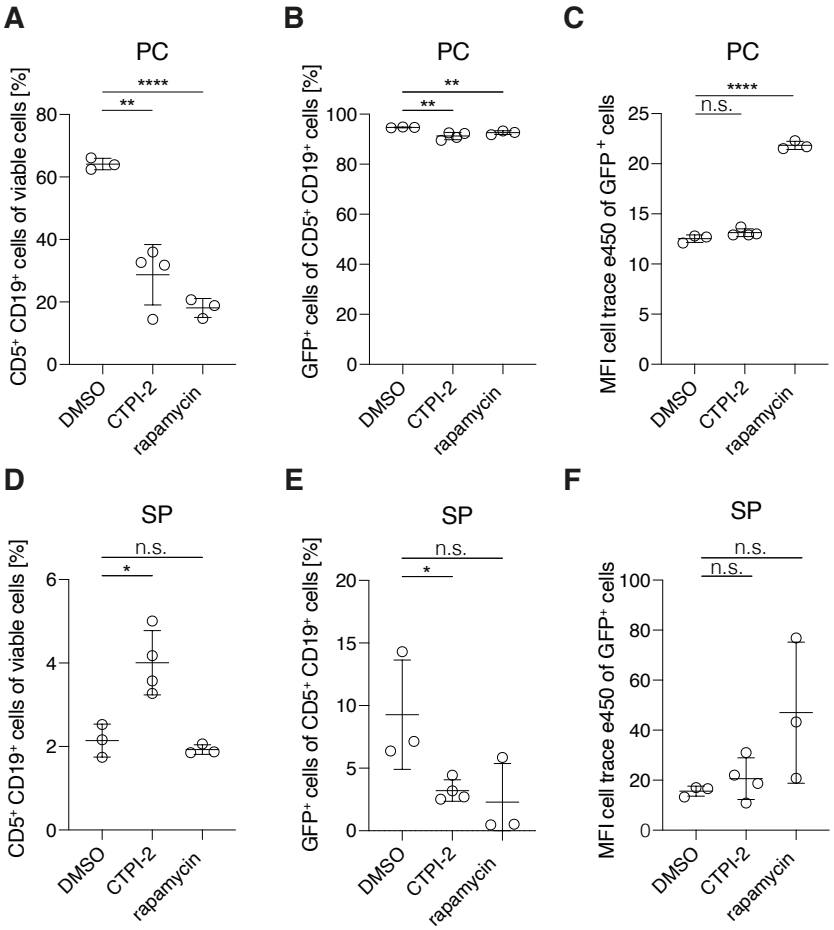

*Figure 47: Analysis of R2b mice transplanted with 2*10⁶ Eμ-TCL1 splenocytes per mouse, seven days after transplantation. The splenocytes were transduced with the pMIG myc plasmid, expanded in vivo, stained with cell trace 450 dye, and transferred into the experimental mice via i.p. injections. The mice were treated with DMSO (control), CTPI-1 (SLC25A1 inhibitor), and rapamycin (mTOR Inhibitor) on day one and day three.* ***A*****-*****C*** *Flow cytometry-based analysis of the peritoneal cavity and* ***D*****+*****E*** *spleen. For statistical analysis, a two-tailed unpaired Student's t-test was performed.* ***A****: **, p=0.0017; ****, p<0.0001.* ***B****: **, p=0.0095; **, p=0.0096.* ***C****: n.s., p=0.0992; ****, p<0.0001.* ***D****: *, p=0.0129; n.s., p=0.4138.* ***E****: *, p=0.0385; n.s., p=0.0864.* ***F****: n.s., p=0.3636; n.s., p=0.1274. Data is presented as mean values ± SD.*

Based on the PC niche preference of MYC-expressing lymphoma, we hypothesized that the metabolic environment is responsible for this effect. To test this, we applied the inhibitors CTPI-2 and rapamycin *in vivo* upon i.p. transplantation of splenocytes containing MYC^+ and MYC^- lymphoma cells. CTPI-2 inhibits the mitochondrial citrate carrier SLC25A1 and thereby limits cytosolic citrate pools, the source of acetyl-Coenzyme A (Ac-CoA). However, it can also allosterically regulate metabolic enzymes of glycolysis, lipogenesis, and gluconeogenesis.[106-108] Rapamycin inhibits mTOR, the mammalian target of rapamycin, regulating cell proliferation, autophagy, and apoptosis through the involvement in several intracellular signaling pathways.[109] Lymphoma cells transduced with pMIG myc and labeled with cell trace e450 were i.p. transplanted into R2b mice and treated with CTPI-2, rapamycin, or DMSO as a control on day 1 and day 3 after transplantation, also via i.p. injections. Seven days after transplantation, we analyzed the lymphoma cells of SP and PC. In the PC, we detected significantly decreased lymphoma cell levels (indicating general toxicity of the drugs) and decreased ratios of GFP-positive lymphoma cells after treatment with CTPI-2 and rapamycin, suggesting selective disadvantage in the presence of MYC (Figure 47A+B).

After seven days *in vivo*, the lymphoma cells contained only low amounts of cell proliferation dye, suggesting they had undergone several rounds of proliferation. Nevertheless, after rapamycin treatment, lymphoma cells in the PC contained significantly higher levels of cell trace dye implying they experienced impaired cell proliferation (Figure 47C). Since the experiment was terminated after seven days, the lymphoma amount in the spleen was still comparatively low. CPTI-2 treatment increased lymphoma cell content in the spleen but decreased GFP-positive cell ratios (Figure 47D+E). In the spleen, the treatments did not affect cell proliferation (Figure 47F).

This data shows that a genetical induction of additional MYC expression did not affect lymphoma cells strongly *in vitro*. After induced transcription of *MYC* in immunocompetent mice, we could not detect reporter-positive lymphoma cells at first. However, it appears that the cells need to adapt to the enhanced *MYC* transcription, to finally express high levels of MYC and to outgrow reporter-negative lymphoma cells. We hypothesize that this adaption takes place primarily in the lymphoid tissue, as we found hints of a starting outgrowth in the iLN and detected significant differences only in the iLN of our transplantation model. Further, we found that the peritoneal cavity might provide a microenvironment supporting excessive MYC expression.

Injections into the PC favored the engraftment of MYC-positive lymphoma cells and altered intracellular signaling pathways. An immune response against MYC-positive cells was primarily detected in the spleen. With these promising mouse models showing outgrowing lymphoma cells resembling RT, we continued to characterize MYC-positive cells in the hopes of working with models that correspond to RT, to find the reason for the RT-induced shift to an aggressive lymphoma, and to find possibilities to avoid or treat RT.

4.3.6. Metabolic and proteomic profiling of MYC-overexpressing RT cells

To study the metabolism of the MYC-overexpressing lymphoma cells, we performed a broad metabolic protein expression analysis using a CyTOF-based approach (Figure 48A+B). We collected splenocytes of mice transplanted with pMIG myc transduced cells once the GFP-positive lymphoma portion equaled approximately 50%. This enables the comparison of the MYC-GFP-positive RT cells with their internal controls, the GFP-negative cells from the same donor mouse. Due to technical issues, the spleens of only 2 mice were analyzed, therefore no statistical evaluation was performed. The analysis of CyTOF data using the software CYANUS revealed an upregulated expression of Ki-67, ATP citrate synthase (ACLY), CD5, glucose-6-phosphat-dehydrogenase (G6PDH), lactate dehydrogenase (LDHA), HIF-1α, isocitrate dehydrogenase 2 (IDH2), glucose transporter 1 (GLUT1), and acetyl-CoA carboxylase (ACC) in both samples in MYC-positive CLL cells (Figure 48A). The expression of the other listed metabolic proteins showed inconsistent trends. The TSNE projection showed a clear metabolic distinction between both groups (Figure 48B).

In parallel, we validated the significant MYC overexpression in GFP-positive RT cells transduced with the pMIG myc plasmid using a flow cytometry-based analysis (Figure 48C). Also, we were able to confirm the upregulation of the proliferation marker Ki-67 and the metabolic transporter GLUT1 (Figure 48D+E). Additionally, we could show that hexokinase 2 was upregulated upon excessive MYC signaling, hexokinase 1 was screened in the CyTOF analysis and did not show a significant upregulation. (Figure 48F). Upregulation of HIF-1α in MYC-positive RT cells could also be validated using flow cytometry 48G.

To further study the metabolic pathways fueling MYC-positive RT cells, we harvested splenocytes and treated them with the metabolic inhibitors 2-DG, Telaglenastat, and Etomoxir. As previously described, 2-DG prevents glycolysis, while Telaglenastat inhibits glutamine metabolism. Etomoxir irreversibly inhibits the carnitine palmitoyltransferase 1A (CPT1A) and therefore interferes with fatty acid oxidation (FAO). After inhibitor treatment, we analyzed the total viability of lymphoma cells, but more importantly the fold change of GFP-positive RT cells under the described conditions. The inhibition of all three mentioned metabolic pathways led to significant reductions of MYC-GFP-positive RT cells compared to GFP-positive control cells transduced with the pMIG empty plasmid (Figure 48H-J). The total viability of lymphoma cells in both groups is affected similarly by the treatments (Figure 48K-M).

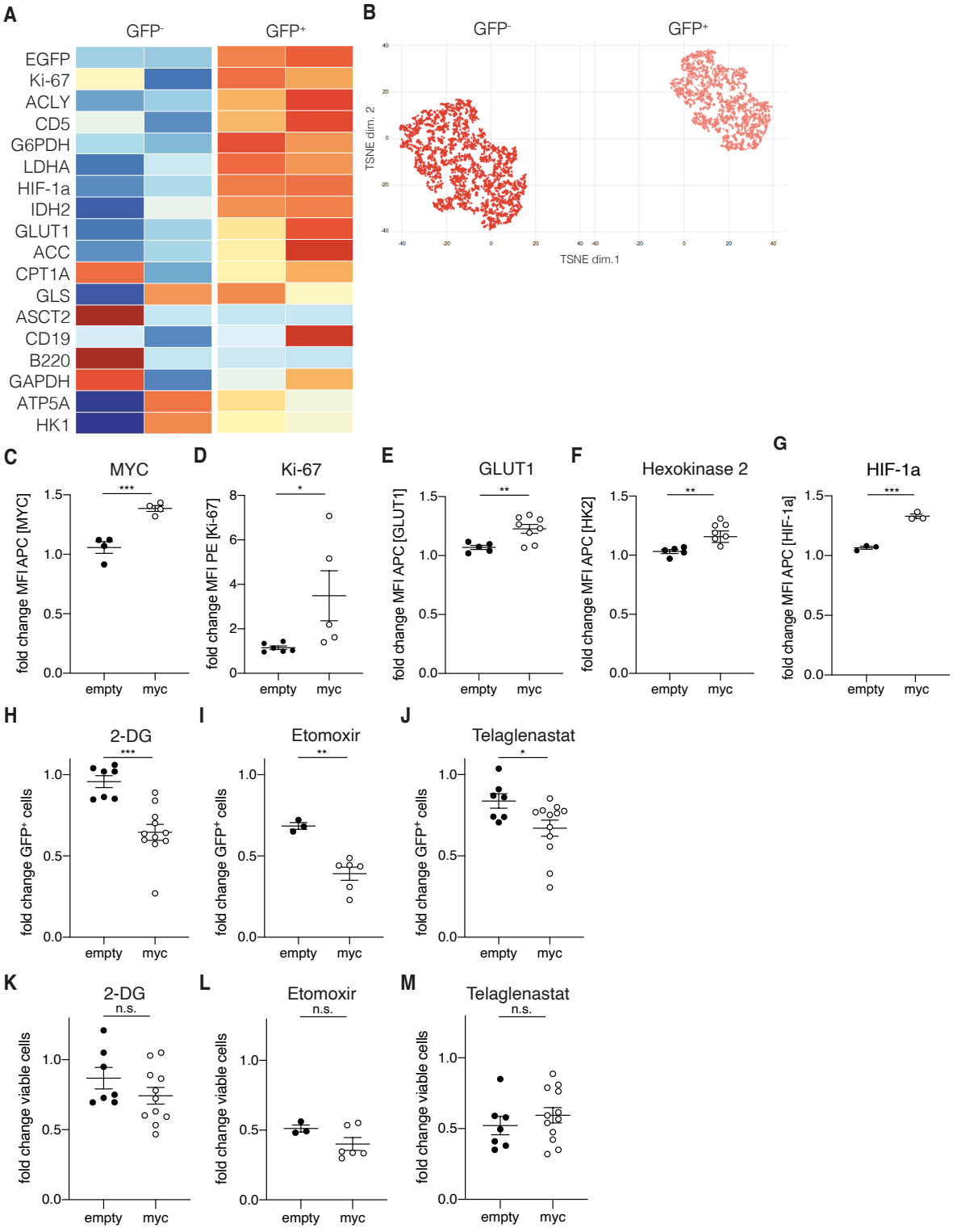

*Figure 48: Metabolic analysis of lymphoma cells expressing MYC after retroviral transduction – **A** Differential expression analysis using differential cluster abundance testing of TSNE clusters. n=2. **B** TSNE projection related to A. Analysis was performed with CYANUS (CYtometry ANalysis Using Shiny) software. **C**-**G** Intracellular flow cytometry analysis of splenocytes of R2b mice after transplantation of transduced cells. **C**: p=0.0010 **D**: p=0.0472 **E**: p=0.0092 **F**: p=0.0018 **G**: p=0.0003. **H**-**M** Flow cytometric analysis of GFP+ cells and viability by DAPI staining after in vitro treatment of splenocytes with 2-DG (0.625 µM), Etomoxir (75 µM), or Telaglenastat (25 µM) for 24 h. **H**: p= 0.0003, **I**: p=0.0019, **J**: p=0.0363. For statistical analyses, two-tailed unpaired Student's t-tests were performed. Pooled data from 3 experiments is shown. Data is presented as mean values ± SD.*

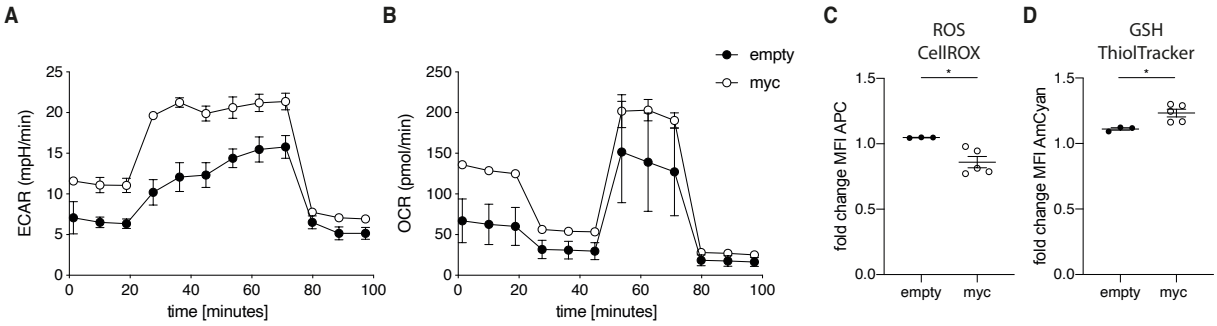

*Figure 49: Metabolic Seahorse and mitochondrial analysis of lymphoma cells expressing MYC after retroviral transduction – **A+B** Seahorse XF Glycolysis Stress Test and Seahorse XF Cell Mito Stress Test. One experiment is shown, empty: n=2, myc: n=3. **C+D** Flow cytometric analysis of intracellular ROS and GSH levels **C:** p=0.0170, **D:** p=0.0218. Pooled data from 2 experiments. Data is presented as mean values ± SD. For statistical analyses, two-tailed unpaired Student's t-tests were performed.*

Additionally, to analyze the glycolytic capacities and aerobic mitochondrial respiration of MYC-positive RT cells, we performed the Agilent Seahorse XF glycolysis stress test and mito stress test assays (Figure 49A+B). As the readout of both assays is not single-cell-based, but based on the oxygen concentration and the pH inside a 96-well plate well, it is not possible to internally compare GFP-positive RT and GFP-negative control cells from the same mouse. Technically, it would be possible to separate GFP-positive and -negative cells using a FACS sorter. However, during this process, the cells are put under physical pressure and remain under suboptimal conditions for a long period, which led to alterations of the metabolic profiles in previous experiments. Therefore, we harvested splenocytes of mice with at least 85% MYC-positive RT cells transduced with the pMIG myc plasmid in the spleen and compared them to control cells which are transduced with the pMIG empty plasmid. Using this approach, we detected a strong increase in glycolytic capacities, as well as aerobic mitochondrial respiration, in MYC-expressing RT cells.

As ROS are a byproduct of mitochondrial respiration, we further analyzed intracellular ROS levels using single-cell-based flow cytometry. Thereby, we were able to calculate the fold change of ROS in GFP^+/GFP^- cells within a sample. We were surprised to detect significantly decreased intracellular ROS levels and vice versa increased amounts of the reduced GSH (Figure 49C+D) in MYC-expressing RT cells compared to their control.

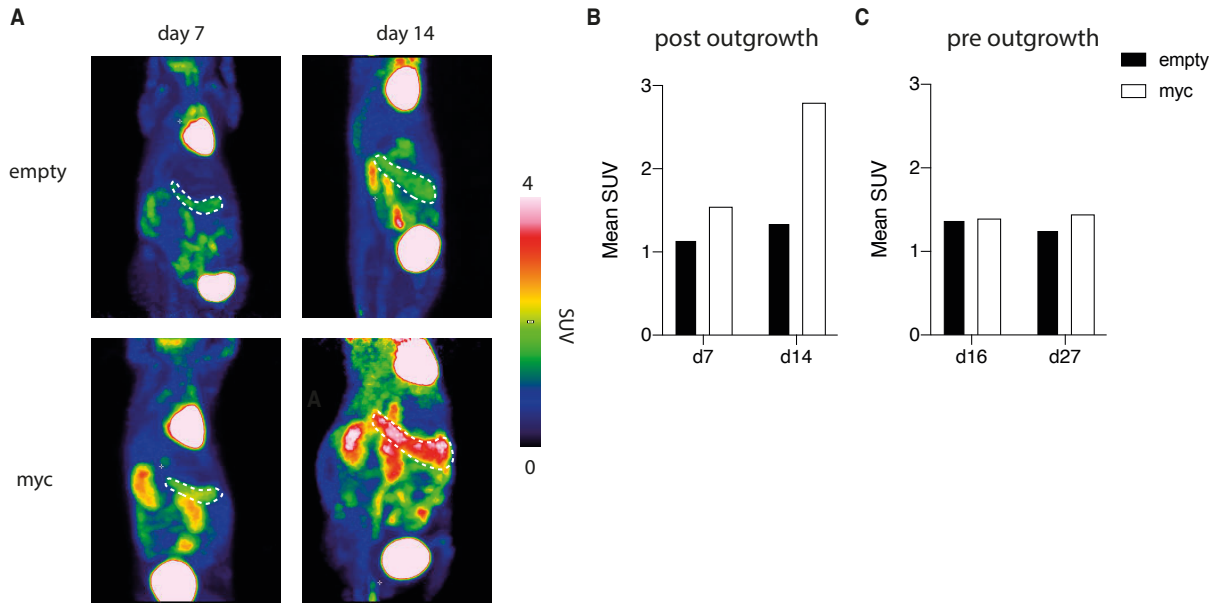

*Figure 50: PET-MRI imaging of ^{18}F-glucose uptake in R2b mice transplanted with lymphoma cells, which were retrovirally transduced with the pMIG empty or pMIG myc vector – **A** PET-MRI images on day 7 and day 14 after transplantation. Spleen outlines are marked with dotted lines. **B** Mean standardized uptake values (SUV) corresponding to the experiment depicted in **A**. **C** Mean SUV of an experimental repetition, in which CLL cells did not show outgrowth of MYC$^+$ lymphoma cells until the measured time points.*

Further, we performed PET-MRI imaging of R2b mice transplanted with lymphoma cells transduced with the plasmids pMIG empty and pMIG myc to visualize the uptake of radioactively labeled ^{18}F-glucose. The first imaging was completed on day 7 after transplantation. At this time point, spleens were about the same size (white outline) (Figure 50A) and the mean ^{18}F-glucose uptake was largely similar (Figure 50B). The second imaging was performed on day 14 after transplantation. Visibly, spleen sizes and mean ^{18}F-glucose were drastically increased on that day. Due to technical issues, we can only show the results for one mouse each for this experiment. When we imaged mice with MYC-positive lymphoma cells that did not progress over time, we could not detect increased ^{18}F-glucose uptake between both dates or both mice (Figure 50C). This indicated that the metabolic boost is coupled to the progression of MYC-expressing lymphoma cells, while it remains to be determined, whether metabolic reprogramming is a prerequisite or a consequence of MYC-driven lymphoma progression.

To analyze differences between outgrowing MYC-expressing RT cells and control cells on a protein level, we performed the array-based protein expression analysis scioDiscover of splenocytes transduced with the pMIG empty vector and the pMIG myc vector with the company Sciomics (Figure 51). The cells were harvested after the animals' individual endpoint. This assay utilizes antibodies recognizing primarily human peptides. Murine proteins that are similar in amino acid sequence to the human equivalent can be detected with this array-based protein expression analysis. Murine peptide sequences that don't resemble the human analog might not be detected, although they are differentially expressed in our samples.

The volcano blot in Figure 51A separates proteins according to their increased abundance in control or RT samples and on the statistical significance. Every event above the red horizontal line is significantly deregulated indicated by an adj. p-value > 0.05. Some of the strongest and most interesting deregulated proteins in MYC-positive RT cells are PARP1, PACA, FURIN, and CDN2B (marked with orange underlining). Figure 51B+C depict the corresponding differential expression according to adjusted thresholds |logFC| > 1 and adj. p-value < 0.001.

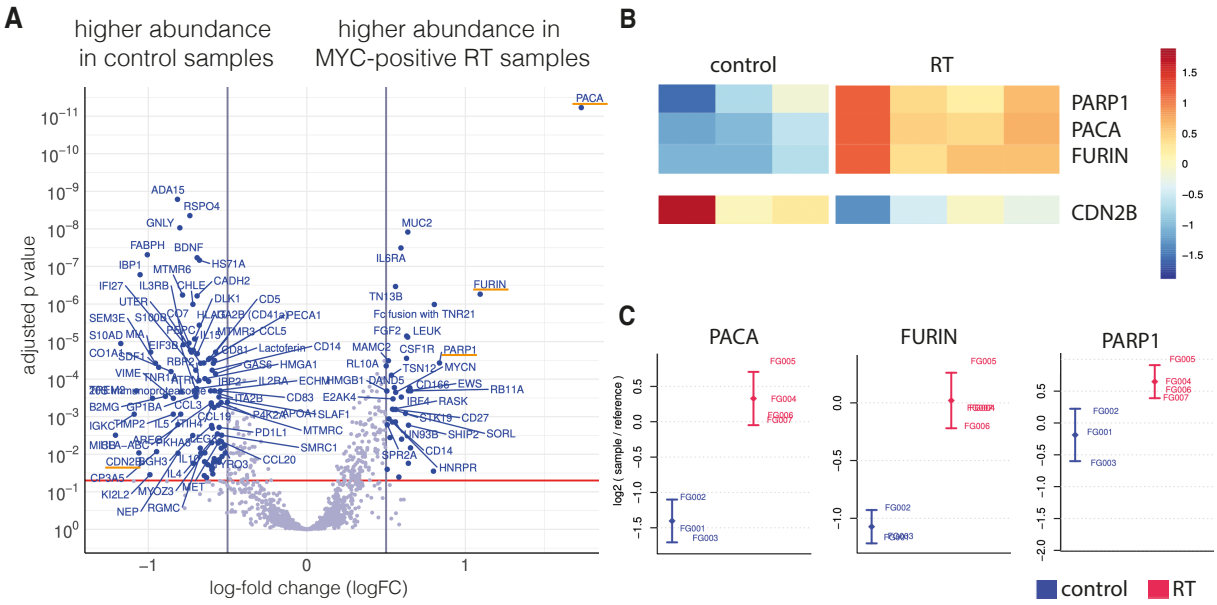

*Figure 51: Array-based protein expression analysis scioDiscover of lymphoma cells transduced with the pMIG empty vector (n=3) and RT cells transduced with the pMIG myc vector (n=4) – **A** Volcano plot showing distinct protein abundance between the two groups by visualizing p-values (adjusted for multiple testing) vs. corresponding log-fold changes (logFC). A significance level of adj. p-value = 0.05 is indicated as a horizontal red line. The logFC cutoffs are indicated as vertical lines. Proteins with a positive logFC had a higher abundance in RT samples and proteins with a negative value in control samples. Proteins with |logFC| > 0.5 and a significant adj. p-value are defined as differential and displayed with blue names (complete list in Suppl. Table 2). **B** Heatmap displaying the relative expression of proteins identified as differential according to adjusted thresholds |logFC| > 1 and adj. p-value < 0.001 in comparison myc vs control. Values were centered and scaled by proteins. **C** For selected proteins relative protein levels are presented. Individual array values for a set of differential proteins. Each sample is measured by four replicate spots per array. Rhombs indicate sample group means. Whiskers indicate one standard deviation. PACA: logFC=1.73, adj. p-value=5.89e-12. FURIN: logFC=1.09, adj. p-value=5.46e-07. PARP1: logFC=0.84, adj. p-value=3.71e-05.*

In summary, in our model, it became clear that induced *MYC* transcription does not automatically induce a phenotypical shift towards RT in lymphoma cells. Upon overcoming cell-intrinsic and T-cell control-mediated checkpoints (which remain to be characterized in detail), progressing MYC reporter-positive RT cells showed a district metabolic and proteomic profile. In strongly proliferating MYC-expressing RT cells, we saw a metabolic reprogramming characterized by increased proliferation, glucose uptake, and glycolysis. Furthermore, a wide range of metabolic proteins were upregulated in a CyTOF-based screening. Additionally, inhibition of glycolysis, glutamine metabolism, or fatty acid oxidation significantly interfered with the viability of MYC-positive RT cells. Even though we detected enhanced mitochondrial respiration, ROS levels were significantly decreased in GFP-reporter-positive cells, potentially due to an upregulation of the glutathione-based anti-ROS defense machinery. PET MRI imaging validated enhanced glucose uptake in MYC-expressing cells and emphasized that although *MYC* transcription is induced in lymphoma cells, they must adapt to increased MYC signaling to exhibit MYC-GFP expression and altered metabolic properties. Finally, we detected a broad range of changes in the proteasome of MYC-positive RT cells, that distinguish them from standard lymphoma cells, and that might help to explain, how MYC expression transforms CLL towards the aggressive RT lymphoma.

5. Discussion and outlook

5.1. Effects of diets with different fat contents on blood parameters and CLL pathogenesis

5.1.1. Effects of Western diet and PB low fat diet on murine CLL pathogenesis in immunocompetent wt mice

Phenotype of mice on a Western diet

Obesity is associated with an increased risk of developing many serious health conditions, including hypertension, coronary heart disease, stroke, osteoarthritis, and cancer.[110] It has been shown that people who follow a Western dietary pattern are more likely to be diagnosed with CLL than people who adhere to a Mediterranean diet.[111] To study the effects of a plant-based low fat diet and a Western diet on murine CLL pathogenesis, we used a mouse model in which mice were transplanted with murine CLL cells after being fed specific diets for several weeks. The chosen Western diet mirrors the average macronutrient consumption of adults in the United States from 2013 to 2016 (Figure 52). The main component of the Western and American diet is carbohydrates, followed by almost as high amounts of animal fats. Proteins make up the smallest part of the diet. Monitoring of the body weight from the beginning of the dietary change pointed out that the increase in weight can be successfully controlled with the different diets in immunocompetent C57Bl6/J mice. Parallel to this, the blood parameters cholesterol, LDL, and HDL increased due to the Western diet as described in the literature.[112] Originally, two additional experimental groups were analyzed, in which the mice had access to running wheels. It was not possible to document the actual usage of the running wheel and we could not detect differences in weight gain or blood parameters, which is why these experimental conditions were not continued.

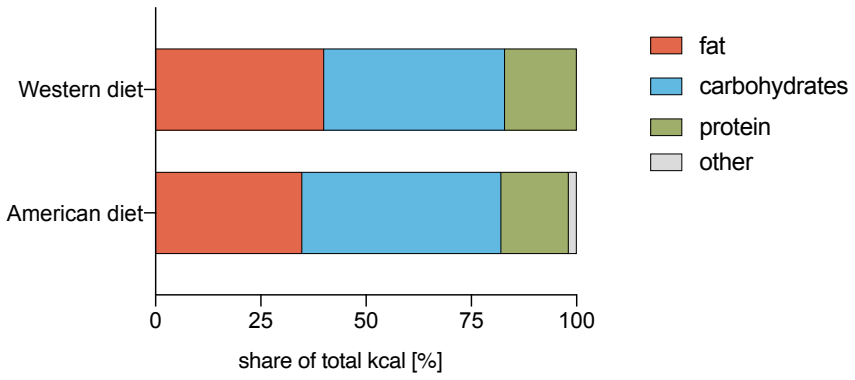

Figure 52: Composition of the utilized murine Western diet (40% fat, 43% carbohydrates, 17% protein) and the mean macronutrient intake of adults in the United States of America between 2013 and 2016 (age-adjusted to the year 2000 standard population using four age groups: 20–44 years, 45–64 years, 65–74 years, and 75 years and over) (34.8% fat, 47.3% carbohydrates, 16% protein).[113] Detailed data can be found in Suppl. Table 1.

To mimic a Western lifestyle the mice were fed the Western diet or the PB low fat diet for at least 10 weeks, before receiving CLL transplantations. When transplanted with CLL splenocytes, the engraftment in the PB over the time course of the disease showed no significant differences between both groups. Once the mice were terminally ill, the spleen size did not reveal significant differences between mice on the PB low fat diet and Western diet. However, the fact that mice on the Western diet show a reduced lifespan after CLL transplantation suggests that splenic progression was promoted by the diet. We did not compare total viable CLL cell numbers in the spleen, nor in the bone marrow, as some mice in this survival study have been found dead, and therefore no reliable counts could have been performed. Nevertheless, this suggests that the effects of the diet require long observation periods to unravel their effect on CLL progression. To further analyze the engraftment behavior, a possible next step would be a proliferation analysis, for instance with a Ki-67 staining, as differences in proliferation and cell viability cannot be ruled out.

Indication of systemic inflammation upon Western diet

Our study suggests that mice on a Western diet may have slightly higher levels of the pro-inflammatory cytokines MCP-1 (monocyte chemoattractant protein-1) and IL-1α in their plasma compared to mice on a PB low fat diet. MCP-1, also known as CCL2, is one of the key factors regulating migration and infiltration of monocytes and macrophages via the binding to its receptor CCR2.[114] It is known that MCP-1 levels are elevated in the serum of CLL patients.[115] Cancer cells are considered to be the main source of MCP-1, nevertheless, non-cancer cell in the stroma also produce MCP-1 in response to stimuli.[116] One example of non-malignant cells producing MCP-1 is the macrophage subgroup of M1 macrophages. Both “classical” M1 macrophages and “alternative” M2 macrophages are closely related to inflammatory responses, whereby M1 macrophages are associated with pro-inflammatory processes and M2 macrophages are primarily involved in the anti-inflammatory responses.[117] Published findings have revealed elevated MCP-1 levels in WT mice subjected to obesity through a high fat diet. Furthermore, MCP-1 transgene mouse models have demonstrated insulin resistance, adipose tissue infiltration by macrophages, and increased hepatic triglyceride levels.[118,119] Unfortunately, we could not make a statement about the usage of the running wheels given to the mice in our pilot experiment. In high fat diet experiments with strict timing of physical activity, it was shown that exercise did not induce loss of body or adipose tissue mass, but led to phenotype switching from M1 macrophage to M2 macrophage in obese adipose tissue besides inhibiting M1 macrophage infiltration into adipose tissue. Consequently, physical exercise inhibits inflammation in adipose tissue.[120]

Additionally, research has indicated that a high fat diet can activate inflammatory signaling through IL-1R1, which binds to IL-1α and IL-1β.[121,122] Moreover, the administration of an IL-1R antagonist has been shown to enhance glucose tolerance and insulin secretion in a mouse model exposed to a Western diet, offering protection against hyperglycemia.[123] In light of this data, we propose that the consumption of a Western diet can trigger inflammation within adipose tissue, accompanied by the infiltration of M1 macrophage and global upregulation of proinflammatory cytokines.

Cancer cell- and inflammation-promoting microenvironment through Western diet

Further, we detected that different diets affect the quantitative composition of the cell populations of the spleen. Percentage change in cell populations can be caused by cell migration, cell death, or enhanced cell proliferation of specific cells. Mice on Western diet showed a reduction in NK cells, macrophages, and dendritic cells in their spleens. This reduction could be caused by migration into adipose tissue and adjacent lymph nodes conveyed through chemoattractants like MCP-1, or metabolites like lactic acid.[124-128] As CLL cells persist in the peripheral blood and the secondary lymphoid organs,[71,129] a further step in this project could be the analysis of lymph nodes adjoining fatty tissue in Western diet mice. As high rates of infiltrating tumor-associated macrophages (TAMs) correlate with a poor clinical outcome in cancer diseases, cytokines that promote immune escape, anti-apoptotic effects, and chemoresistance of tumor cells,[130] migration of macrophages into the TME of the lymph nodes could explain the reduced survival of CLL-burdened mice on the Western diet.

Analyzing further cell populations, we found that CD3 TCRβ double-positive T cells are found in the same quantity in the spleens of both diet groups, but the activation stages were unequally represented. Mice on the Western diet showed a higher percentage of CD25 CD4 double-positive T cells. CD25 is a prominent cellular activation marker, which is upregulated within 24 hours of TCR stimulation and remains elevated for several days. Constitutively, it is expressed on T-cell subsets, such as regulatory and resting memory T cells.[131-133] Further analysis of the intracellular expression of FoxP3, which characterizes CD25 CD4 double-positive T cells as regulatory T cells, is required to clearly define the Treg population in our model. However, the reduction of naive CD4 and CD8 T cells and an increase in effector memory CD4 and CD8 T cells, with significant changes only in the subset of CD4 T cells. In summary, our data indicates an elapsed activation of T-cell populations due to the feeding of a Western diet, which could be induced due to inflammation.

This suggests that an intake of the different diets can alter the abundance of specific immune cell populations in the spleens of our experimental mice through changes in migration patterns and differential activation. Especially enhanced activation of T-cell populations in mice on the Western diet indicates a proinflammatory environment, which can affect CLL engraftment and progression in our model. Further, it should be evaluated to which degree Tregs are affected by different diets and how much their involvement influences CLL disease progression.

Microbial changes upon the Western diet

Analyzing 16S rRNA sequencing data, we could show that the gut microbiome of mice on the PB low fat diet and the Western diet differ significantly in their composition. This is described by the beta diversity, the distance between two groups of samples. Also, it was detected that die gut bacteria richness within a sample, also known as alpha diversity, is strongly reduced in the cecal content of mice on the Western diet. The richness of microbiota species characterizes a healthy digestive microbiome.[134] The microbiome itself, but also microbial metabolites affect the human overall health, fitness of the immune system, and cancer therapy.[135]

For example, it was shown that immune checkpoint blockade therapy can induce lymph node remodeling, DC activation, and translocation of gut bacteria into lymph nodes facilitating anti-tumor immunity.[136] Also, it was described that a reduction of gut bacteria due to antibiotic treatment leads to the transit of Tr17 cells to tumors and associated lymph nodes, where they reduce immune checkpoint blockade therapy success.[137]

Further, we detected reduced relative abundances of gut bacteria belonging to the Muribaculaceae and Colidextribacter family and an increased relative abundance of gut microbiota of the Desulfovibrionaceae family in mice on Western diet. Bacteria of the Muribaculaceae family are generally classified as beneficial to the host as they are associated with strengthened intestinal mucosal barrier function.[138] Additionally, the loss of Muribaculaceae was correlated with inflammation-associated parameters and contributed to colitis development.[139] Abundance of Muribaculaceae was firmly correlated with the production of the short fatty acid propionic acid and its salts through the fermentation of microbial macronutrients.[140] Propionate was found to inhibit the activation of CD8 T cells[141], which could explain the described negative correlation between Muribaculaceae and inflammation, and the observed T-cell activation in our mouse model.

Colidextribacter have also been found with greater abundance in mice on PB low fat diet, as well as in human studies in non-obese participants.[142] However, other sources report a positive correlation of Colidextribacter with high fat diets, fat accumulation, and specific bile acid monomers in mice [143-145] This suggests that the abundance of Colidextribacter is regulated in a more complex manner.

Bile acids however play a crucial part in the composition and function of the gut microbiome. In the host system, they are an important end product of cholesterol metabolism and are crucial for fat digestion, as they emulsify fat to enable lipid absorption in the small intestine. Microbes in the gut respond to bile acids, can modify levels of bile acids, and transform bile acids affecting host lipid metabolism.[146,147] Enhanced bile acid levels were described to alter the gut microbiota significantly, with an increased abundance in Desulfovibrionaceae.[148,149] With elevated dietary fats leading to high levels of bile acids,[150] this explains the strong increase of the thermophilic sulfate-reducing bacteria in our mouse model on the Western diet. Most bile acids are reabsorbed during small intestinal transit recirculating to the liver, but remaining bile acids entering the colon undergo various transformations by the gut microbiota, resulting in secondary bile acids with signaling functions.[150,151] Through interactions of transformed bile acids with host receptors, colon bacteria, including the Desulfovibrionaceae family, can regulate not only lipid absorption, but also lipid, glucose, and energy metabolism, inflammation, and tumorigenesis of the host.[152,153]

Therefore, we suggest that the reduced richness of alpha diversity, as well as an altered composition of the gut microbiome, could be jointly responsible for the observed inflammation, immune cell migration, and finally, the reduced overall survival of CLL-burdened mice.

One aspect that has been neglected in our research, is the development of CLL under the conditions of a Western diet, as a transplantation model, in which Eμ-*TCL1* transgenic mice develop CLL on a regular chow diet, was used. It is very likely that a Western diet also influences the initial emergence of CLL. To investigate in that manner, a long-term experiment could be performed, in which Eμ-*TCL1* transgenic littermates are fed with the specific diets from birth until CLL development. Unfortunately, it is not possible to co-house mice on different diets, which has an impact on their gut microbiome, but this could be addressed by exchanging dirty bedding from the mice fed with different diets.

5.1.2. Effects of Western diet and whole food plant-based diet on human blood values *in vivo*

Already in the early 1990s, the Malmö Diet and Cancer Study (MDCS) started a long-term screening survey to establish possible causalities between diet and cancer incidence.[154] In our human study, we wanted to examine the alterations in blood parameters after a change in diet, to find the causes of the link between diet and CLL. Therefore, our healthy volunteer participants changed their diet for 7 consecutive days, followed by blood draws. Then the participants were asked to increase their uptake of animal fats, processed foods, and refined sugar in the week of the designated Western diet. This resulted in significant changes in serum LDL and cholesterol already after only 7 days on a whole food plant-based diet compared to a Western diet, as most published studies cover a period of 16 weeks up to 16 years.[155-157] This short period might have been beneficial for the results, as it is easier to stick to strict dietary restrictions for only 7 days than for a longer period.

Also surprising to us was the fact that there were hardly any differences in blood lipids after the participants' usual diet compared to the intentionally unhealthy Western diet. This might suggest that to see even small differences in blood lipids, it is necessary to perform significant changes in the dietary uptake. Besides changes in cholesterol and LDL, a significant increase in thrombocytes and the trend of amplified leukocytes were detected. The collected serum was used in the following to perform *in vitro* experiments with primary human CLL cells.

5.1.3. Effects of high lipid concentrations on human CLL cells *in vitro*

CLL cell survival in medium supplemented with Western diet serum

To determine whether serum factors that vary depending on the diet impact CLL viability and proliferation, the collected serum of the volunteer study was used as a culture supplement. In general, primary human CLL cells do not proliferate and viability decreases rapidly *in vitro.* Western diet serum could not enhance the proliferation of primary CLL cells, but it was possible to enhance the CLL cell viability after 48 h significantly.

The CLL cell lines MEC-1 and OSU-CLL proliferate vigorously in culture. This might be the reason why the proliferation of the cell lines could not be further enhanced. Nevertheless, cell viability increased after incubation in Western diet serum. This indicates that increased concentrations of blood lipids and possible alterations in blood cytokines have a positive effect on CLL cell fitness and survival. Although many cytokine levels can be elevated through the intake of a high fat diet, only some promote CLL survival. One factor that could play a role in Western diet-induced CLL viability is B-cell-activating factor (BAFF), a cytokine belonging to the TNF family. Interestingly, serum BAFF levels are positively correlated with high fat diets and body fat in human and murine studies.[158,159] Further, BAFF and its receptors are closely related to the physiological activity of adipose tissues.[158,160] Also, a proliferation-inducing ligand (APRIL) was found to be expressed by mature adipocytes.[160] Both, BAFF and APRIL, enhance CLL and support CLL survival through activation of the canonical NF-κB pathway[161] and could therefore be responsible for enhanced CLL viability after incubation with human serum. An additional adipocytokine supporting CLL survival is CXCL13, which can promote CLL cell survival through inactivation of transcription factor FOXO3a.[162,163] In a more complex manner, also insulin growth factor-1 (IGF-1) levels can be increased in obesity and by dietary intake of animal proteins.[164] In patient CLL, IGF-1 receptor expression is positively correlated with the antiapoptotic protein Bcl-2,[165] therefore, a Western diet-induced increase in IGF-1 levels could be responsible for improved CLL cell viability.

CLL signaling in Western diet serum

To generate different cholesterol conditions *in vitro*, soluble cholesterol was added with final concentrations of 25 µM and 75 µM based on published data.[166,167] Signaling analysis of MEC-1 cells incubated with 75 µM of added cholesterol showed increased phosphorylation of PLCγ, IKKα/β, AKT, ERK1/2, STAT3, and p65 compared to cells incubated with 25 µM or 0 µM already after 15 min. The elevated signaling is detected also at 1 h but decreased after 4 h of incubation. Interestingly, not only the phosphorylation events were upregulated, but global protein concentrations as well. The metabolic proteins PFK-1 and aldolase were also upregulated after incubation with 75 µM of soluble cholesterol after 15 min. Cholesterol homeostasis is tightly regulated by cholesterol synthesis in the endoplasmic reticulum (ER), uptake from lipoprotein particles, and efflux to extracellular acceptors enabling adaption to high or low cellular cholesterol levels.[168] Intracellular transport mechanisms translocate cholesterol into the plasma membrane forming lipid rafts, which play a critical role in the activation of signaling pathways including cell growth, adhesion, migration, invasion, and apoptosis.[169] Cancer cells contain higher levels of intracellular cholesterol and lipid rafts than non-cancer cell populations, additionally, it is known that many signal pathways involved in cancer progression, e.g. the PI3K/AKT pathway are modulated by lipid rafts.[170] Therefore, we hypothesize that the observed increase in cell survival and phosphorylation events are caused by amplified lipid raft formation. The reduction of signal transmission after 4 h is most likely caused by negative feedback regulation and restoration of intracellular cholesterol homeostasis orchestrated by the ER.

With the collected data, we provide clear evidence of dietary effects on CLL. However, it is important to separate the effect of high lipid levels on the CLL cells but also the whole organism, including the immune system and gut microbiome.

5.2. Negative feedback regulation of MAPK signaling in CLL

ERK1/2 phosphorylation is tightly linked to DUSP6 protein levels

Under steady-state conditions, intracellular MAPK signaling is strictly regulated and drives cells towards proliferation and differentiation.[171,172] DUSP1 and DUSP6 function as downstream negative regulators to maintain essential signaling homeostasis.[173] We showed that MAPK signaling levels, measured via the phosphorylation of ERK1/2, are tightly linked to DUSP6 protein levels in CLL cells. Additionally, ERK1/2 binding regulates DUSP6 enzymatic activity in a substrate-induced activating manner.[174] In line with that, increased DUSP6 levels are found in more aggressive RAS/BRAF mutant CLL samples.[93]

Excessive MAPK pathway activation induces cell death in CLL cells

Therapeutic approaches in CLL treatment are largely focused on the application of potent tyrosine kinase inhibitors to suppress oncogenic signaling below a minimum threshold for survival. Contrarily, in this project, we discovered that BCI-induced inhibition of DUSP1/6 in CLL cells doesn't enhance cell survival, but rather drives CLL into cell death. This means that an increase in MAPK signaling in CLL cells above a given threshold leads to unavoidable cell death. This is not entirely a new concept as hypersignaling has been described in CLL[92] and acute lymphoblastic leukemia (ALL)[175] as a means of inducing cell death before. Also, it was previously described that excessive levels of MAPK signaling led to cell death in melanoma cells,[176] proving that balanced MAPK signaling is crucial, especially for cancer cell survival. RAS mutations, upstream of the RAS/RAF/MEK/ERK signaling cascade, are found in approximately 19% of all cancer patients.[177] Among other things, this is the reason why the RAS/RAF/MEK/ERK signaling cascade proteins have been studied heavily to determine whether it is possible to suppress their activity in cancer. Besides, this signaling pathway is often implicated in the resistance to therapeutic approaches.[178-183] This emphasizes the necessity to find alternative therapies, such as cell death through hypersignaling, with the MAPK-negative regulators DUSP1 and DUSP6 as novel targets in the treatment of CLL.

MAPK signaling-induced mitochondrial ROS production leads to DNA damage

Mechanistically, we discovered that increased MAPK signaling led to mitochondrial ROS accumulation, which subsequently resulted in DNA damage (Figure 53). ROS describe a family of short-lived radicals such as the hyperoxide anion (O2-), hydroxyl radical (OH·), and the peroxyl radical (ROO·), as well as stable molecular oxidants such as hydrogen peroxide (H2O2), hydroperoxide (ROOH), and ozone (O3). Although recent studies have shown ROS' supporting functions in the immune response[72] and as a signaling molecule,[184,185] they are primarily known as harmful byproducts of mitochondrial respiration. ROS are well known to cause DNA damage, such as strand breakage, or formation of 8-oxo guanine,

finally resulting in DNA degradation.[52,53] Additionally, ROS are described to trigger DNA replication stress after RAS activation.[186,187] Therefore, we suggest that mitochondrial ROS are a deciding factor in the fate of keeping the balance between cell survival and cell death. Further, leakage of mitochondrial DNA (mtDNA) into the cytosol can appear as a result of mitochondrial metabolic balance disruption due to cellular stress, or upon infection.[188] Several receptors and pathways are involved in the sensing of cytoplasmic mtDNA leading to innate immune activation.[189] Thus, also the complex interplay of innate immune cells could lead to a depletion of CLL cells after DUSP1/6 inhibition *in vivo.*

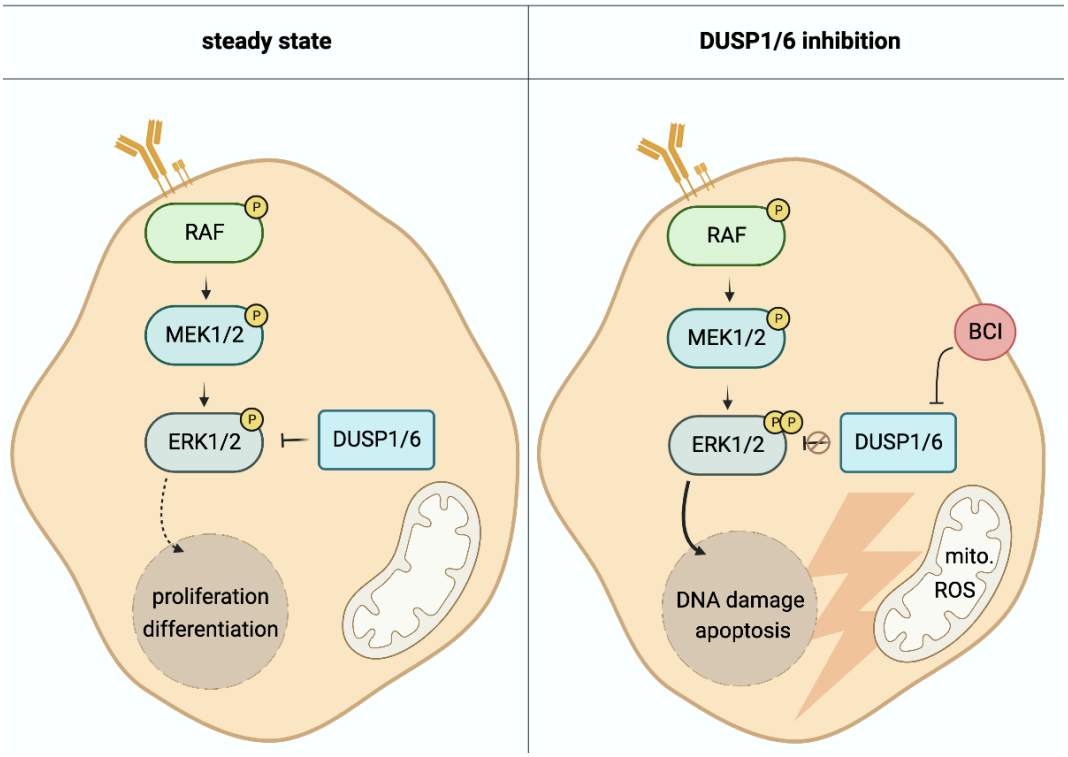

Figure 53: Graphical summary of the intracellular signaling events after DUSP1/6 inhibition in CLL cells. MAPK deregulation by DUSP1/6 inhibition is highly effective inducing apoptosis via the DNA damage response pathway in CLL cells. Hence, DUSP1/6 inhibition is a promising novel treatment concept to eliminate CLL cells including drug-resistant cases.

Taken together, this data shows high levels of DUSP6 are associated with poor clinical outcome and linked to high levels of MAPK signaling. Further, enhanced MAPK signaling through chemical inhibition results in impaired survival of CLL cells. We suggest that a controlled MAPK signaling homeostasis in CLL cells is crucial to avoid ROS-induced DNA damage and apoptotic cell death. Consequently, we propose DUSP1/6 inhibition as a novel approach to treating naive or kinase inhibitor-resistant CLL cases.

5.3. Mutations and their potential to drive lymphoma towards RT

5.3.1. Constitutively active CARD11 expression in murine and human CLL

As part of the CBM complex, CARD11 plays a crucial part in the induction of NF-κB and JNK signaling. CARD11 mutations are found in cases of CLL, but more commonly in DLBCL and RT.[22,40,190] Therefore, we tried to generate a model for RT via the induction of constitutive active CARD11 in mature CLL cells. With the expression of CARD11^{L225LI} the CBM complex is permanently assembled and downstream signaling cascades are constantly induced.

Altered proliferation and metabolism in CARD11^{L225LI} expressing CLL cells

CARD11^{L225LI} expression in human CLL cell lines and murine CLL splenocytes led to increased cell proliferation, upregulation of metabolic proteins, and glycolysis *in vitro*. This confirms the described link between the CBM complex and NF-κB signaling, as enhanced NF-κB signaling is known to drive proliferation in lymphocytes and increase the expression of GLUT1, which enables enhanced glucose uptake allowing a tumor-promoting upregulation in glycolysis.[191,192]

Differential chemokine receptor profile in CARD11^{L225LI} expressing CLL cells

Additionally, we detected an upregulation of CXCR4, CXCR5, and MYC in CARD11^{L225LI} expressing splenocytes *in vitro*. The extracellular chemokine receptors CXCR4 and CXCR5 coordinate CLL migration and homing. Their respective ligands CXCL12 and CXCL13 are highly expressed in lymphoid tissue, facilitating migration towards lymph nodes.[193,194] A relocation of CLL cells from the PB into lymph nodes is an occurrence detected in RT.[195] Additionally, it was described that Eμ-*TCL1* mice with gain of function mutations in CXCR4 show B-cell enrichment with a transcriptional signature resembling RT. Notably, MYC activation was associated with increased CXCR4 expression.[196]

CARD11^{L225LI}-GFP expression in CLL cells induces CD8 T-cell response in mice

In vivo, the most striking was the reduction of CLL cells in the PB, the comprehensive absence of GFP-positive CLL cells, and increased overall survival of TAM-treated mice. Reasons for these observations could be CLL cell death due to intrinsic events, cell death due to extrinsic factors, or migration of CLL cells into other tissues. The latter can be ruled out, as GFP-positive CLL cells couldn't be found in any other organ of TAM-treated mice. Cell death due to intracellular events could occur *in vivo*, as we detected reduced cell viability in CARD11^{L225LI}xTCL1xMb1CreERT2 splenocytes treated with 4OHT *in vitro*. Also, as in point 4.2. discussed, elevated signaling above a certain threshold can induce cell death in CLL. Nevertheless, we did not detect affected viability in CLL cell lines after CARD11^{L225L} expression, therefore, we do not suggest cell death as the main reason for the complete absence of CARD11^{L225L}-GFP-expressing CLL cells *in vivo*. The most likely reason, why we could not detect GFP-positive CLL cells in experimental mice and the collapsed CLL content in PB after TAM treatment is a cytotoxic T-cell response, as we observed enhanced CD8 T-cell activation after CARD11^{L225LI} expression in CLL *in vivo* and *in vitro*.

One reason for the immune response could be the intracellular expression of the human CARD11 mutant and GFP, which are presented on MHCI molecules after degradation. This is a weak point of our transplantation model, as recipient T cells undergo negative selection without being exposed to these xenoantigens. N. Knies et al.[40] and A. Kratzert from the Ruland lab worked with B cells constitutively expressing the CARD11^{L225L}-GFP construct, which didn't lead to an immune response.

Another reason for the observed T-cell activation could be the loss of CLL's immunosuppressive functions, which could be part of the RT transformation process, as it is described that CLL and RT have very distinct immune signatures.[197] During the CLL disease course, elements of the innate and the adaptive immune system are altered to induce a tolerant environment that favors CLL development. Main dysfunctions are found in the T cell compartment, with inhibition of CD8 and CD4 activated effector T cells, exchanged by exhausted subsets.[100] Mice after tamoxifen treatment and a low percentage of CLL cells in the PB showed the highest ratio of CD8 effector T cells. We hypothesize that the CARD11^{L225L} expression results in a shift of CLL cells towards RT cells, which lack immunosuppressive characteristics and therefore induce a T-cell response leading to CLL depletion. Additionally, PB T-cell receptor clonality was found to be significantly decreased in RT compared to CLL patients, proposing higher T-cell diversity in RT.[197]

We originally performed a transplantation experiment in R2b mice, which lack B and T cells, to confirm or rule out the responsibility of the immune system in our collected data. However, since donor T cells are strongly engrafted, these experiments were not conclusive and should be repeated with T-cell depletion to be able to conclude.

Even though activating mutations of CARD11 are relatively rare in RT (5-12.5%),[22,23] this model is still interesting to investigate. Since the retroviral transduction of primary murine CLL cells was established during the work for this thesis, it would be a final possibility to transduce fresh Eμ-*TCL1* transgene splenocytes with our existing pMIG CARD11^{L225LI} plasmid and repeat transplantation experiments with the steadily transduced cells in R2b mice. In the absence of a T-cell response, it would also be interesting to follow the possible migration of the CARD11^{L225LI}-expressing cells. This would be possible with our CLL cell lines expressing the bioluminescent luciferase-luciferin system, which were not yet transduced with our plasmids used to mimic RT mutations. These cell lines express the firefly luciferase *in vivo* and *in vitro*. In transplantation experiments, i.p. injections of D-luciferin (D-LH2), the luciferase catalyzes the reaction between D-luciferin and ATP resulting in light emission. This bioluminescent signal can penetrate the skin and therefore can be detected in anesthetized mice to visualize the location and quantify the presence of the transduced cells.[198,199] Interestingly, in a subset of RT and the first RT cell line U-RT1, the assembly of a CBM is implemented using CARD9 instead of CARD11. That's a remarkable insight, as until now, CARD9 has been known to be an activator of NF-κB signaling in myeloid cells.[200]

In summary, the induction of CARD11^{L225LI} in CLL cells led to the appearance of some RT characteristics, like the upregulation of glycolysis, expression of LN homing receptors, and differential modulation of T-cell subsets. Most importantly, a mouse model has to be generated, in which the influence of T cells can be specifically examined and in which CARD11^{L225LI}-positive lymphoma cells can be detected and studied. For further analyses, the retroviral transduction model, or gain of function mutations of CARD9, could be used to mimic constitutive CBM singling in murine splenocytes.

5.3.2. Constitutively active AKT expression in murine CLL *in vivo*

Active AKT signaling was described to trigger CLL towards RT via Notch1 signaling in mouse models with a constitutive expression of a gain of function mutant of AKT in B cells.[34] However, in contrast, we observed that acute activation of AKT induces cell death in CLL.[92] Therefore, we hypothesized that CLL cells must adapt to high AKT signaling and acquire strategies to prevent cell death. Understanding these adaptation strategies may be important to understand and potentially treat or prevent the malignant transformation. We thus tested whether we could establish a mouse model for RT with an induction of AKT signaling in matured CLL cells, which resembles the natural formation of RT. However, none of our experiments were successful in promoting RT by AKT activation. We can rule out a reduced effect of 4OHT and TAM and application errors in our studies since the tamoxifen derivates showed full effect in other experiments in parallel. Therefore, acute expression of constitutively active AKT signaling is lethal in murine CLL, and in the performed long-term transplantation experiments we did not see evidence of adapted AKT^{E17K}-GFP-positive CLL cells, which resemble RT.

5.3.3. MYC overexpression in murine and human lymphoma cells

MYC was found to be involved in several germinal center-derived lymphomas, whereby oncogenic events leading to enhanced MYC signaling can overcome the inhibitory effect of physiological repressors, such as Bcl-6 or BLIMP1.[201] In RT, MYC alterations are found in up to 70% of all cases and co-occur with specific aberrations such as the loss of p53, CDKN2A/B, or gain of Bcl-2/ Bcl-6.[30] To mimic a shift towards RT, we first overexpressed MYC in human CLL cell lines and murine primary CLL cells *in vitro*. There, no effects on cell viability, proliferation, cell size, and metabolic pathways after MYC induction were detected. However, when overexpressing MYC in mature CLL cells *in vivo*, we generated a model that displays an acquired shift towards stronger proliferative lymphoma with a distinct metabolic and proteomic profile that resembles multiple features of RT.

MYC overexpression in lymphoma cells induces initial cell depletion

After TAM-induced transcription of *MYC* in transplanted splenocytes in immunocompetent mice, we detected a reduction of MYCxTCL1xMb1CreERT2 cells and no appearance of reporter-positive cells in the blood. However, in immunocompetent R2b mice, we did not see distinctive engraftment patterns between the tamoxifen-treated and the control group. When re-transplanting prior induced MYCxTCL1xMb1CreERT2 splenocytes or pMIG myc transduced lymphoma cells, we could detect depletion of MYC-reporter-positive cells in the PB and other secondary organs in the presence of cytotoxic CD8 T cells. The observed immune response towards these cells could be triggered by various factors. The reporter protein CD2, as well as the induced MYC, consist of human amino acid sequences, which could potentially induce immune responses in mice. Since we transplant the cells of interest in mature mice, their T cells recognize the xenoantigens, which can result in the depletion of the cells.

Another reason for the disappearance of lymphoma cells in the PB after tamoxifen treatment could be cell death due to elevated activation of MYC signaling pathways leading to oncogene-induced cell death. Our data showed that MYC signaling results in enhanced metabolic processes and intracellular signaling. Spontaneous induction of these processes could lead to cell death due to exceeding signaling thresholds, the insufficient presence of necessary metabolites, or too high generated stress levels.

Lymphoma cells adapt to high MYC signaling

However, we detected outgrowth of MYC-positive cells up to 90 days after tamoxifen application, or after transplantation of pMIG myc transduced lymphoma cells. This indicates that although *MYC* transcription is induced, MYC expression or function is suppressed intracellularly until the cells have adapted to excessive MYC signaling and its consequences. Interestingly, the fact that we could not detect any differences *in vitro* speaks for the strict regulation of MYC expression, for which the cells first have to adapt. In line with that, it was shown that it can take up to 19 years before the transformation towards a RT phenotype in a long-term study of human RT patients.[202] The reasons for the observed delayed metabolic and phenotypic shift in lymphoma cells after MYC expression are complex and have not yet been clarified.

HIF-1α alters extracellular pH in MYC-positive lymphoma cells possibly enabling cell transformation

Among other things, the transcription factor HIF-1α was found to be increased in the analyzed MYC-positive RT cells. Its transcriptional activity is enhanced by hypoxic conditions, but also by intracellular signaling (RAS/RAF/MEK/ERK, PI3K/AKT/mTOR, or MYC), as well as end products of glycolysis.[203-207] At the same time, HIF-1α stabilization induces an increased expression of glycolytic enzymes.[207] Additionally, besides oncogene activation and cancer cell transformation, HIF-1α is described to induce the expression of different pH-regulating systems, to cope with acidosis in the TME, such as the lymph nodes.[208,209] For once, HIF-1α can regulate proton distribution through the upregulation of the proprotein convertase FURIN,[210] which was verified to be strongly upregulated in MYC-positive RT cells by proteomics analysis.

FURIN enables proteolytic activation of different precursor proteins, such as pro-Ac45, in different cell types and *ex vivo*.[211,212] Ac45 is a subunit of the vacuolar-type ATPase (V-ATPase) and therefore a part of a transmembrane proton pump system responsible for an alkaline intracellular and acidic extracellular environment.[213] Enhanced employment of V-ATPases in the plasma membranes of cancer cells to maintain an extracellular alkaline pH is a confirmed survival strategy in acidic TMEs[214] and was shown to be responsible for tumorigenic transformations of fibroblasts.[215]

Due to a possible HIF-1α-enabled alkalization of the TME in MYC-positive lymphoma, the cells could experience the necessary adaption to the increased MYC expression and a first shift towards RT, as among other things MYC-induced enhanced glucose metabolism increases extracellular acidification. The ability of MYC-expressing lymphoma cells to maintain an alkaline intracellular milieu via the overexpression of FURIN and the linked upregulation of V-ATPase may also enable the observed invasion into the lymph nodes in our mouse model, resembling RT. Interestingly, a proximity extension assay (PEA) analysis of patient plasma proteins revealed a relative upregulation of FURIN in the blood of DLBCL patients, but not in CLL patients.[216] This further supports the resemblance of the analyzed MYC-positive lymphoma cells with DLBCL-type RT.

MYC RT cells show enhanced glycolysis

We found that enhanced MYC signaling in our mouse models leads to increased glycolysis (see Figure 2 for an overview of metabolic pathways). On the one hand, we detected upregulation of the glucose transporter GLUT1, hexokinase 2 (HK2), and lactate dehydrogenase A (LDHA) as described in the literature.[217-219] Additionally, we detected increased glucose uptake using PET-MRI and measured elevated ECAR values in the Seahorse glycolysis stress test. Enhancing glycolysis as a means of energy production under aerobic conditions is rather ineffective, but fast, and therefore often discovered in invading cancer cells. This phenomenon is described as the Warburg effect.[47]

MYC RT cells depend on glutaminolysis and β-oxidation to fuel the TCA cycle

To satisfy the energy demand for fast proliferation, cancer cells have to generate ATP alternatively, incorporating glutamine through for example glutamine-driven oxidative phosphorylation,[220] Although we could not detect an increase of glutaminase 1 (GLS1), or glutamine transporter (ASCT2) in our CyTOF screen we detected reduced viability of MYC-positive RT cells after GLS1 inhibitor treatment. Glutamine metabolism is highly regulated by several factors, including MYC and HIF-1α.[221] It is described that MYC signaling induces mitochondrial glutaminolysis, which can lead to glutamine addiction, among other things, through enhanced GLS1 activity and glutamine transporter expression.[222-224] Thus, the stimulation of mitochondrial glutamine metabolism can result in reduced glucose carbon entering the TCA cycle, as glutamine can replenish the TCA cycle to enable high OXPHOS, despite citrate exports from the mitochondria for fatty acid synthesis, required for membrane generation.[221] Not only glutaminolysis can be utilized as an alternative source of energy, but also fatty acids through β-oxidation.[225]

Again, we could not detect an increase of carnitine palmitoyltransferase 1A (CPT1A) in our CyTOF screen but saw impaired viability of MYC-positive RT cells after CPT1A inhibitor treatment, indicating MYC RT cells need for β-oxidation-derived acetyl-CoA entering the TCA cycle. Additionally, the byproducts of β-oxidation, $FADH_2$ and NADH, can fuel the ETC directly to generate ATP. In lymphoma-burdened mice, *in vivo* inhibition of glycolysis led to a reduction of total double-positive CD5 CD19 cells, while the proliferation of MYC-positive RT cells was not impaired. This further confirms glutaminolysis and fatty acid oxidation as main sources for TCA cycle substrates enabling cancer cell proliferation.

Protection from ROS and DNA damage in MYC RT cells

ROS are known to be mainly toxic byproducts of mitochondrial respiration. However, they have been described to a role in intracellular signaling as well, as ROS are also involved in inactivating phosphatases[226] and modulating of HIF-1α stability.[227] To avoid potentially harmful consequences of ROS production, cells can induce antioxidant systems that orchestrate the reduction of surrounding ROS. Consequently, only the imbalance between ROS production and the antioxidant capacity leads to oxidative stress, and not oxidant occurrence itself.[228] As previously described, ROS are well known to cause DNA damage resulting in DNA degradation and potentially causing cell death.[52,53] We hypothesize that MYC-positive lymphoma cells experience proliferative and metabolic stress before during, and after the adaption to excessive MYC signaling. We detected increased oxygen consumption during the Seahorse mito stress test in MYC-positive RT cells. The enhanced mitochondrial respiration fueled by acetyl-CoA originating from glutaminolysis and β-oxidation is linked to increased intracellular ROS levels. However, we detected decreased intracellular ROS and increased glutathione (GSH) levels in adapted MYC-positive RT cells compared to control cells. Therefore, we hypothesize that to transform towards RT cells, MYC lymphoma cells adapt to elevated ROS levels by the upregulation of protective mechanisms. One mechanism to avoid oxidative harm and drive oncogenic transformation is the overexpression of glucose-6-phosphate dehydrogenase (G6PD),[229] as detected in our CyTOF screen. G6PD catalyzes the first step of the pentose phosphate pathway, during which GSH is regenerated from its oxidized form (GSSG)[230]. Thus, G6PD activity can prevent increased ROS levels and resulting apoptosis.[231,232]

Another strategy to reduce harmful ROS levels in MYC-positive RT cells is the upregulation of PACA, also known as “pituitary adenylate cyclase-activating polypeptide” (PACAP), as detected in the proteomic screen. PACAP is mostly characterized as a neuropeptide, but can also be found in B and T lymphocytes in the spleen, lymph nodes, and peritoneum.[233] It prevents intracellular ROS overproduction and was shown to protect astroglial cells and cerebellar granule neurons from oxidative stress-induced apoptosis.[234,235,236] PACAP could play an even more decisive role in the cells’ transformation, as the peptide was additionally shown to inhibit apoptosis through induction of Bcl-2 expression and inhibition of the expression of proapoptotic factors, such as c-Jun or Bax.[237] Moreover, PACAP was found to increase intracellular glutamate uptake via transporters and glutamate metabolism through the upregulation of the enzyme glutamine synthetase.[238]

Further, our proteomic screen indicated an increase of poly [ADP-ribose] polymerase 1 (PARP1) in MYC-positive RT cells. PARP1 is employed in DNA damage repair in CLL lymphoma cells.[239,240] Next to the nucleus, PARP1 was also found in the mitochondria regulating DNA damage in a NAD^+-dependent manner, implicating a role in the control of mitochondrial function under oxidative stress.[241,242] Also it was shown that an ATM- and p53-deficiency in murine CLL is associated with a sensitivity against PARP inhibition.[243] Thus, PARP plays an important role in aggressive CLL lymphoma models, could contribute to RT, and provides a preclinical rationale for the use of PARP inhibitors.

Richter transformation potentially originates in lymph nodes

Further, we hypothesize that the lymph nodes are the origin of the shift towards RT, as we detected CD2-positive RT cells in the LN of a mouse without any prior detection of reporter-positive cells. As addressed previously, MYC expression and nodal hypoxic conditions stabilize HIF-1α, enabling an adaption to the acidic TME of the LN.[100,244-246] Additionally, we have evidence indicating that MYC-expressing cells may be protected from T-cell immune responses in the LN. Supporting this observation, it was described that interactions with stroma cells lead to MYC-mediated expression of the immune checkpoint molecule PD-L1 *in vitro*, reducing T-cell responses.[247] Finally, MYC overexpression goes in hand with enhanced CXCR4 levels, which recruit cells into the LNs.[196]

Signaling in MYC RT cells

When analyzing phosphorylation events, we saw increased AKT, ERK, mTOR, and 4E-BP1 signaling in MYC-positive RT cells compared to control cells after i.v. transplantation. It was described that activated mTOR signaling and 4E-BP1/eIF4E signaling cascades downstream of mTOR are essential for MYC-dependent tumor transformation through an upregulation of the glutamine metabolism.[222] After *in vivo* therapy with the mTOR inhibitor rapamycin, we detected reduced proliferation and decreased viability of MYC-positive RT cells harvested from the PC, validating that MYC overexpressing lymphoma cells depend on mTOR signaling for survival and fitness. However, mTOR singling also leads to elevated oxygen consumption and increased ROS levels, resulting in lactate production through HIF-1α, and sensitivity to nutrient starvation.[248] Therefore we suggest that mTOR and 4E-BP1 signaling create a link between increased HIF-1α levels and elevated glutaminolysis in MYC-positive lymphoma cells resembling RT.

MYC RT cells experience an advantage in the peritoneal cavity

During our studies, we also identified the PC as a favored compartment of MYC-expressing RT cells. After i.p. transplantations, higher ratios of reporter-positive lymphoma cells engrafted, indicating the PC creates a microenvironment that favors the survival and proliferation of MYC-expressing cells in comparison to cells without enhanced MYC signaling. However, mTOR signaling and 4E-BP1/eIF4E signaling were significantly reduced in MYC-positive RT cells after i.p. injections compared to MYC-positive RT cells after i.v. injections. Therefore, we hypothesize that the microenvironment of the PC, including metabolites and cellular compartment, can create conditions which make it possible to withstand high MYC signaling, due to adjusted mTOR signaling.

MYC signaling controls tumor suppressor CDKN2B expression

Further, CLL lymphoma cells do not proliferate *in vitro*, even upon BCR activation as mentioned earlier. This suggests that their proliferation is regulated in a complex manner by negative regulators, such as CDKN2A, CDKN2B, and p53, which block cell cycle progression. Inactivating lesions in these regulators frequently co-occur with MYC alterations in RT.[30,42] Our proteomics screen revealed significantly higher levels of CDKN2B in control cells compared to MYC-positive RT cells, further validating our model as a physiological RT.

We would like to confirm our hypotheses with the support of RNA sequencing, whole exome sequencing, and mass spectrometry data of MYC-positive RT cells, as well as with gas chromatography-mass spectrometry data of metabolites of MYC-expressing RT cells.

Summing up, we found that enhanced MYC expression in lymphoma cells is strongly regulated and allegedly lethal in non-adapted cells. Over some time, we could observe an adaption to enhanced MYC signaling after tamoxifen induction in approximately 50% of mice through all performed experiments. Together with adjustments in metabolic processes and the oxidative controlling machinery, the oncogenic potential of MYC can be exploited and lymphoma cells appear to shift towards RT phenotype. However, the molecular mechanisms whereby MYC exerts its oncogenic activity remain not fully understood. Here, we hypothesize that mTOR signaling and HIF-1α stabilization are involved in MYC-dependent Richter transformation through the upregulation of glycolysis and glutaminolysis. Further, we would like to emphasize the importance of the regulation of antioxidant systems in transforming cells that enable metabolic adaption and increased proliferation of MYC-positive cells with RT phenotype. These findings open up new possibilities, as targeting the mTOR pathway, antioxidant systems, and metabolic pathways may be an effective and novel therapeutic option for the treatment of RT with activated MYC signaling.

6. References

1. Murphy, K.W., C. (2018). Janeway's immunobiology, 9th Edition Edition (Garland Science, Taylor & Francis Group).
2. Chaplin, D.D. (2010). Overview of the immune response. J Allergy Clin Immunol *125*, S3-23. 10.1016/j.jaci.2009.12.980.
3. Christie, S.M., Fijen, C., and Rothenberg, E. (2022). V(D)J Recombination: Recent Insights in Formation of the Recombinase Complex and Recruitment of DNA Repair Machinery. Front Cell Dev Biol *10*, 886718. 10.3389/fcell.2022.886718.
4. Shinkai, Y., Rathbun, G., Lam, K.P., Oltz, E.M., Stewart, V., Mendelsohn, M., Charron, J., Datta, M., Young, F., Stall, A.M., and et al. (1992). RAG-2-deficient mice lack mature lymphocytes owing to inability to initiate V(D)J rearrangement. Cell *68*, 855-867. 10.1016/0092-8674(92)90029-c.
5. Klein, L., Kyewski, B., Allen, P.M., and Hogquist, K.A. (2014). Positive and negative selection of the T cell repertoire: what thymocytes see (and don't see). Nat Rev Immunol *14*, 377-391. 10.1038/nri3667.
6. Hanahan, D., and Weinberg, R.A. (2000). The hallmarks of cancer. Cell *100*, 57-70. 10.1016/s0092-8674(00)81683-9.
7. Hanahan, D., and Weinberg, R.A. (2011). Hallmarks of cancer: the next generation. Cell *144*, 646-674. 10.1016/j.cell.2011.02.013.
8. Itchaki, G., and Brown, J.R. (2016). The potential of venetoclax (ABT-199) in chronic lymphocytic leukemia. Ther Adv Hematol *7*, 270-287. 10.1177/2040620716655350.
9. Hallek, M. (2017). Chronic lymphocytic leukemia: 2017 update on diagnosis, riskstratification, and treatment. American Journal of Hematology *92*, 946-965.
10. Hallek, M. (2019). Chronic lymphocytic leukemia: 2020 update on diagnosis, risk stratification and treatment. Am J Hematol *94*, 1266-1287. 10.1002/ajh.25595.
11. Duhren-von Minden, M., Ubelhart, R., Schneider, D., Wossning, T., Bach, M.P., Buchner, M., Hofmann, D., Surova, E., Follo, M., Kohler, F., et al. (2012). Chronic lymphocytic leukaemia is driven by antigen-independent cell-autonomous signalling. Nature *489*, 309-312. 10.1038/nature11309.
12. Burger, J.A., and Chiorazzi, N. (2013). B cell receptor signaling in chronic lymphocytic leukemia. Trends Immunol *34*, 592-601. 10.1016/j.it.2013.07.002.
13. Cargnello, M., and Roux, P.P. (2011). Activation and function of the MAPKs and their substrates, the MAPK-activated protein kinases. Microbiol Mol Biol Rev *75*, 50-83. 10.1128/MMBR.00031-10.
14. Turner, N.A., and Blythe, N.M. (2019). Cardiac Fibroblast p38 MAPK: A Critical Regulator of Myocardial Remodeling. J Cardiovasc Dev Dis *6*. 10.3390/jcdd6030027.
15. Johnson, G.L., and Lapadat, R. (2002). Mitogen-activated protein kinase pathways mediated by ERK, JNK, and p38 protein kinases. Science *298*, 1911-1912. 10.1126/science.1072682.
16. Svanberg, R., Janum, S., Patten, P.E.M., Ramsay, A.G., and Niemann, C.U. (2021). Targeting the tumor microenvironment in chronic lymphocytic leukemia. Haematologica *106*, 2312-2324. 10.3324/haematol.2020.268037.
17. Smolej, L., Vodarek, P., Ecsiova, D., and Simkovic, M. (2021). Chemoimmunotherapy in the First-Line Treatment of Chronic Lymphocytic Leukaemia: Dead Yet, or Alive and Kicking? Cancers (Basel) *13*. 10.3390/cancers13133134.
18. Woyach, J.A., and Johnson, A.J. (2015). Targeted therapies in CLL: mechanisms of resistance and strategies for management. Blood *126*, 471-477. 10.1182/blood-2015-03-585075.
19. Tadmor, T., and Levy, I. (2021). Richter Transformation in Chronic Lymphocytic Leukemia: Update in the Era of Novel Agents. Cancers (Basel) *13*. 10.3390/cancers13205141.
20. Wang, Y., Tschautscher, M.A., Rabe, K.G., Call, T.G., Leis, J.F., Kenderian, S.S., Kay, N.E., Muchtar, E., Van Dyke, D.L., Koehler, A.B., et al. (2020). Clinical characteristics and outcomes of Richter transformation: experience of 204 patients from a single center. Haematologica *105*, 765-773. 10.3324/haematol.2019.224121.
21. Rossi, D., Spina, V., and Gaidano, G. (2018). Biology and treatment of Richter syndrome. Blood *131*, 2761-2772. 10.1182/blood-2018-01-791376.
22. Rossi, D., Spina, V., Deambrogi, C., Rasi, S., Laurenti, L., Stamatopoulos, K., Arcaini, L., Lucioni, M., Rocque, G.B., Xu-Monette, Z.Y., et al. (2011). The genetics of Richter syndrome reveals disease heterogeneity and predicts survival after transformation. Blood *117*, 3391-3401. 10.1182/blood-2010-09-302174.
23. Fabbri, G., Khiabanian, H., Holmes, A.B., Wang, J., Messina, M., Mullighan, C.G., Pasqualucci, L., Rabadan, R., and Dalla-Favera, R. (2013). Genetic lesions associated with chronic lymphocytic leukemia transformation to Richter syndrome. J Exp Med *210*, 2273-2288. 10.1084/jem.20131448.
24. Condoluci, A., and Rossi, D. (2021). Richter Syndrome. Curr Oncol Rep *23*, 26. 10.1007/s11912-020-01001-x.
25. Conacci-Sorrell, M., McFerrin, L., and Eisenman, R.N. (2014). An overview of MYC and its interactome. Cold Spring Harb Perspect Med *4*, a014357. 10.1101/cshperspect.a014357.
26. Nie, Z., Hu, G., Wei, G., Cui, K., Yamane, A., Resch, W., Wang, R., Green, D.R., Tessarollo, L., Casellas, R., et al. (2012). c-Myc is a universal amplifier of expressed genes in lymphocytes and embryonic stem cells. Cell *151*, 68-79. 10.1016/j.cell.2012.08.033.
27. Iyer, P., Zhang, B., Liu, T., Jin, M., Hart, K., Zhang, J., Song, J., Chan, W.C., Siddiqi, T., Rosen, S.T., et al. (2023). MGA deletion leads to Richter's transformation via modulation of mitochondrial OXPHOS. bioRxiv. 10.1101/2023.02.07.527502.
28. Yu, L., Yu, T.T., and Young, K.H. (2019). Cross-talk between Myc and p53 in B-cell lymphomas. Chronic Dis Transl Med *5*, 139-154. 10.1016/j.cdtm.2019.08.001.
29. Hemann, M.T., Bric, A., Teruya-Feldstein, J., Herbst, A., Nilsson, J.A., Cordon-Cardo, C., Cleveland, J.L., Tansey, W.P., and Lowe, S.W. (2005). Evasion of the p53 tumour surveillance network by tumour-derived MYC mutants. Nature *436*, 807-811. 10.1038/nature03845.
30. Filip, D., and Mraz, M. (2020). The role of MYC in the transformation and aggressiveness of 'indolent' B-cell malignancies. Leuk Lymphoma *61*, 510-524. 10.1080/10428194.2019.1675877.
31. Stine, Z.E., Walton, Z.E., Altman, B.J., Hsieh, A.L., and Dang, C.V. (2015). MYC, Metabolism, and Cancer. Cancer Discov *5*, 1024-1039. 10.1158/2159-8290.CD-15-0507.
32. Dang, C.V. (2012). MYC on the path to cancer. Cell *149*, 22-35. 10.1016/j.cell.2012.03.003.
33. Tao, J., Zhao, X., and Tao, J. (2014). c-MYC-miRNA circuitry: a central regulator of aggressive B-cell malignancies. Cell Cycle *13*, 191-198. 10.4161/cc.27646.
34. Kohlhaas, V., Blakemore, S.J., Al-Maarri, M., Nickel, N., Pal, M., Roth, A., Hovelmeyer, N., Schafer, S.C., Knittel, G., Lohneis, P., et al. (2021). Active Akt signaling triggers CLL toward Richter transformation via overactivation of Notch1. Blood *137*, 646-660. 10.1182/blood.2020005734.
35. Mendes, R.D., Cante-Barrett, K., Pieters, R., and Meijerink, J.P. (2016). The relevance of PTEN-AKT in relation to NOTCH1-directed treatment strategies in T-cell acute lymphoblastic leukemia. Haematologica *101*, 1010-1017. 10.3324/haematol.2016.146381.

36. Carpten, J.D., Faber, A.L., Horn, C., Donoho, G.P., Briggs, S.L., Robbins, C.M., Hostetter, G., Boguslawski, S., Moses, T.Y., Savage, S., et al. (2007). A transforming mutation in the pleckstrin homology domain of AKT1 in cancer. Nature *448*, 439-444. 10.1038/nature05933.
37. Ruland, J., and Hartjes, L. (2019). CARD-BCL-10-MALT1 signalling in protective and pathological immunity. Nat Rev Immunol *19*, 118-134. 10.1038/s41577-018-0087-2.
38. Lenz, G., Davis, R.E., Ngo, V.N., Lam, L., George, T.C., Wright, G.W., Dave, S.S., Zhao, H., Xu, W., Rosenwald, A., et al. (2008). Oncogenic CARD11 mutations in human diffuse large B cell lymphoma. Science *319*, 1676-1679. 10.1126/science.1153629.
39. Chan, W., Schaffer, T.B., and Pomerantz, J.L. (2013). A quantitative signaling screen identifies CARD11 mutations in the CARD and LATCH domains that induce Bcl10 ubiquitination and human lymphoma cell survival. Mol Cell Biol *33*, 429-443. 10.1128/MCB.00850-12.
40. Knies, N., Alankus, B., Weilemann, A., Tzankov, A., Brunner, K., Ruff, T., Kremer, M., Keller, U.B., Lenz, G., and Ruland, J. (2015). Lymphomagenic CARD11/BCL10/MALT1 signaling drives malignant B-cell proliferation via cooperative NF-kappaB and JNK activation. Proc Natl Acad Sci U S A *112*, E7230-7238. 10.1073/pnas.1507459112.
41. Nadeu, F., Royo, R., Massoni-Badosa, R., Playa-Albinyana, H., Garcia-Torre, B., Duran-Ferrer, M., Dawson, K.J., Kulis, M., Diaz-Navarro, A., Villamor, N., et al. (2022). Detection of early seeding of Richter transformation in chronic lymphocytic leukemia. Nat Med *28*, 1662-1671. 10.1038/s41591-022-01927-8.
42. Chakraborty, S., Martines, C., Porro, F., Fortunati, I., Bonato, A., Dimishkovska, M., Piazza, S., Yadav, B.S., Innocenti, I., Fazio, R., et al. (2021). B-cell receptor signaling and genetic lesions in TP53 and CDKN2A/CDKN2B cooperate in Richter transformation. Blood *138*, 1053-1066. 10.1182/blood.2020008276.
43. Varano, G., Raffel, S., Sormani, M., Zanardi, F., Lonardi, S., Zasada, C., Perucho, L., Petrocelli, V., Haake, A., Lee, A.K., et al. (2017). The B-cell receptor controls fitness of MYC-driven lymphoma cells via GSK3beta inhibition. Nature *546*, 302-306. 10.1038/nature22353.
44. Condoluci, A., and Rossi, D. (2022). Biology and Treatment of Richter Transformation. Front Oncol *12*, 829983. 10.3389/fonc.2022.829983.
45. Smyth, M.J., Ngiow, S.F., Ribas, A., and Teng, M.W. (2016). Combination cancer immunotherapies tailored to the tumour microenvironment. Nat Rev Clin Oncol *13*, 143-158. 10.1038/nrclinonc.2015.209.
46. Lunt, S.Y., and Vander Heiden, M.G. (2011). Aerobic glycolysis: meeting the metabolic requirements of cell proliferation. Annu Rev Cell Dev Biol *27*, 441-464. 10.1146/annurev-cellbio-092910-154237.
47. Warburg, O. (1956). On respiratory impairment in cancer cells. Science *124*, 269-270.
48. Nie, Y., Yun, X., Zhang, Y., and Wang, X. (2022). Targeting metabolic reprogramming in chronic lymphocytic leukemia. Exp Hematol Oncol *11*, 39. 10.1186/s40164-022-00292-z.
49. Weinberg, S.E., and Chandel, N.S. (2015). Targeting mitochondria metabolism for cancer therapy. Nat Chem Biol *11*, 9-15. 10.1038/nchembio.1712.
50. Liu, Y., Sun, Y., Guo, Y., Shi, X., Chen, X., Feng, W., Wu, L.L., Zhang, J., Yu, S., Wang, Y., and Shi, Y. (2023). An Overview: The Diversified Role of Mitochondria in Cancer Metabolism. Int J Biol Sci *19*, 897-915. 10.7150/ijbs.81609.
51. Pfeiffer, T., Schuster, S., and Bonhoeffer, S. (2001). Cooperation and competition in the evolution of ATP-producing pathways. Science *292*, 504-507. 10.1126/science.1058079.
52. Srinivas, U.S., Tan, B.W.Q., Vellayappan, B.A., and Jeyasekharan, A.D. (2019). ROS and the DNA damage response in cancer. Redox Biol *25*, 101084. 10.1016/j.redox.2018.101084.
53. Salehi, F., Behboudi, H., Kavoosi, G., and Ardestani, S.K. (2018). Oxidative DNA damage induced by ROS-modulating agents with the ability to target DNA: A comparison of the biological characteristics of citrus pectin and apple pectin. Sci Rep *8*, 13902. 10.1038/s41598-018-32308-2.
54. Martinez-Reyes, I., and Chandel, N.S. (2020). Mitochondrial TCA cycle metabolites control physiology and disease. Nat Commun *11*, 102. 10.1038/s41467-019-13668-3.
55. Bornstein, R., Mulholland, M.T., Sedensky, M., Morgan, P., and Johnson, S.C. (2023). Glutamine metabolism in diseases associated with mitochondrial dysfunction. Mol Cell Neurosci *126*, 103887. 10.1016/j.mcn.2023.103887.
56. Yoo, H., Antoniewicz, M.R., Stephanopoulos, G., and Kelleher, J.K. (2008). Quantifying reductive carboxylation flux of glutamine to lipid in a brown adipocyte cell line. J Biol Chem *283*, 20621-20627. 10.1074/jbc.M706494200.
57. Mayer, R.L., Schwarzmeier, J.D., Gerner, M.C., Bileck, A., Mader, J.C., Meier-Menches, S.M., Gerner, S.M., Schmetterer, K.G., Pukrop, T., Reichle, A., et al. (2018). Proteomics and metabolomics identify molecular mechanisms of aging potentially predisposing for chronic lymphocytic leukemia. Mol Cell Proteomics *17*, 290-303. 10.1074/mcp.RA117.000425.
58. Brose, S.A., Marquardt, A.L., and Golovko, M.Y. (2014). Fatty acid biosynthesis from glutamate and glutamine is specifically induced in neuronal cells under hypoxia. J Neurochem *129*, 400-412. 10.1111/jnc.12617.
59. Bartlett, K., and Eaton, S. (2004). Mitochondrial beta-oxidation. Eur J Biochem *271*, 462-469. 10.1046/j.1432-1033.2003.03947.x.
60. Rozovski, U., Harris, D.M., Li, P., Liu, Z., Jain, P., Ferrajoli, A., Burger, J., Thompson, P., Jain, N., Wierda, W., et al. (2018). Ibrutinib inhibits free fatty acid metabolism in chronic lymphocytic leukemia. Leuk Lymphoma *59*, 2686-2691. 10.1080/10428194.2018.1439167.
61. Liu, P.P., Liu, J., Jiang, W.Q., Carew, J.S., Ogasawara, M.A., Pelicano, H., Croce, C.M., Estrov, Z., Xu, R.H., Keating, M.J., and Huang, P. (2016). Elimination of chronic lymphocytic leukemia cells in stromal microenvironment by targeting CPT with an antiangina drug perhexiline. Oncogene *35*, 5663-5673. 10.1038/onc.2016.103.
62. Rohrl, C., and Stangl, H. (2018). Cholesterol metabolism-physiological regulation and pathophysiological deregulation by the endoplasmic reticulum. Wien Med Wochenschr *168*, 280-285. 10.1007/s10354-018-0626-2.
63. Mullen, P.J., Yu, R., Longo, J., Archer, M.C., and Penn, L.Z. (2016). The interplay between cell signalling and the mevalonate pathway in cancer. Nat Rev Cancer *16*, 718-731. 10.1038/nrc.2016.76.
64. Larson, R.A., and Yachnin, S. (1984). Mevalonic acid induces DNA synthesis in chronic lymphocytic leukemia cells. Blood *64*, 257-262.
65. Righolt, C.H., Zhang, G., Ye, X., Banerji, V., Johnston, J.B., Gibson, S., and Mahmud, S.M. (2019). Statin Use and Chronic Lymphocytic Leukemia Incidence: A Nested Case-Control Study in Manitoba, Canada. Cancer Epidemiology, Biomarkers & Prevention: Home *28*, 1495-1501. 10.1158/1055-9965.EPI-19-0107.
66. Ding, X., Zhang, W., Li, S., and Yang, H. (2019). The role of cholesterol metabolism in cancer. Am J Cancer Res *9*, 219-227.
67. Feingold, K.R. (2000). Introduction to Lipids and Lipoproteins. In Endotext, K.R. Feingold, B. Anawalt, M.R. Blackman, A. Boyce, G. Chrousos, E. Corpas, W.W. de Herder, K. Dhatariya, K. Dungan, J. Hofland, et al., eds.
68. Boren, J., Chapman, M.J., Krauss, R.M., Packard, C.J., Bentzon, J.F., Binder, C.J., Daemen, M.J., Demer, L.L., Hegele, R.A., Nicholls, S.J., et al. (2020). Low-density lipoproteins cause atherosclerotic cardiovascular disease: pathophysiological, genetic, and therapeutic insights: a consensus statement from the European Atherosclerosis Society Consensus Panel. Eur Heart J *41*, 2313-2330. 10.1093/eurheartj/ehz962.
69. Tabet, F., and Rye, K.A. (2009). High-density lipoproteins, inflammation and oxidative stress. Clin Sci (Lond) *116*, 87-98. 10.1042/CS20080106.

70. Smith, L.C., Pownall, H.J., and Gotto, A.M., Jr. (1978). The plasma lipoproteins: structure and metabolism. Annu Rev Biochem *47*, 751-757. 10.1146/annurev.bi.47.070178.003535.
71. Bichi, R., Shinton, S.A., Martin, E.S., Koval, A., Calin, G.A., Cesari, R., Russo, G., Hardy, R.R., and Croce, C.M. (2002). Human chronic lymphocytic leukemia modeled in mouse by targeted TCL1 expression. Proc Natl Acad Sci U S A *99*, 6955-6960. 10.1073/pnas.102181599.
72. Cepko, C., and Pear, W. (2001). Overview of the retrovirus transduction system. Curr Protoc Mol Biol *Chapter 9*, Unit9 9. 10.1002/0471142727.mb0909s36.
73. Sena-Esteves, M., and Gao, G. (2018). Production of High-Titer Retrovirus and Lentivirus Vectors. Cold Spring Harb Protoc *2018*. 10.1101/pdb.prot095687.
74. Das, A.T., Tenenbaum, L., and Berkhout, B. (2016). Tet-On Systems For Doxycycline-inducible Gene Expression. Curr Gene Ther *16*, 156-167. 10.2174/1566523216666160524144041.
75. Berens, C., and Hillen, W. (2003). Gene regulation by tetracyclines. Constraints of resistance regulation in bacteria shape TetR for application in eukaryotes. Eur J Biochem *270*, 3109-3121. 10.1046/j.1432-1033.2003.03694.x.
76. Sternberg, N., Sauer, B., Hoess, R., and Abremski, K. (1986). Bacteriophage P1 cre gene and its regulatory region. Evidence for multiple promoters and for regulation by DNA methylation. J Mol Biol *187*, 197-212. 10.1016/0022-2836(86)90228-7.
77. Indra, A.K., Warot, X., Brocard, J., Bornert, J.M., Xiao, J.H., Chambon, P., and Metzger, D. (1999). Temporally-controlled site-specific mutagenesis in the basal layer of the epidermis: comparison of the recombinase activity of the tamoxifen-inducible Cre-ER(T) and Cre-ER(T2) recombinases. Nucleic Acids Res *27*, 4324-4327. 10.1093/nar/27.22.4324.
78. Kim, H., Kim, M., Im, S.K., and Fang, S. (2018). Mouse Cre-LoxP system: general principles to determine tissue-specific roles of target genes. Lab Anim Res *34*, 147-159. 10.5625/lar.2018.34.4.147.
79. Feil, S., Valtcheva, N., and Feil, R. (2009). Inducible Cre mice. Methods Mol Biol *530*, 343-363. 10.1007/978-1-59745-471-1_18.
80. Mahmood, T., and Yang, P.C. (2012). Western blot: technique, theory, and trouble shooting. N Am J Med Sci *4*, 429-434. 10.4103/1947-2714.100998.
81. Hnasko, T.S., and Hnasko, R.M. (2015). The Western Blot. Methods Mol Biol *1318*, 87-96. 10.1007/978-1-4939-2742-5_9.
82. McKinnon, K.M. (2018). Flow Cytometry: An Overview. Curr Protoc Immunol *120*, 5 1 1-5 1 11. 10.1002/cpim.40.
83. Nolan, J.P., and Condello, D. (2013). Spectral flow cytometry. Curr Protoc Cytom *Chapter 1*, 1 27 21-21 27 13. 10.1002/0471142956.cy0127s63.
84. Givan, A.L. (2011). Flow cytometry: an introduction. Methods Mol Biol *699*, 1-29. 10.1007/978-1-61737-950-5_1.
85. Iyer, A., Hamers, A.A.J., and Pillai, A.B. (2022). CyTOF((R)) for the Masses. Front Immunol *13*, 815828. 10.3389/fimmu.2022.815828.
86. Bandura, D.R., Baranov, V.I., Ornatsky, O.I., Antonov, A., Kinach, R., Lou, X., Pavlov, S., Vorobiev, S., Dick, J.E., and Tanner, S.D. (2009). Mass cytometry: technique for real time single cell multitarget immunoassay based on inductively coupled plasma time-of-flight mass spectrometry. Anal Chem *81*, 6813-6822. 10.1021/ac901049w.
87. Rahmim, A., Lodge, M.A., Karakatsanis, N.A., Panin, V.Y., Zhou, Y., McMillan, A., Cho, S., Zaidi, H., Casey, M.E., and Wahl, R.L. (2019). Dynamic whole-body PET imaging: principles, potentials and applications. Eur J Nucl Med Mol Imaging *46*, 501-518. 10.1007/s00259-018-4153-6.
88. Deshmane, A., Gulani, V., Griswold, M.A., and Seiberlich, N. (2012). Parallel MR imaging. J Magn Reson Imaging *36*, 55-72. 10.1002/jmri.23639.
89. Caines, J.K., Barnes, D.A., and Berry, M.D. (2022). The Use of Seahorse XF Assays to Interrogate Real-Time Energy Metabolism in Cancer Cell Lines. Methods Mol Biol *2508*, 225-234. 10.1007/978-1-0716-2376-3_17.
90. Gray, M.W., Sankoff, D., and Cedergren, R.J. (1984). On the evolutionary descent of organisms and organelles: a global phylogeny based on a highly conserved structural core in small subunit ribosomal RNA. Nucleic Acids Res *12*, 5837-5852. 10.1093/nar/12.14.5837.
91. Yang, B., Wang, Y., and Qian, P.Y. (2016). Sensitivity and correlation of hypervariable regions in 16S rRNA genes in phylogenetic analysis. BMC Bioinformatics *17*, 135. 10.1186/s12859-016-0992-y.
92. Ecker, V., Stumpf, M., Brandmeier, L., Neumayer, T., Pfeuffer, L., Engleitner, T., Ringshausen, I., Nelson, N., Jucker, M., Wanninger, S., et al. (2021). Targeted PI3K/AKT-hyperactivation induces cell death in chronic lymphocytic leukemia. Nat Commun *12*, 3526. 10.1038/s41467-021-23752-2.
93. Zenz, T., Luetge, A., Lu, J., J., H., S., D., L., S., and Huber, W. (2019). Transcriptional Profiling Reveals Strong Impact of Major Molecular Disease Subgroups and Mixed Epistasis in Chronic Lymphocytic Leukemia. Blood *134*.
94. Landau, D.A., Tausch, E., Taylor-Weiner, A.N., Stewart, C., Reiter, J.G., Bahlo, J., Kluth, S., Bozic, I., Lawrence, M., Bottcher, S., et al. (2015). Mutations driving CLL and their evolution in progression and relapse. Nature *526*, 525-530. 10.1038/nature15395.
95. Hamblin, T.J., Davis, Z., Gardiner, A., Oscier, D.G., and Stevenson, F.K. (1999). Unmutated Ig V(H) genes are associated with a more aggressive form of chronic lymphocytic leukemia. Blood *94*, 1848-1854.
96. Sharma, A., Singh, K., and Almasan, A. (2012). Histone H2AX phosphorylation: a marker for DNA damage. Methods Mol Biol *920*, 613-626. 10.1007/978-1-61779-998-3_40.
97. He, K., and Aizenman, E. (2010). ERK signaling leads to mitochondrial dysfunction in extracellular zinc-induced neurotoxicity. J Neurochem *114*, 452-461. 10.1111/j.1471-4159.2010.06762.x.
98. Pyakurel, A., Savoia, C., Hess, D., and Scorrano, L. (2015). Extracellular regulated kinase phosphorylates mitofusin 1 to control mitochondrial morphology and apoptosis. Mol Cell *58*, 244-254. 10.1016/j.molcel.2015.02.021.
99. Juan, C.A., Perez de la Lastra, J.M., Plou, F.J., and Perez-Lebena, E. (2021). The Chemistry of Reactive Oxygen Species (ROS) Revisited: Outlining Their Role in Biological Macromolecules (DNA, Lipids and Proteins) and Induced Pathologies. Int J Mol Sci *22*. 10.3390/ijms22094642.
100. Arruga, F., Gyau, B.B., Iannello, A., Vitale, N., Vaisitti, T., and Deaglio, S. (2020). Immune Response Dysfunction in Chronic Lymphocytic Leukemia: Dissecting Molecular Mechanisms and Microenvironmental Conditions. Int J Mol Sci *21*. 10.3390/ijms21051825.
101. Andersen, P.S., Menne, C., Mariuzza, R.A., Geisler, C., and Karjalainen, K. (2001). A response calculus for immobilized T cell receptor ligands. J Biol Chem *276*, 49125-49132. 10.1074/jbc.M109396200.
102. Neumann, K., Castineiras-Vilarino, M., Hockendorf, U., Hannesschlager, N., Lemeer, S., Kupka, D., Meyermann, S., Lech, M., Anders, H.J., Kuster, B., et al. (2014). Clec12a is an inhibitory receptor for uric acid crystals that regulates inflammation in response to cell death. Immunity *40*, 389-399. 10.1016/j.immuni.2013.12.015.
103. Chan, T.O., Rittenhouse, S.E., and Tsichlis, P.N. (1999). AKT/PKB and other D3 phosphoinositide-regulated kinases: kinase activation by phosphoinositide-dependent phosphorylation. Annu Rev Biochem *68*, 965-1014. 10.1146/annurev.biochem.68.1.965.
104. Carroll, P.A., Freie, B.W., Mathsyaraja, H., and Eisenman, R.N. (2018). The MYC transcription factor network: balancing metabolism, proliferation and oncogenesis. Front Med *12*, 412-425. 10.1007/s11684-018-0650-z.

105. Ozturk, S., Paul, Y., Afzal, S., Gil-Farina, I., Jauch, A., Bruch, P.M., Kalter, V., Hanna, B., Arseni, L., Roessner, P.M., et al. (2022). Longitudinal analyses of CLL in mice identify leukemia-related clonal changes including a Myc gain predicting poor outcome in patients. Leukemia *36*, 464-475. 10.1038/s41375-021-01381-4.
106. Kunji, E.R.S., King, M.S., Ruprecht, J.J., and Thangaratnarajah, C. (2020). The SLC25 Carrier Family: Important Transport Proteins in Mitochondrial Physiology and Pathology. Physiology (Bethesda) *35*, 302-327. 10.1152/physiol.00009.2020.
107. Palmieri, F., Scarcia, P., and Monne, M. (2020). Diseases Caused by Mutations in Mitochondrial Carrier Genes SLC25: A Review. Biomolecules *10*. 10.3390/biom10040655.
108. Mosaoa, R., Kasprzyk-Pawelec, A., Fernandez, H.R., and Avantaggiati, M.L. (2021). The Mitochondrial Citrate Carrier SLC25A1/CIC and the Fundamental Role of Citrate in Cancer, Inflammation and Beyond. Biomolecules *11*. 10.3390/biom11020141.
109. Zou, Z., Tao, T., Li, H., and Zhu, X. (2020). mTOR signaling pathway and mTOR inhibitors in cancer: progress and challenges. Cell Biosci *10*, 31. 10.1186/s13578-020-00396-1.
110. Pi-Sunyer, X. (2009). The medical risks of obesity. Postgrad Med *121*, 21-33. 10.3810/pgm.2009.11.2074.
111. Solans, M., Castello, A., Benavente, Y., Marcos-Gragera, R., Amiano, P., Gracia-Lavedan, E., Costas, L., Robles, C., Gonzalez-Barca, E., de la Banda, E., et al. (2018). Adherence to the Western, Prudent, and Mediterranean dietary patterns and chronic lymphocytic leukemia in the MCC-Spain study. Haematologica *103*, 1881-1888. 10.3324/haematol.2018.192526.
112. Chawla, S., Tessarolo Silva, F., Amaral Medeiros, S., Mekary, R.A., and Radenkovic, D. (2020). The Effect of Low-Fat and Low-Carbohydrate Diets on Weight Loss and Lipid Levels: A Systematic Review and Meta-Analysis. Nutrients *12*. 10.3390/nu12123774.
113. Statistics, N.C.f.H. (2018). Mean macronutrient intake among adults aged 20 and over, by sex and age: United States, selected years 1988-1994 through 2013-2016.
114. Deshmane, S.L., Kremlev, S., Amini, S., and Sawaya, B.E. (2009). Monocyte chemoattractant protein-1 (MCP-1): an overview. J Interferon Cytokine Res *29*, 313-326. 10.1089/jir.2008.0027.
115. Mesaros, O., Jimbu, L., Neaga, A., Popescu, C., Berceanu, I., Tomuleasa, C., Fetica, B., and Zdrenghea, M. (2020). Macrophage Polarization in Chronic Lymphocytic Leukemia: Nurse-Like Cells Are the Caretakers of Leukemic Cells. Biomedicines *8*. 10.3390/biomedicines8110516.
116. Yoshimura, T. (2018). The chemokine MCP-1 (CCL2) in the host interaction with cancer: a foe or ally? Cell Mol Immunol *15*, 335-345. 10.1038/cmi.2017.135.
117. Chylikova, J., Dvorackova, J., Tauber, Z., and Kamarad, V. (2018). M1/M2 macrophage polarization in human obese adipose tissue. Biomed Pap Med Fac Univ Palacky Olomouc Czech Repub *162*, 79-82. 10.5507/bp.2018.015.
118. Kanda, H., Tateya, S., Tamori, Y., Kotani, K., Hiasa, K., Kitazawa, R., Kitazawa, S., Miyachi, H., Maeda, S., Egashira, K., and Kasuga, M. (2006). MCP-1 contributes to macrophage infiltration into adipose tissue, insulin resistance, and hepatic steatosis in obesity. J Clin Invest *116*, 1494-1505. 10.1172/JCI26498.
119. van der Heijden, R.A., Sheedfar, F., Morrison, M.C., Hommelberg, P.P., Kor, D., Kloosterhuis, N.J., Gruben, N., Youssef, S.A., de Bruin, A., Hofker, M.H., et al. (2015). High-fat diet induced obesity primes inflammation in adipose tissue prior to liver in C57BL/6j mice. Aging (Albany NY) *7*, 256-268. 10.18632/aging.100738.
120. Kawanishi, N., Yano, H., Yokogawa, Y., and Suzuki, K. (2010). Exercise training inhibits inflammation in adipose tissue via both suppression of macrophage infiltration and acceleration of phenotypic switching from M1 to M2 macrophages in high-fat-diet-induced obese mice. Exerc Immunol Rev *16*, 105-118.
121. Dinarello, C.A. (2018). Overview of the IL-1 family in innate inflammation and acquired immunity. Immunol Rev *281*, 8-27. 10.1111/imr.12621.
122. Kim, S.J., Choi, Y., Jun, H.S., Kim, B.M., Na, H.K., Surh, Y.J., and Park, T. (2010). High-fat diet stimulates IL-1 type I receptor-mediated inflammatory signaling in the skeletal muscle of mice. Mol Nutr Food Res *54*, 1014-1020. 10.1002/mnfr.200800512.
123. Sauter, N.S., Schulthess, F.T., Galasso, R., Castellani, L.W., and Maedler, K. (2008). The antiinflammatory cytokine interleukin-1 receptor antagonist protects from high-fat diet-induced hyperglycemia. Endocrinology *149*, 2208-2218. 10.1210/en.2007-1059.
124. Gendelman, H.E., Ding, S., Gong, N., Liu, J., Ramirez, S.H., Persidsky, Y., Mosley, R.L., Wang, T., Volsky, D.J., and Xiong, H. (2009). Monocyte chemotactic protein-1 regulates voltage-gated K+ channels and macrophage transmigration. J Neuroimmune Pharmacol *4*, 47-59. 10.1007/s11481-008-9135-1.
125. Allavena, P., Bianchi, G., Zhou, D., van Damme, J., Jilek, P., Sozzani, S., and Mantovani, A. (1994). Induction of natural killer cell migration by monocyte chemotactic protein-1, -2 and -3. Eur J Immunol *24*, 3233-3236. 10.1002/eji.1830241249.
126. Zhu, K., Shen, Q., Ulrich, M., and Zheng, M. (2000). Human monocyte-derived dendritic cells expressing both chemotactic cytokines IL-8, MCP-1, RANTES and their receptors, and their selective migration to these chemokines. Chin Med J (Engl) *113*, 1124-1128.
127. Casazza, A., Laoui, D., Wenes, M., Rizzolio, S., Bassani, N., Mambretti, M., Deschoemaeker, S., Van Ginderachter, J.A., Tamagnone, L., and Mazzone, M. (2013). Impeding macrophage entry into hypoxic tumor areas by Sema3A/Nrp1 signaling blockade inhibits angiogenesis and restores antitumor immunity. Cancer Cell *24*, 695-709. 10.1016/j.ccr.2013.11.007.
128. Colegio, O.R., Chu, N.Q., Szabo, A.L., Chu, T., Rhebergen, A.M., Jairam, V., Cyrus, N., Brokowski, C.E., Eisenbarth, S.C., Phillips, G.M., et al. (2014). Functional polarization of tumour-associated macrophages by tumour-derived lactic acid. Nature *513*, 559-563. 10.1038/nature13490.
129. Fabbri, G., and Dalla-Favera, R. (2016). The molecular pathogenesis of chronic lymphocytic leukaemia. Nat Rev Cancer *16*, 145-162. 10.1038/nrc.2016.8.
130. Ohtaki, Y., Ishii, G., Nagai, K., Ashimine, S., Kuwata, T., Hishida, T., Nishimura, M., Yoshida, J., Takeyoshi, I., and Ochiai, A. (2010). Stromal macrophage expressing CD204 is associated with tumor aggressiveness in lung adenocarcinoma. J Thorac Oncol *5*, 1507-1515. 10.1097/JTO.0b013e3181eba692.
131. Jackson, A.L., Matsumoto, H., Janszen, M., Maino, V., Blidy, A., and Shye, S. (1990). Restricted expression of p55 interleukin 2 receptor (CD25) on normal T cells. Clin Immunol Immunopathol *54*, 126-133. 10.1016/0090-1229(90)90012-f.
132. Reddy, M., Eirikis, E., Davis, C., Davis, H.M., and Prabhakar, U. (2004). Comparative analysis of lymphocyte activation marker expression and cytokine secretion profile in stimulated human peripheral blood mononuclear cell cultures: an in vitro model to monitor cellular immune function. J Immunol Methods *293*, 127-142. 10.1016/j.jim.2004.07.006.
133. Bajnok, A., Ivanova, M., Rigo, J., Jr., and Toldi, G. (2017). The Distribution of Activation Markers and Selectins on Peripheral T Lymphocytes in Preeclampsia. Mediators Inflamm *2017*, 8045161. 10.1155/2017/8045161.
134. Heiman, M.L., and Greenway, F.L. (2016). A healthy gastrointestinal microbiome is dependent on dietary diversity. Mol Metab *5*, 317-320. 10.1016/j.molmet.2016.02.005.
135. Postler, T.S., and Ghosh, S. (2017). Understanding the Holobiont: How Microbial Metabolites Affect Human Health and Shape the Immune System. Cell Metab *26*, 110-130. 10.1016/j.cmet.2017.05.008.
136. Choi, Y., Lichterman, J.N., Coughlin, L.A., Poulides, N., Li, W., Del Valle, P., Palmer, S.N., Gan, S., Kim, J., Zhan, X., et al. (2023). Immune checkpoint blockade induces gut microbiota translocation that augments extraintestinal antitumor immunity. Sci Immunol *8*, eabo2003. 10.1126/sciimmunol.abo2003.

137. Fidelle, M., Rauber, C., Alves Costa Silva, C., Tian, A.L., Lahmar, I., de La Varende, A.M., Zhao, L., Thelemaque, C., Lebhar, I., Messaoudene, M., et al. (2023). A microbiota-modulated checkpoint directs immunosuppressive intestinal T cells into cancers. Science *380*, eabo2296. 10.1126/science.abo2296.
138. Xu, Y., Duan, J., Wang, D., Liu, J., Chen, X., Qin, X.Y., and Yu, W. (2023). Akkermansia muciniphila Alleviates Persistent Inflammation, Immunosuppression, and Catabolism Syndrome in Mice. Metabolites *13*. 10.3390/metabo13020194.
139. Shang, L., Liu, H., Yu, H., Chen, M., Yang, T., Zeng, X., and Qiao, S. (2021). Core Altered Microorganisms in Colitis Mouse Model: A Comprehensive Time-Point and Fecal Microbiota Transplantation Analysis. Antibiotics (Basel) *10*. 10.3390/antibiotics10060643.
140. Smith, B.J., Miller, R.A., Ericsson, A.C., Harrison, D.C., Strong, R., and Schmidt, T.M. (2019). Changes in the gut microbiome and fermentation products concurrent with enhanced longevity in acarbose-treated mice. BMC Microbiol *19*, 130. 10.1186/s12866-019-1494-7.
141. Nastasi, C., Fredholm, S., Willerslev-Olsen, A., Hansen, M., Bonefeld, C.M., Geisler, C., Andersen, M.H., Odum, N., and Woetmann, A. (2017). Butyrate and propionate inhibit antigen-specific CD8(+) T cell activation by suppressing IL-12 production by antigen-presenting cells. Sci Rep *7*, 14516. 10.1038/s41598-017-15099-w.
142. Ecklu-Mensah, G., Choo-Kang, C., Maseng, M.G., Donato, S., Bovet, P., Viswanathan, B., Bedu-Addo, K., Plange-Rhule, J., Oti Boateng, P., Forrester, T.E., et al. (2023). Gut microbiota and fecal short chain fatty acids differ with adiposity and country of origin: the METS-microbiome study. Nat Commun *14*, 5160. 10.1038/s41467-023-40874-x.
143. Song, E.J., Shin, N.R., Jeon, S., Nam, Y.D., and Kim, H. (2022). Lorcaserin and phentermine exert anti-obesity effects with modulation of the gut microbiota. Front Microbiol *13*, 1109651. 10.3389/fmicb.2022.1109651.
144. Kumar, V., Kumar, V., Mahajan, N., Kaur, J., Devi, K., Dharavath, R.N., Singh, R.P., Kondepudi, K.K., and Bishnoi, M. (2022). Mucin secretory action of capsaicin prevents high fat diet-induced gut barrier dysfunction in C57BL/6 mice colon. Biomed Pharmacother *145*, 112452. 10.1016/j.biopha.2021.112452.
145. Sun, J., Fan, J., Li, T., Yan, X., and Jiang, Y. (2022). Nuciferine Protects Against High-Fat Diet-Induced Hepatic Steatosis via Modulation of Gut Microbiota and Bile Acid Metabolism in Rats. J Agric Food Chem *70*, 12014-12028. 10.1021/acs.jafc.2c04817.
146. Schoeler, M., and Caesar, R. (2019). Dietary lipids, gut microbiota and lipid metabolism. Rev Endocr Metab Disord *20*, 461-472. 10.1007/s11154-019-09512-0.
147. Staley, C., Weingarden, A.R., Khoruts, A., and Sadowsky, M.J. (2017). Interaction of gut microbiota with bile acid metabolism and its influence on disease states. Appl Microbiol Biotechnol *101*, 47-64. 10.1007/s00253-016-8006-6.
148. Just, S., Mondot, S., Ecker, J., Wegner, K., Rath, E., Gau, L., Streidl, T., Hery-Arnaud, G., Schmidt, S., Lesker, T.R., et al. (2018). The gut microbiota drives the impact of bile acids and fat source in diet on mouse metabolism. Microbiome *6*, 134. 10.1186/s40168-018-0510-8.
149. Tsuji, Y., Kaji, K., Kitade, M., Kaya, D., Kitagawa, K., Ozutsumi, T., Fujinaga, Y., Takaya, H., Kawaratani, H., Namisaki, T., et al. (2020). Bile Acid Sequestrant, Sevelamer Ameliorates Hepatic Fibrosis with Reduced Overload of Endogenous Lipopolysaccharide in Experimental Nonalcoholic Steatohepatitis. Microorganisms *8*. 10.3390/microorganisms8060925.
150. Ocvirk, S., and O'Keefe, S.J.D. (2021). Dietary fat, bile acid metabolism and colorectal cancer. Semin Cancer Biol *73*, 347-355. 10.1016/j.semcancer.2020.10.003.
151. Li, T., and Chiang, J.Y. (2014). Bile acid signaling in metabolic disease and drug therapy. Pharmacol Rev *66*, 948-983. 10.1124/pr.113.008201.
152. Ozcan, E., Lum, G.R., and Hsiao, E.Y. (2022). Interactions between the gut microbiome and ketogenic diet in refractory epilepsy. Int Rev Neurobiol *167*, 217-249. 10.1016/bs.irn.2022.06.002.
153. Yu, Y., Raka, F., and Adeli, K. (2019). The Role of the Gut Microbiota in Lipid and Lipoprotein Metabolism. J Clin Med *8*. 10.3390/jcm8122227.
154. Manjer, J., Carlsson, S., Elmstahl, S., Gullberg, B., Janzon, L., Lindstrom, M., Mattisson, I., and Berglund, G. (2001). The Malmo Diet and Cancer Study: representativity, cancer incidence and mortality in participants and non-participants. Eur J Cancer Prev *10*, 489-499. 10.1097/00008469-200112000-00003.
155. Kahleova, H., Dort, S., Holubkov, R., and Barnard, N.D. (2018). A Plant-Based High-Carbohydrate, Low-Fat Diet in Overweight Individuals in a 16-Week Randomized Clinical Trial: The Role of Carbohydrates. Nutrients *10*. 10.3390/nu10091302.
156. Kahleova, H., Petersen, K.F., Shulman, G.I., Alwarith, J., Rembert, E., Tura, A., Hill, M., Holubkov, R., and Barnard, N.D. (2020). Effect of a Low-Fat Vegan Diet on Body Weight, Insulin Sensitivity, Postprandial Metabolism, and Intramyocellular and Hepatocellular Lipid Levels in Overweight Adults: A Randomized Clinical Trial. JAMA Netw Open *3*, e2025454. 10.1001/jamanetworkopen.2020.25454.
157. Sonestedt, E., Hellstrand, S., Drake, I., Schulz, C.A., Ericson, U., Hlebowicz, J., Persson, M.M., Gullberg, B., Hedblad, B., Engstrom, G., and Orho-Melander, M. (2016). Diet Quality and Change in Blood Lipids during 16 Years of Follow-up and Their Interaction with Genetic Risk for Dyslipidemia. Nutrients *8*. 10.3390/nu8050274.
158. Hamada, M., Abe, M., Miyake, T., Kawasaki, K., Tada, F., Furukawa, S., Matsuura, B., Hiasa, Y., and Onji, M. (2011). B cell-activating factor controls the production of adipokines and induces insulin resistance. Obesity (Silver Spring) *19*, 1915-1922. 10.1038/oby.2011.165.
159. Bienertova-Vasku J, B.P., Zlamal F, Tomandl J, Forejt M, Tomandlova M, Vavrina M, Kudelková J, Splichal Z, Vasku A (2012). B-cell activating factor (BAFF) – a new factor linking immunity to diet? Open Medicine *7* (*3*), 275-283. 10.2478/s11536-011-0153-7.
160. Alexaki, V.I., Notas, G., Pelekanou, V., Kampa, M., Valkanou, M., Theodoropoulos, P., Stathopoulos, E.N., Tsapis, A., and Castanas, E. (2009). Adipocytes as immune cells: differential expression of TWEAK, BAFF, and APRIL and their receptors (Fn14, BAFF-R, TACI, and BCMA) at different stages of normal and pathological adipose tissue development. J Immunol *183*, 5948-5956. 10.4049/jimmunol.0901186.
161. Endo, T., Nishio, M., Enzler, T., Cottam, H.B., Fukuda, T., James, D.F., Karin, M., and Kipps, T.J. (2007). BAFF and APRIL support chronic lymphocytic leukemia B-cell survival through activation of the canonical NF-kappaB pathway. Blood *109*, 703-710. 10.1182/blood-2006-06-027755.
162. Kusuyama, J., Bandow, K., Ohnishi, T., Amir, M.S., Shima, K., Semba, I., and Matsuguchi, T. (2019). CXCL13 is a differentiation- and hypoxia-induced adipocytokine that exacerbates the inflammatory phenotype of adipocytes through PHLPP1 induction. Biochem J *476*, 3533-3548. 10.1042/BCJ20190709.
163. Ticchioni, M., Essafi, M., Jeandel, P.Y., Davi, F., Cassuto, J.P., Deckert, M., and Bernard, A. (2007). Homeostatic chemokines increase survival of B-chronic lymphocytic leukemia cells through inactivation of transcription factor FOXO3a. Oncogene *26*, 7081-7091. 10.1038/sj.onc.1210519.
164. AsghariHanjani, N., and Vafa, M. (2019). The role of IGF-1 in obesity, cardiovascular disease, and cancer. Med J Islam Repub Iran *33*, 56. 10.34171/mjiri.33.56.
165. Schillaci, R., Galeano, A., Becu-Villalobos, D., Spinelli, O., Sapia, S., and Bezares, R.F. (2005). Autocrine/paracrine involvement of insulin-like growth factor-I and its receptor in chronic lymphocytic leukaemia. Br J Haematol *130*, 58-66. 10.1111/j.1365-2141.2005.05579.x.

166. Gamerdinger, M., Clement, A.B., and Behl, C. (2007). Cholesterol-like effects of selective cyclooxygenase inhibitors and fibrates on cellular membranes and amyloid-beta production. Mol Pharmacol *72*, 141-151. 10.1124/mol.107.034009.
167. Lim, S.C., Parajuli, K.R., Duong, H.Q., Choi, J.E., and Han, S.I. (2014). Cholesterol induces autophagic and apoptotic death in gastric carcinoma cells. Int J Oncol *44*, 805-811. 10.3892/ijo.2014.2246.
168. Bloch, K. (1992). Sterol molecule: structure, biosynthesis, and function. Steroids *57*, 378-383. 10.1016/0039-128x(92)90081-j.
169. Vona, R., Iessi, E., and Matarrese, P. (2021). Role of Cholesterol and Lipid Rafts in Cancer Signaling: A Promising Therapeutic Opportunity? Front Cell Dev Biol *9*, 622908. 10.3389/fcell.2021.622908.
170. Mollinedo, F., and Gajate, C. (2020). Lipid rafts as signaling hubs in cancer cell survival/death and invasion: implications in tumor progression and therapy: Thematic Review Series: Biology of Lipid Rafts. J Lipid Res *61*, 611-635. 10.1194/jlr.TR119000439.
171. Zhang, W., and Liu, H.T. (2002). MAPK signal pathways in the regulation of cell proliferation in mammalian cells. Cell Res *12*, 9-18. 10.1038/sj.cr.7290105.
172. Sun, Y., Liu, W.Z., Liu, T., Feng, X., Yang, N., and Zhou, H.F. (2015). Signaling pathway of MAPK/ERK in cell proliferation, differentiation, migration, senescence and apoptosis. J Recept Signal Transduct Res *35*, 600-604. 10.3109/10799893.2015.1030412.
173. Jeffrey, K.L., Camps, M., Rommel, C., and Mackay, C.R. (2007). Targeting dual-specificity phosphatases: manipulating MAP kinase signalling and immune responses. Nat Rev Drug Discov *6*, 391-403. 10.1038/nrd2289.
174. Farooq, A., and Zhou, M.M. (2004). Structure and regulation of MAPK phosphatases. Cell Signal *16*, 769-779. 10.1016/j.cellsig.2003.12.008.
175. Chen, Z., Shojaee, S., Buchner, M., Geng, H., Lee, J.W., Klemm, L., Titz, B., Graeber, T.G., Park, E., Tan, Y.X., et al. (2015). Signalling thresholds and negative B-cell selection in acute lymphoblastic leukaemia. Nature *521*, 357-361. 10.1038/nature14231.
176. Leung, G.P., Feng, T., Sigoillot, F.D., Geyer, F.C., Shirley, M.D., Ruddy, D.A., Rakiec, D.P., Freeman, A.K., Engelman, J.A., Jaskelioff, M., and Stuart, D.D. (2019). Hyperactivation of MAPK Signaling Is Deleterious to RAS/RAF-mutant Melanoma. Mol Cancer Res *17*, 199-211. 10.1158/1541-7786.MCR-18-0327.
177. Prior, I.A., Hood, F.E., and Hartley, J.L. (2020). The Frequency of Ras Mutations in Cancer. Cancer Res *80*, 2969-2974. 10.1158/0008-5472.CAN-19-3682.
178. Steelman, L.S., Chappell, W.H., Abrams, S.L., Kempf, R.C., Long, J., Laidler, P., Mijatovic, S., Maksimovic-Ivanic, D., Stivala, F., Mazzarino, M.C., et al. (2011). Roles of the Raf/MEK/ERK and PI3K/PTEN/Akt/mTOR pathways in controlling growth and sensitivity to therapy-implications for cancer and aging. Aging (Albany NY) *3*, 192-222. 10.18632/aging.100296.
179. Chappell, W.H., Steelman, L.S., Long, J.M., Kempf, R.C., Abrams, S.L., Franklin, R.A., Basecke, J., Stivala, F., Donia, M., Fagone, P., et al. (2011). Ras/Raf/MEK/ERK and PI3K/PTEN/Akt/mTOR inhibitors: rationale and importance to inhibiting these pathways in human health. Oncotarget *2*, 135-164. 10.18632/oncotarget.240.
180. McCubrey, J.A., Steelman, L.S., Kempf, C.R., Chappell, W.H., Abrams, S.L., Stivala, F., Malaponte, G., Nicoletti, F., Libra, M., Basecke, J., et al. (2011). Therapeutic resistance resulting from mutations in Raf/MEK/ERK and PI3K/PTEN/Akt/mTOR signaling pathways. J Cell Physiol *226*, 2762-2781. 10.1002/jcp.22647.
181. McCubrey, J.A., Steelman, L.S., Chappell, W.H., Abrams, S.L., Franklin, R.A., Montalto, G., Cervello, M., Libra, M., Candido, S., Malaponte, G., et al. (2012). Ras/Raf/MEK/ERK and PI3K/PTEN/Akt/mTOR cascade inhibitors: how mutations can result in therapy resistance and how to overcome resistance. Oncotarget *3*, 1068-1111. 10.18632/oncotarget.659.
182. Little, A.S., Smith, P.D., and Cook, S.J. (2013). Mechanisms of acquired resistance to ERK1/2 pathway inhibitors. Oncogene *32*, 1207-1215. 10.1038/onc.2012.160.
183. McCubrey, J.A., Steelman, L.S., Chappell, W.H., Abrams, S.L., Montalto, G., Cervello, M., Nicoletti, F., Fagone, P., Malaponte, G., Mazzarino, M.C., et al. (2012). Mutations and deregulation of Ras/Raf/MEK/ERK and PI3K/PTEN/Akt/mTOR cascades which alter therapy response. Oncotarget *3*, 954-987. 10.18632/oncotarget.652.
184. Dahlgren, C., and Karlsson, A. (1999). Respiratory burst in human neutrophils. J Immunol Methods *232*, 3-14. 10.1016/s0022-1759(99)00146-5.
185. Zhang, J., Wang, X., Vikash, V., Ye, Q., Wu, D., Liu, Y., and Dong, W. (2016). ROS and ROS-Mediated Cellular Signaling. Oxid Med Cell Longev *2016*, 4350965. 10.1155/2016/4350965.
186. Maya-Mendoza, A., Ostrakova, J., Kosar, M., Hall, A., Duskova, P., Mistrik, M., Merchut-Maya, J.M., Hodny, Z., Bartkova, J., Christensen, C., and Bartek, J. (2015). Myc and Ras oncogenes engage different energy metabolism programs and evoke distinct patterns of oxidative and DNA replication stress. Mol Oncol *9*, 601-616. 10.1016/j.molonc.2014.11.001.
187. Park, M.T., Kim, M.J., Suh, Y., Kim, R.K., Kim, H., Lim, E.J., Yoo, K.C., Lee, G.H., Kim, Y.H., Hwang, S.G., et al. (2014). Novel signaling axis for ROS generation during K-Ras-induced cellular transformation. Cell Death Differ *21*, 1185-1197. 10.1038/cdd.2014.34.
188. West, A.P., and Shadel, G.S. (2017). Mitochondrial DNA in innate immune responses and inflammatory pathology. Nat Rev Immunol *17*, 363-375. 10.1038/nri.2017.21.
189. Sakai, A., and Matsui, H. (2022). Cellular response against cytosolic leakage of mitochondrial DNA: insights into the pathology of Parkinson's disease. Neural Regen Res *17*, 2682-2684. 10.4103/1673-5374.335816.
190. Lu, H.Y., Bauman, B.M., Arjunaraja, S., Dorjbal, B., Milner, J.D., Snow, A.L., and Turvey, S.E. (2018). The CBM-opathies-A Rapidly Expanding Spectrum of Human Inborn Errors of Immunity Caused by Mutations in the CARD11-BCL10-MALT1 Complex. Front Immunol *9*, 2078. 10.3389/fimmu.2018.02078.
191. Zhang, T., Ma, C., Zhang, Z., Zhang, H., and Hu, H. (2021). NF-kappaB signaling in inflammation and cancer. MedComm (2020) *2*, 618-653. 10.1002/mco2.104.
192. Kracht, M., Muller-Ladner, U., and Schmitz, M.L. (2020). Mutual regulation of metabolic processes and proinflammatory NF-kappaB signaling. J Allergy Clin Immunol *146*, 694-705. 10.1016/j.jaci.2020.07.027.
193. Li, S.H., Dong, W.C., Fan, L., and Wang, G.S. (2016). Suppression of chronic lymphocytic leukemia progression by CXCR4 inhibitor WZ811. Am J Transl Res *8*, 3812-3821.
194. Burkle, A., Niedermeier, M., Schmitt-Graff, A., Wierda, W.G., Keating, M.J., and Burger, J.A. (2007). Overexpression of the CXCR5 chemokine receptor, and its ligand, CXCL13 in B-cell chronic lymphocytic leukemia. Blood *110*, 3316-3325. 10.1182/blood-2007-05-089409.
195. Parikh, S.A., Kay, N.E., and Shanafelt, T.D. (2014). How we treat Richter syndrome. Blood *123*, 1647-1657. 10.1182/blood-2013-11-516229.
196. Lewis, R., Maurer, H.C., Singh, N., Gonzalez-Menendez, I., Wirth, M., Schick, M., Zhang, L., Isaakidis, K., Scherger, A.K., Schulze, V., et al. (2021). CXCR4 hyperactivation cooperates with TCL1 in CLL development and aggressiveness. Leukemia *35*, 2895-2905. 10.1038/s41375-021-01376-1.
197. Wang, Y., Sinha, S., Wellik, L.E., Secreto, C.R., Rech, K.L., Call, T.G., Parikh, S.A., Kenderian, S.S., Muchtar, E., Hayman, S.R., et al. (2021). Distinct immune signatures in chronic lymphocytic leukemia and Richter syndrome. Blood Cancer J *11*, 86. 10.1038/s41408-021-00477-5.
198. Li, S., Ruan, Z., Zhang, H., and Xu, H. (2021). Recent achievements of bioluminescence imaging based on firefly luciferin-luciferase system. Eur J Med Chem *211*, 113111. 10.1016/j.ejmech.2020.113111.

199. White, E.H., Rapaport, E., Hopkins, T.A., and Seliger, H.H. (1969). Chemi- and bioluminescence of firefly luciferin. J Am Chem Soc *91*, 2178-2180. 10.1021/ja01036a093.
200. Maier, J., Lechel, A., Marienfeld, R., Barth, T.F.E., Moller, P., and Mellert, K. (2022). CARD9 Forms an Alternative CBM Complex in Richter Syndrome. Cancers (Basel) *14*. 10.3390/cancers14030531.
201. Ott, G., Rosenwald, A., and Campo, E. (2013). Understanding MYC-driven aggressive B-cell lymphomas: pathogenesis and classification. Hematology Am Soc Hematol Educ Program *2013*, 575-583. 10.1182/asheducation-2013.1.575.
202. Renvall, S., and Niinikoski, J. (1980). Kinetics of oxygen in peritoneal cavity. Effects of chemical peritonitis and intraperitoneally administered colloids in rats. J Surg Res *28*, 132-139. 10.1016/0022-4804(80)90156-0.
203. Kierans, S.J., and Taylor, C.T. (2021). Regulation of glycolysis by the hypoxia-inducible factor (HIF): implications for cellular physiology. J Physiol *599*, 23-37. 10.1113/JP280572.
204. Gillies, R.J., Robey, I., and Gatenby, R.A. (2008). Causes and consequences of increased glucose metabolism of cancers. J Nucl Med *49 Suppl 2*, 24S-42S. 10.2967/jnumed.107.047258.
205. Dang, C.V. (2007). The interplay between MYC and HIF in the Warburg effect. Ernst Schering Found Symp Proc, 35-53. 10.1007/2789_2008_088.
206. Semenza, G.L. (2003). Targeting HIF-1 for cancer therapy. Nat Rev Cancer *3*, 721-732. 10.1038/nrc1187.
207. Lu, H., Forbes, R.A., and Verma, A. (2002). Hypoxia-inducible factor 1 activation by aerobic glycolysis implicates the Warburg effect in carcinogenesis. J Biol Chem *277*, 23111-23115. 10.1074/jbc.M202487200.
208. Chiche, J., Brahimi-Horn, M.C., and Pouyssegur, J. (2010). Tumour hypoxia induces a metabolic shift causing acidosis: a common feature in cancer. J Cell Mol Med *14*, 771-794. 10.1111/j.1582-4934.2009.00994.x.
209. Wu, H., Estrella, V., Beatty, M., Abrahams, D., El-Kenawi, A., Russell, S., Ibrahim-Hashim, A., Longo, D.L., Reshetnyak, Y.K., Moshnikova, A., et al. (2020). T-cells produce acidic niches in lymph nodes to suppress their own effector functions. Nat Commun *11*, 4113. 10.1038/s41467-020-17756-7.
210. McMahon, S., Grondin, F., McDonald, P.P., Richard, D.E., and Dubois, C.M. (2005). Hypoxia-enhanced expression of the proprotein convertase furin is mediated by hypoxia-inducible factor-1: impact on the bioactivation of proproteins. J Biol Chem *280*, 6561-6569. 10.1074/jbc.M413248200.
211. Zhang, Y., Gao, X., Bai, X., Yao, S., Chang, Y.Z., and Gao, G. (2022). The emerging role of furin in neurodegenerative and neuropsychiatric diseases. Transl Neurodegener *11*, 39. 10.1186/s40035-022-00313-1.
212. Louagie, E., Taylor, N.A., Flamez, D., Roebroek, A.J., Bright, N.A., Meulemans, S., Quintens, R., Herrera, P.L., Schuit, F., Van de Ven, W.J., and Creemers, J.W. (2008). Role of furin in granular acidification in the endocrine pancreas: identification of the V-ATPase subunit Ac45 as a candidate substrate. Proc Natl Acad Sci U S A *105*, 12319-12324. 10.1073/pnas.0800340105.
213. Pamarthy, S., Kulshrestha, A., Katara, G.K., and Beaman, K.D. (2018). The curious case of vacuolar ATPase: regulation of signaling pathways. Mol Cancer *17*, 41. 10.1186/s12943-018-0811-3.
214. Sennoune, S.R., and Martinez-Zaguilan, R. (2007). Plasmalemmal vacuolar H+-ATPases in angiogenesis, diabetes and cancer. J Bioenerg Biomembr *39*, 427-433. 10.1007/s10863-007-9108-8.
215. Perona, R., and Serrano, R. (1988). Increased pH and tumorigenicity of fibroblasts expressing a yeast proton pump. Nature *334*, 438-440. 10.1038/334438a0.
216. Human Protein Atlas.
217. Shim, H., Dolde, C., Lewis, B.C., Wu, C.S., Dang, G., Jungmann, R.A., Dalla-Favera, R., and Dang, C.V. (1997). c-Myc transactivation of LDH-A: implications for tumor metabolism and growth. Proc Natl Acad Sci U S A *94*, 6658-6663. 10.1073/pnas.94.13.6658.
218. Osthus, R.C., Shim, H., Kim, S., Li, Q., Reddy, R., Mukherjee, M., Xu, Y., Wonsey, D., Lee, L.A., and Dang, C.V. (2000). Deregulation of glucose transporter 1 and glycolytic gene expression by c-Myc. J Biol Chem *275*, 21797-21800. 10.1074/jbc.C000023200.
219. Kim, J.W., Gao, P., Liu, Y.C., Semenza, G.L., and Dang, C.V. (2007). Hypoxia-inducible factor 1 and dysregulated c-Myc cooperatively induce vascular endothelial growth factor and metabolic switches hexokinase 2 and pyruvate dehydrogenase kinase 1. Mol Cell Biol *27*, 7381-7393. 10.1128/MCB.00440-07.
220. Zhdanov, A.V., Waters, A.H., Golubeva, A.V., Dmitriev, R.I., and Papkovsky, D.B. (2014). Availability of the key metabolic substrates dictates the respiratory response of cancer cells to the mitochondrial uncoupling. Biochim Biophys Acta *1837*, 51-62. 10.1016/j.bbabio.2013.07.008.
221. Chen, L., and Cui, H. (2015). Targeting Glutamine Induces Apoptosis: A Cancer Therapy Approach. Int J Mol Sci *16*, 22830-22855. 10.3390/ijms160922830.
222. Liu, P., Ge, M., Hu, J., Li, X., Che, L., Sun, K., Cheng, L., Huang, Y., Pilo, M.G., Cigliano, A., et al. (2017). A functional mammalian target of rapamycin complex 1 signaling is indispensable for c-Myc-driven hepatocarcinogenesis. Hepatology *66*, 167-181. 10.1002/hep.29183.
223. Wise, D.R., DeBerardinis, R.J., Mancuso, A., Sayed, N., Zhang, X.Y., Pfeiffer, H.K., Nissim, I., Daikhin, E., Yudkoff, M., McMahon, S.B., and Thompson, C.B. (2008). Myc regulates a transcriptional program that stimulates mitochondrial glutaminolysis and leads to glutamine addiction. Proc Natl Acad Sci U S A *105*, 18782-18787. 10.1073/pnas.0810199105.
224. Gao, P., Tchernyshyov, I., Chang, T.C., Lee, Y.S., Kita, K., Ochi, T., Zeller, K.I., De Marzo, A.M., Van Eyk, J.E., Mendell, J.T., and Dang, C.V. (2009). c-Myc suppression of miR-23a/b enhances mitochondrial glutaminase expression and glutamine metabolism. Nature *458*, 762-765. 10.1038/nature07823.
225. Carracedo, A., Cantley, L.C., and Pandolfi, P.P. (2013). Cancer metabolism: fatty acid oxidation in the limelight. Nat Rev Cancer *13*, 227-232. 10.1038/nrc3483.
226. Meng, T.C., Fukada, T., and Tonks, N.K. (2002). Reversible oxidation and inactivation of protein tyrosine phosphatases in vivo. Mol Cell *9*, 387-399. 10.1016/s1097-2765(02)00445-8.
227. Liang, S., Dong, S., Liu, W., Wang, M., Tian, S., Ai, Y., and Wang, H. (2021). Accumulated ROS Activates HIF-1alpha-Induced Glycolysis and Exerts a Protective Effect on Sensory Hair Cells Against Noise-Induced Damage. Front Mol Biosci *8*, 806650. 10.3389/fmolb.2021.806650.
228. Thannickal, V.J., and Fanburg, B.L. (2000). Reactive oxygen species in cell signaling. Am J Physiol Lung Cell Mol Physiol *279*, L1005-1028. 10.1152/ajplung.2000.279.6.L1005.
229. Zhang, Y., Xu, Y., Lu, W., Ghergurovich, J.M., Guo, L., Blair, I.A., Rabinowitz, J.D., and Yang, X. (2021). Upregulation of Antioxidant Capacity and Nucleotide Precursor Availability Suffices for Oncogenic Transformation. Cell Metab *33*, 94-109 e108. 10.1016/j.cmet.2020.10.002.
230. Georgakouli, K., Fatouros, I.G., Draganidis, D., Papanikolaou, K., Tsimeas, P., Deli, C.K., and Jamurtas, A.Z. (2019). Exercise in Glucose-6-Phosphate Dehydrogenase Deficiency: Harmful or Harmless? A Narrative Review. Oxid Med Cell Longev *2019*, 8060193. 10.1155/2019/8060193.
231. Fang, Z., Jiang, C., Feng, Y., Chen, R., Lin, X., Zhang, Z., Han, L., Chen, X., Li, H., Guo, Y., and Jiang, W. (2016). Effects of G6PD activity inhibition on the viability, ROS generation and mechanical properties of cervical cancer cells. Biochim Biophys Acta *1863*, 2245-2254. 10.1016/j.bbamcr.2016.05.016.

232. Capece, D., Verzella, D., Flati, I., Arboretto, P., Cornice, J., and Franzoso, G. (2022). NF-kappaB: blending metabolism, immunity, and inflammation. Trends Immunol *43*, 757-775. 10.1016/j.it.2022.07.004.
233. Abad, C., Martinez, C., Leceta, J., Juarranz, M.G., Delgado, M., and Gomariz, R.P. (2002). Pituitary adenylate-cyclase-activating polypeptide expression in the immune system. Neuroimmunomodulation *10*, 177-186. 10.1159/000067180.
234. Shili, I., Hamdi, Y., Marouani, A., Ben Lasfar, Z., Ghrairi, T., Lefranc, B., Leprince, J., Vaudry, D., and Olfa, M.K. (2021). Long-term protective effect of PACAP in a fetal alcohol syndrome (FAS) model. Peptides *146*, 170630. 10.1016/j.peptides.2021.170630.
235. Masmoudi-Kouki, O., Douiri, S., Hamdi, Y., Kaddour, H., Bahdoudi, S., Vaudry, D., Basille, M., Leprince, J., Fournier, A., Vaudry, H., et al. (2011). Pituitary adenylate cyclase-activating polypeptide protects astroglial cells against oxidative stress-induced apoptosis. J Neurochem *117*, 403-411. 10.1111/j.1471-4159.2011.07185.x.
236. Vaudry, D., Pamantung, T.F., Basille, M., Rousselle, C., Fournier, A., Vaudry, H., Beauvillain, J.C., and Gonzalez, B.J. (2002). PACAP protects cerebellar granule neurons against oxidative stress-induced apoptosis. Eur J Neurosci *15*, 1451-1460. 10.1046/j.1460-9568.2002.01981.x.
237. Seaborn, T., Masmoudi-Kouli, O., Fournier, A., Vaudry, H., and Vaudry, D. (2011). Protective effects of pituitary adenylate cyclase-activating polypeptide (PACAP) against apoptosis. Curr Pharm Des *17*, 204-214. 10.2174/138161211795049679.
238. Figiel, M., and Engele, J. (2000). Pituitary adenylate cyclase-activating polypeptide (PACAP), a neuron-derived peptide regulating glial glutamate transport and metabolism. J Neurosci *20*, 3596-3605. 10.1523/JNEUROSCI.20-10-03596.2000.
239. Diamantopoulos, P.T., Sofotasiou, M., Papadopoulou, V., Polonyfi, K., Iliakis, T., and Viniou, N.A. (2014). PARP1-driven apoptosis in chronic lymphocytic leukemia. Biomed Res Int *2014*, 106713. 10.1155/2014/106713.
240. Krishnakumar, R., and Kraus, W.L. (2010). The PARP side of the nucleus: molecular actions, physiological outcomes, and clinical targets. Mol Cell *39*, 8-24. 10.1016/j.molcel.2010.06.017.
241. Herrmann, G.K., Russell, W.K., Garg, N.J., and Yin, Y.W. (2021). Poly(ADP-ribose) polymerase 1 regulates mitochondrial DNA repair in an NAD-dependent manner. J Biol Chem *296*, 100309. 10.1016/j.jbc.2021.100309.
242. Szczesny, B., Brunyanszki, A., Olah, G., Mitra, S., and Szabo, C. (2014). Opposing roles of mitochondrial and nuclear PARP1 in the regulation of mitochondrial and nuclear DNA integrity: implications for the regulation of mitochondrial function. Nucleic Acids Res *42*, 13161-13173. 10.1093/nar/gku1089.
243. Knittel, G., Rehkamper, T., Korovkina, D., Liedgens, P., Fritz, C., Torgovnick, A., Al-Baldawi, Y., Al-Maarri, M., Cun, Y., Fedorchenko, O., et al. (2017). Two mouse models reveal an actionable PARP1 dependence in aggressive chronic lymphocytic leukemia. Nat Commun *8*, 153. 10.1038/s41467-017-00210-6.
244. Firmino, N.S., Cederberg, R.A., Lee, C.M., Shi, R., Wadsworth, B.J., Franks, S.E., Thomas, K.N., Decotret, L.R., and Bennewith, K.L. (2021). Germinal center hypoxia in tumor-draining lymph nodes negatively regulates tumor-induced humoral immune responses in mouse models of breast cancer. Oncoimmunology *10*, 1959978. 10.1080/2162402X.2021.1959978.
245. Gan, E.S., and Ooi, E.E. (2020). Oxygen: viral friend or foe? Virol J *17*, 115. 10.1186/s12985-020-01374-2.
246. Caldwell, C.C., Kojima, H., Lukashev, D., Armstrong, J., Farber, M., Apasov, S.G., and Sitkovsky, M.V. (2001). Differential effects of physiologically relevant hypoxic conditions on T lymphocyte development and effector functions. J Immunol *167*, 6140-6149. 10.4049/jimmunol.167.11.6140.
247. Bottcher, M., Bruns, H., Volkl, S., Lu, J., Chartomatsidou, E., Papakonstantinou, N., Mentz, K., Buttner-Herold, M., Zenz, T., Herling, M., et al. (2021). Control of PD-L1 expression in CLL-cells by stromal triggering of the Notch-c-Myc-EZH2 oncogenic signaling axis. J Immunother Cancer *9*. 10.1136/jitc-2020-001889.
248. Dermit, M., Casado, P., Rajeeve, V., Wilkes, E.H., Foxler, D.E., Campbell, H., Critchlow, S., Sharp, T.V., Gribben, J.G., Unwin, R., and Cutillas, P.R. (2017). Oxidative stress downstream of mTORC1 but not AKT causes a proliferative defect in cancer cells resistant to PI3K inhibition. Oncogene *36*, 2762-2774. 10.1038/onc.2016.435.

7. Supplementary tables

Suppl. Table 1: Nutrition values of the different diets used in the experimental setup

	Western diet (D12079B)	Low fat diet (D19011501)	Chow diet (altromin)	Mean American diet (2013-2016)[113]
Ingredient [% kcal]				
Protein	17	17	27	16.0
Carbohydrates	43	73	55	47.3
Fat	40	10	18	34.8
kcal/g	4.68	3.91	3.47	
Ingredient [kcal]				
Casein, 80 Mesh	780	0		
Soy Protein, Supro 661	0	780		
Corn Starch	200	1617.6		
Milk Fat, Anhydrous	1800	0		
Cholesterol	0	0		
Corn Oil	90	472.5		
Choline Bitartrate	0	0		
DL-Methionine	12	12		
Maltodextrin 10	400	400		
Sucrose	1364	1364		
Cellulose, BW200	0	0		
Ethoxyquin	0	0		
Mineral Mix S10001	0	0		
Calcium Carbonate	0	0		
Vitamin Mix V10001	40	40		
Total	**4686**	**4686.1**		
Ingredient [% of g]				
Protein	20	17		
Carbohydrates	50	71		
Fat	21	4		
Ingredient [g]				
Casein, 80 Mesh	195	0		
Soy Protein, Supro 661	0	195		
Corn Starch	50	404.4		
Milk Fat, Anhydrous	200	0		
Cholesterol	1.5	0		
Corn Oil	10	52.5		
Choline Bitartrate	2	2		
DL-Methionine	3	3		
Maltodextrin 10	100	100		
Sucrose	341	341		
Cellulose, BW200	50	50		
Ethoxyquin	0.04	0.04		
Mineral Mix S10001	35	35		
Calcium Carbonate	4	4		
Vitamin Mix V10001	10	10		
Total	**1001.54**	**1197.04**		

Suppl. Table 2: Proteins with differential abundance in MYC-positive RT samples and control samples. Proteins with a positive logFC value had a higher abundance in RT samples than in control samples, vis versa, proteins with a negative logFC value had a higher abundance in control samples than in RT samples. In addition, p-values adjusted for multiple testing are listed.

Protein	AntibodyID	Uniprot-Entry-Name	Uniprot-Entry	HGNC	logFC	AveExp	adj.p val
PACA	ab2913	PACA_HUMAN	P18509	ADCYAP1	1.73	12.71	5.9e-12
FURIN	ab1740	FURIN_HUMAN	P09958	FURIN	1.09	14.20	5.5e-07
PARP1	ab1125	PARP1_HUMAN	P09874	PARP1	0.84	12.03	3.7e-05
Fc fusion with TNR21	ab0517				0.80	13.38	1.0e-06
CCL8	ab1870	CCL8_HUMAN	P80075	CCL8	0.80	11.59	2.8e-02
RB11A	ab3202	RB11A_HUMAN	P62491	RAB11A	0.66	10.39	2.1e-04
IL10	ab1898	IL10_HUMAN	P22301	IL10	0.65	11.35	6.8e-03
CD166	ab2246	CD166_HUMAN	Q13740	ALCAM	0.65	14.26	1.7e-04
SHIP2	ab3137	SHIP2_HUMAN	O15357	INPPL1	0.64	12.15	1.7e-03
EWS	ab3531	EWS_HUMAN	Q01844	EWSR1	0.64	11.46	2.1e-04
AMBP	ab2682	AMBP_HUMAN	P02760	AMBP	0.64	13.70	1.7e-02
MUC2	ab0504	MUC2_HUMAN	Q02817	MUC2	0.64	12.65	1.2e-08
LEUK	ab0991	LEUK_HUMAN	P16150	SPN	0.64	13.45	7.6e-06
FGF2	ab1714	FGF2_HUMAN	P09038	FGF2	0.63	13.72	7.1e-06
CSF1R	ab1925	CSF1R_HUMAN	P07333	CSF1R	0.63	13.72	2.8e-05
SORL	ab0522	SORL_HUMAN	Q92673	SORL1	0.62	12.51	8.2e-04
ASNS	ab3524	ASNS_HUMAN	P08243	ASNS	0.60	11.70	4.0e-03
IRF4	ab1208	IRF4_HUMAN	Q15306	IRF4	0.60	11.65	3.0e-04
IL6RA	ab1706	IL6RA_HUMAN	P08887	IL6R	0.59	13.67	3.2e-08
RSPO1	ab2675	RSPO1_HUMAN	Q2MKA7	RSPO1	0.58	12.52	4.0e-02
CD27	ab0718	CD27_HUMAN	P26842	CD27	0.56	12.39	6.4e-04
MYCN	ab0745	MYCN_HUMAN	P04198	MYCN	0.56	12.49	2.2e-04
TN13B	ab1711	TN13B_HUMAN	Q9Y275	TNFSF13B	0.56	12.08	3.4e-07
UN93B	ab0079	UN93B_HUMAN	Q9H1C4	UNC93B1	0.56	13.53	1.4e-03
DAND5	ab2381	DAND5_HUMAN	Q8N907	DAND5	0.55	12.88	1.7e-04
STK19	ab1296	STK19_HUMAN	P49842	STK19	0.55	13.60	6.4e-04
E2AK4	ab0744	E2AK4_HUMAN	Q9P2K8	EIF2AK4	0.54	14.10	3.4e-04
RASK	ab1140	RASK_HUMAN	P01116	KRAS	0.54	12.87	6.3e-04
HNRPR	ab0702	HNRPR_HUMAN	O43390	HNRNPR	0.54	13.08	1.4e-03
TSN12	ab0696	TSN12_HUMAN	O95859	TSPAN12	0.53	13.75	7.9e-05
CXL11	ab2115	CXL11_HUMAN	O14625	CXCL11	0.52	11.87	3.6e-03
CD14	ab2267	CD14_HUMAN	P08571	CD14	0.52	11.30	1.1e-03
MAMC2	ab0844	MAMC2_HUMAN	Q7Z304	MAMDC2	0.51	13.37	3.2e-05
SPR2A	ab0826	SPR2A_HUMAN	P35326	SPRR2A	0.51	14.04	1.6e-03
ITA5	ab1565	ITA5_HUMAN	P08648	ITGA5	0.51	13.70	2.5e-02
HMGB1	ab1215	HMGB1_HUMAN	P09429	HMGB1	0.51	13.46	2.1e-04
RL10A	ab1279	RL10A_HUMAN	P62906	RPL10A	0.50	12.32	4.5e-05
APOA1	ab2771	APOA1_HUMAN	P02647	APOA1	-0.50	14.27	4.1e-04
S10A6	ab1027	S10A6_HUMAN	P06703	S100A6	-0.51	9.38	9.3e-03
CD3E	ab1359	CD3E_HUMAN	P07766	CD3E	-0.52	11.70	5.9e-03
EPOR	ab1938	EPOR_HUMAN	P19235	EPOR	-0.54	10.37	1.1e-02
SMRC1	ab2875	SMRC1_HUMAN	Q92922	SMARCC1	-0.54	11.49	3.1e-03
TYRO3	ab2186	TYRO3_HUMAN	Q06418	TYRO3	-0.54	11.68	4.6e-03
PERM	ab1514	PERM_HUMAN	P05164	MPO	-0.54	11.76	6.9e-03
P4K2A	ab3152	P4K2A_HUMAN	Q9BTU6	PI4K2A	-0.54	11.01	4.2e-04
CD83	ab3502	CD83_HUMAN	Q01151	CD83	-0.55	14.07	2.1e-04
CCL20	ab1598	CCL20_HUMAN	P78556	CCL20	-0.55	11.73	4.4e-03
KLKB1	ab2866	KLKB1_HUMAN	P03952	KLKB1	-0.55	12.44	1.4e-02
PD1L1	ab1823	PD1L1_HUMAN	Q9NZQ7	CD274	-0.55	12.96	1.9e-03
UFO	ab2306	UFO_HUMAN	P30530	AXL	-0.55	12.17	1.6e-02
SLAF1	ab2132	SLAF1_HUMAN	Q13291	SLAMF1	-0.55	13.45	3.0e-04
MTMRC	ab3142	MTMRC_HUMAN	Q9C0I1	MTMR12	-0.56	13.46	4.9e-04
MET	ab1790	MET_HUMAN	P08581	MET	-0.56	12.31	5.0e-03
IL4	ab1658	IL4_HUMAN	P05112	IL4	-0.56	12.85	2.9e-03
MTMR3	ab3145	MTMR3_HUMAN	Q13615	MTMR3	-0.58	12.39	1.9e-05
GAS6	ab2740	GAS6_HUMAN	Q14393	GAS6	-0.58	13.92	7.2e-05
CD81	ab0993	CD81_HUMAN	P60033	CD81	-0.58	12.92	3.2e-05
ECHM	ab0593	ECHM_HUMAN	P30084	ECHS1	-0.58	14.24	2.1e-04

Protein	AntibodyID	Uniprot-Entry-Name	Uniprot-Entry	HGNC	logFC	AveExp	adj.p val
GAS1	ab2390	GAS1_HUMAN	P54826	GAS1	-0.58	11.82	1.3e-02
CCL19	ab1585	CCL19_HUMAN	Q99731	CCL19	-0.59	11.37	5.7e-04
DLX4	ab1242	DLX4_HUMAN	Q92988	DLX4	-0.59	10.64	1.6e-02
Lactoferin	ab1611	TRFL_HUMAN	P02788	LTF	-0.59	12.76	3.8e-05
ALBU	ab0217	ALBU_HUMAN	P02768	ALB	-0.59	11.21	3.3e-02
MUC5B	ab0505	MUC5B_HUMAN	Q9HC84	MUC5B	-0.59	12.77	2.3e-02
LEG3	ab1738	LEG3_HUMAN	P17931	LGALS3	-0.60	11.43	2.0e-03
CD14	ab1627	CD14_HUMAN	P08571	CD14	-0.60	13.30	5.8e-05
VEGFA	ab2945	VEGFA_HUMAN	P15692	VEGFA	-0.60	13.99	2.6e-02
MYOZ3	ab2021	MYOZ3_HUMAN	Q8TDC0	MYOZ3	-0.60	10.86	4.9e-03
ITIH4	ab2676	ITIH4_HUMAN	Q14624	ITIH4	-0.60	12.82	5.0e-04
PKHA8	ab3218	PKHA8_HUMAN	Q96JA3	PLEKHA8	-0.60	11.54	1.7e-03
CD20	ab1594	CD20_HUMAN	P11836	MS4A1	-0.60	11.75	2.1e-02
EDA	ab1905	EDA_HUMAN	Q92838	EDA	-0.60	10.46	2.2e-02
HLA-ABC	ab1493				-0.60	11.96	4.3e-04
ITA2B	ab1432	ITA2B_HUMAN	P08514	ITGA2B	-0.61	10.97	2.1e-04
CD5	ab1529	CD5_HUMAN	P06127	CD5	-0.61	12.61	2.8e-05
IBP2	ab1835	IBP2_HUMAN	P18065	IGFBP2	-0.62	14.03	1.1e-04
PECA1	ab1535	PECA1_HUMAN	P16284	PECAM1	-0.62	11.39	3.0e-05
MICA	ab2324	MICA_HUMAN	Q29983	MICA	-0.63	10.79	1.9e-02
TNR6	ab1478	TNR6_HUMAN	P25445	FAS	-0.63	11.88	4.2e-02
HMGA1	ab0969	HMGA1_HUMAN	P17096	HMGA1	-0.64	13.39	9.7e-05
FGF2	ab2374	FGF2_HUMAN	P09038	FGF2	-0.64	12.88	9.2e-03
INHBA	ab2176	INHBA_HUMAN	P08476	INHBA	-0.65	9.85	1.6e-02
TNF14	ab2301	TNF14_HUMAN	O43557	TNFSF14	-0.65	11.72	3.7e-02
CCL5	ab1672	CCL5_HUMAN	P13501	CCL5	-0.65	12.24	3.7e-05
RGMC	ab2819	RGMC_HUMAN	Q6ZVN8	HJV	-0.67	12.16	9.3e-03
S100B	ab2775	S100B_HUMAN	P04271	S100B	-0.67	14.12	3.8e-05
IL10	ab1684	IL10_HUMAN	P22301	IL10	-0.67	12.84	6.9e-03
HS71A	ab2080	HS71A_HUMAN	P0DMV8	HSPA1A	-0.68	13.15	6.8e-08
HLAG	ab1609	HLAG_HUMAN	P17693	HLA-G	-0.68	12.30	3.7e-06
RBP2	ab3544	RBP2_HUMAN	P49792	RANBP2	-0.68	11.76	1.1e-04
ITA2B (CD41a)	ab1538		P08514	ITGA2B	-0.69	12.54	2.1e-05
BDNF	ab2106	BDNF_HUMAN	P23560	BDNF	-0.69	13.78	5.9e-08
CADH2	ab2760	CADH2_HUMAN	P19022	CDH2	-0.69	14.32	6.1e-07
IL2RA	ab1831	IL2RA_HUMAN	P01589	IL2RA	-0.69	12.93	1.8e-04
EIF3B	ab0968	EIF3B_HUMAN	P55884	EIF3B	-0.70	12.85	2.1e-04
CCL3	ab0985	CCL3_HUMAN	P10147	CCL3	-0.70	11.96	2.9e-04
GP1BA	ab1433	GP1BA_HUMAN	P07359	GP1BA	-0.70	13.78	2.6e-04
IFI27	ab1065	IFI27_HUMAN	P40305	IFI27	-0.70	11.60	5.8e-05
DLK1	ab1801	DLK1_HUMAN	P80370	DLK1	-0.71	13.27	8.5e-06
ATRN	ab2721	ATRN_HUMAN	O75882	ATRN	-0.71	12.85	2.1e-04
IL15	ab1510	IL15_HUMAN	P40933	IL15	-0.72	12.53	1.7e-05
VCAM1	ab1090	VCAM1_HUMAN	P19320	VCAM1	-0.72	12.47	1.7e-02
CHLE	ab2685	CHLE_HUMAN	P06276	BCHE	-0.72	13.58	1.0e-06
BGH3	ab2334	BGH3_HUMAN	Q15582	TGFBI	-0.72	11.44	3.2e-03
UTER	ab2119	UTER_HUMAN	P11684	SCGB1A1	-0.73	12.51	1.9e-05
PEPC	ab2697	PEPC_HUMAN	P20142	PGC	-0.73	14.34	1.7e-05
RSPO4	ab2690	RSPO4_HUMAN	Q2I0M5	RSPO4	-0.74	12.80	4.4e-09
CO7	ab2843	CO7_HUMAN	P10643	C7	-0.74	12.81	1.1e-05
IL3RB	ab0902	IL3RB_HUMAN	P32927	CSF2RB	-0.78	14.15	1.2e-05
MTMR6	ab3147	MTMR6_HUMAN	Q9Y217	MTMR6	-0.78	12.24	5.8e-07
TNR1A	ab2332	TNR1A_HUMAN	P19438	TNFRSF1A	-0.79	12.78	2.2e-04
IL5	ab2431	IL5_HUMAN	P05113	IL5	-0.80	11.86	8.6e-04
GNLY	ab2801	GNLY_HUMAN	P22749	GNLY	-0.80	14.32	9.3e-09
NEP	ab1381	NEP_HUMAN	P08473	MME	-0.81	11.12	9.3e-03
AREG	ab1991	AREG_HUMAN	P15514	AREG	-0.81	10.81	1.6e-03
ADA15	ab2088	ADA15_HUMAN	Q13444	ADAM15	-0.82	13.37	1.6e-09
VIME	ab1164	VIME_HUMAN	P08670	VIM	-0.84	13.01	3.2e-04
TIMP2	ab2266	TIMP2_HUMAN	P16035	TIMP2	-0.84	11.04	8.6e-04
CO1A1	ab2123	CO1A1_HUMAN	P02452	COL1A1	-0.86	13.85	6.3e-05

Protein	AntibodyID	Uniprot-Entry-Name	Uniprot-Entry	HGNC	logFC	AveExp	adj.p val
B2MG	ab2878	B2MG_HUMAN	P61769	B2M	-0.89	9.95	2.9e-04
SDF1	ab2491	SDF1_HUMAN	P48061	CXCL12	-0.93	13.23	4.8e-05
CP3A5	ab0893	CP3A5_HUMAN	P20815	CYP3A5	-0.95	11.42	8.5e-03
SEM3E	ab1913	SEM3E_HUMAN	O15041	SEMA3E	-0.95	13.07	3.8e-05
20S Immunoproteasome	ab2722		P28062	PSMB8	-0.97	11.23	3.2e-04
MIA	ab2702	MIA_HUMAN	Q16674	MIA	-0.99	13.89	1.9e-05
KI2L2	ab1134	KI2L2_HUMAN	P43627	KIR2DL2	-0.99	10.70	3.5e-02
FABPH	ab2686	FABPH_HUMAN	P05413	FABP3	-1.01	12.63	4.9e-08
IBP1	ab2347	IBP1_HUMAN	P08833	IGFBP1	-1.05	12.77	1.7e-07
CDN2B	ab2922	CDN2B_HUMAN	P42772	CDKN2B	-1.06	11.48	9.2e-03
TREM2	ab3556	TREM2_HUMAN	Q9NZC2	TREM2	-1.08	12.41	2.1e-04
IGKC	ab3241	IGKC_HUMAN	P01834	IGKC	-1.09	10.71	8.6e-04
S10AD	ab1829	S10AD_HUMAN	Q99584	S100A13	-1.17	11.49	1.1e-05
MICB	ab1762	MICB_HUMAN	Q29980	MICB	-1.21	11.13	3.1e-03

8. Supplementary figures

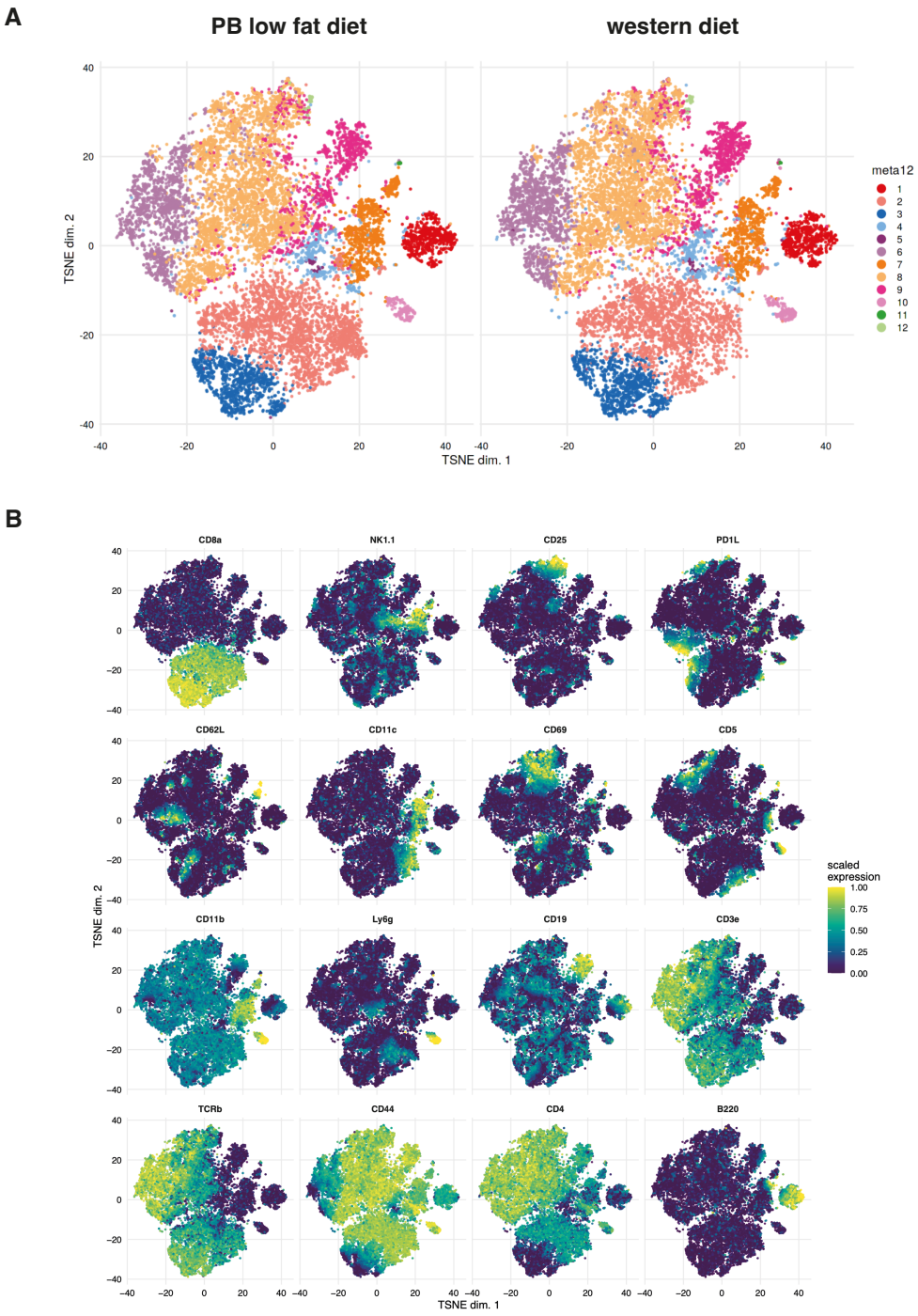

Suppl. Figure 1: TSNE projection of CD19 depleted splenocytes of C57Bl6/J mice (27 weeks on diet, 19 weeks after CLL transplantation) clustered using sixteen extracellular markers. The analysis was performed with CYANUS (CYtometry ANalysis Using Shiny) software. The samples were gated for CD45⁺ expression before analysis. ***A*** *Comparison of low fat diet and Western diet splenocytes with a classification into twelve clusters (meta12).* ***B*** *Localization of the different sixteen extracellular markers inside the TSNE projection.*

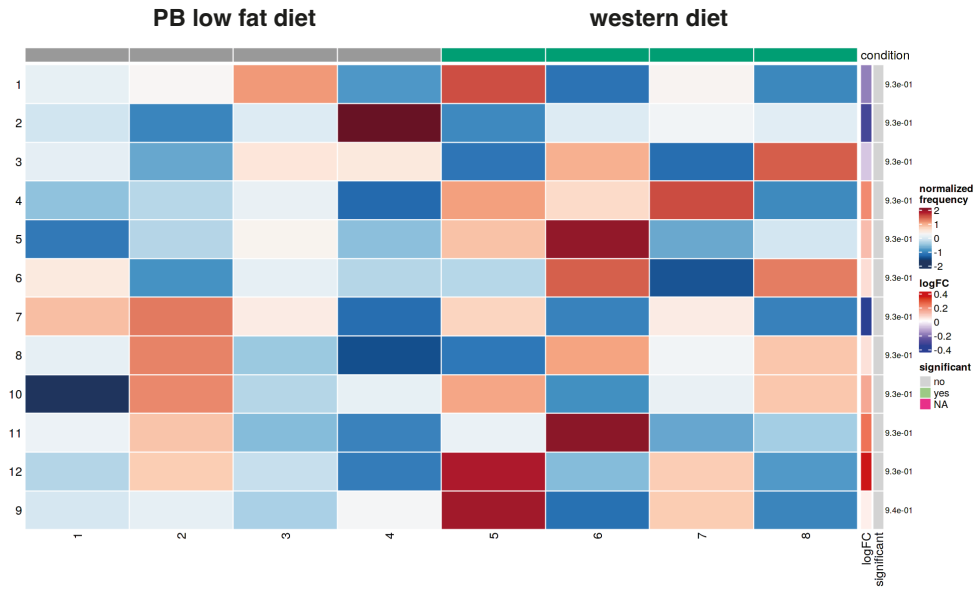

Suppl. Figure 2 Differential expression analysis using differential cluster abundance testing of TSNE clusters. Depicted are the twelve (1-12) defined clusters (meta12) vs. eight experimental mice (1-8). No cluster is significantly differentially expressed. For statistical analysis: method: edgeR, comparison: condition, cluster: meta12, trend method: none, normalized: yes, FDR threshold: 0.05, sorted by: p-adjusted, z-score normalization: yes.

9. Acknowledgments

I would like to express my heartfelt gratitude to all those who have supported and guided me throughout my doctoral journey, making this achievement possible.

First and foremost, I am deeply indebted to my advisor, Maike Buchner-Mayr, whose unwavering guidance, invaluable insights, and encouragement have been the cornerstone of this research. Your mentorship not only shaped the direction of this thesis but also enriched my intellectual growth. Your encouragement to explore new avenues and your unwavering belief in my potential have been instrumental in my growth as a scientist.

I would like to extend my appreciation to the second advisor of my doctoral thesis Matthias Feige and my official mentor Selina Keppler as parts of my doctoral committee for their constructive feedback, rigorous evaluation, and contributions that have enhanced the quality of this work. Selina Keppler and Marc Rosenbaum have been true mentors during the last few years and I am humbled by the support I have received. I am excited to carry forward the lessons and skills I have gained under their mentorship as I embark on new challenges and opportunities. The successful culmination of this work would not have been possible without the unwavering dedication and expertise of my mentors and advisors.

I am thankful to Jürgen Ruland for providing a conducive academic environment and the necessary resources that facilitated my research endeavors. The Institute of Clinical Chemistry and Pathobiochemistry played a pivotal role in providing access to cutting-edge facilities and collaborative opportunities that enriched my research experience. Further, I would like to acknowledge the participants and medical support who volunteered their time and shared their experiences, making this research possible. Your contributions are invaluable and have added depth to the findings of this study.

My gratitude extends to current and past colleagues and fellow researchers who shared their insights and engaged in stimulating discussions, which contributed to shaping the ideas presented in this thesis. Your camaraderie has made this academic journey memorable. Beyond the academic realm, I am deeply appreciative of the personal support and friendship I have received from my colleagues from the second-floor office. Your genuine interest in my well-being, your willingness to lend an ear during moments of uncertainty, and your encouragement during moments of triumph have created a nurturing and motivating environment that transcends academia.

Furthermore, I am above all grateful to my friends outside of this lab, for their unwavering support, encouragement, and understanding during the challenging phases of this journey, even though they might not have a clue what all of this is about. Regardless of whether you have accompanied my life for 15 years or just one, your belief in me kept me motivated and resilient. For you, I would like to quote the famous musicians Bonez MC, RAF Camora, and Maxwell: “Nie ohne mein Team”.

I am profoundly grateful for the unwavering love, support, and encouragement that my family has provided throughout this journey of my whole academic career, as well as during my thesis. Their presence in my life has been a constant source of strength and inspiration, and I am deeply appreciative of their sacrifices and understanding. I especially thank my parents for your belief in my abilities and your unyielding support, which have been the foundation upon which I have built my life pursuits. Your sacrifices, both big and small, have made it possible for me to pursue my dreams. Your words of wisdom, encouragement during moments of self-doubt, and celebrations of my achievements have given me the confidence to overcome challenges. Nevertheless, I am extremely grateful that you stopped asking about the progress of this thesis during difficult times.

Last but not least, I would like to express my appreciation to my husband, for your unwavering patience, understanding, and encouragement. Your belief in my abilities, even during times of stress, has been a driving force in my journey. I am truly thankful for you being by my side for already 15 years through thick and thin, for your support towards my decision to even start a Ph.D. program, and for trying to help with this thesis by any means. Thank you for taking me on involuntarily long bike rides and exploring the world with me.

In conclusion, this thesis stands as a testament to the collective efforts and encouragement of all those who have touched my life. While it is not possible to name everyone individually, please know that your impact has been deeply appreciated and will forever be cherished.

Thank you very much.